Dynamics of Water Interacting with Biomolecules

ISBN 978-94-92323-11-8

Cover art: "Cool blues" by Pery Burge (chronoscapes.com)

Dynamics of Water Interacting with Biomolecules

ACADEMISCH PROEFSCHRIFT

ter verkrijging van de graad van doctor
aan de Universiteit van Amsterdam
op gezag van de Rector Magnificus
prof. dr. ir. K. I. J. Maex
ten overstaan van een door het College voor Promoties
ingestelde commissie,
in het openbaar te verdedigen in de Agnietenkapel
op vrijdag 13 januari 2017, te 10:00 uur

door

Catharina Cecile Maria Groot

geboren te Nijmegen

Promotiecommissie

Promotor:	prof. dr. H. J. Bakker	Universiteit van Amsterdam
Overige leden:	prof. dr. P. G. Bolhuis	Universiteit van Amsterdam
	prof. dr. A. M. Brouwer	Universiteit van Amsterdam
	prof. dr. M. Havenith	Ruhr-Universität Bochum
	prof. dr. J. L. Herek	Universiteit Twente
	prof. dr. J. Oomens	Universiteit van Amsterdam
	prof. dr. K. P. Velikov	Universiteit Utrecht

Faculteit der Natuurwetenschappen, Wiskunde en Informatica

This thesis is part of NanoNextNL, a micro and nanotechnology innovation consortium of the Government of the Netherlands and 130 partners from academia and industry.
The work described in this thesis was performed at the FOM Institute AMOLF, Science Park 104, 1098 XG Amsterdam, The Netherlands. This work is part of the research programme of the Foundation for Fundamental Research on Matter (FOM), which is financially supported by the Netherlands Organisation for Scientific Research (NWO).

Publications covered in this thesis

C. C. M. Groot and H. J. Bakker. Hydration dynamics of aqueous glucose probed with polarization-resolved fs-IR spectroscopy. *J. Chem. Phys. 140*, 234503, 2014. - *chapter 5*

C. C. M. Groot and H. J. Bakker. A femtosecond mid-infrared study of the dynamics of water in aqueous sugar solutions. *Phys. Chem. Chem. Phys. 17*, 8449, 2015. - *chapter 5*

C. C. M. Groot and H. J. Bakker. Proteins take up water before unfolding. *J. Phys. Chem. Lett. 7*, 1800-1804, 2016. - *chapter 6*

C. C. M. Groot, K. P. Velikov and H. J. Bakker. Structure and dynamics of water confined in triglyceride oils. *Phys. Chem. Chem. Phys. 18*, 29361-29368, 2016. - *chapter 8*

C. C. M. Groot, K. Meister, A. L. DeVries and H. J. Bakker. Dynamics of the hydration water of antifreeze glycoproteins. *J. Phys. Chem. Lett. 7*, 4836-4840, 2016. - *chapter 7*

Other publications

S. Lotze, C. C. M. Groot, C. Vennehaug and H. J. Bakker. Femtosecond mid-infrared study of the dynamics of water molecules in water-acetone and water-dimethyl sulfoxide mixtures. *J. Phys. Chem. B 119*, 5228-5239 (2015).

Z. F. Brotzakis, C. C. M. Groot, W. H. Brandeburgo, H. J. Bakker and P. G. Bolhuis. Dynamics of hydration water around native and misfolded α-lactalbumin. *J. Phys. Chem. B 120*, 4756-4766 (2016).

Contents

1 Introduction

1.1 Water

The most familiar liquid to humanity is undoubtedly water. It is also a liquid that continues to be the subject of intense study. Despite its chemical simplicity, a single oxygen atom with two hydrogen atoms, water has some unusual chemical properties. It has an anomalously high melting and boiling point, high surface tension, high heat capacity and a maximum density in the liquid phase, to name a few of the more than 70 anomalies of water [1,2]. Exactly these peculiarities (or rather, the underlying reasons for these) make water such an excellent solvent, reactant and energy transporter, and very important in biology, as we will see further on.

Most anomalous properties of water arise from water's tendency to form hydrogen bonds. This tendency in turn arises from the distribution of electrons in a water molecule. A water molecule has four pairs of valence electrons, two of which are shared between the oxygen and the hydrogens to form covalent bonds, and two lone pairs. Since all electrons repel each other, the most stable configuration is a tetrahedron, with the hydrogen atoms residing in two corners, and the lone pairs smeared out over the other two (fig. 1.1A). (Because of the slightly higher electrostatic repulsion between the lone pairs, the angle between the two OH bonds is 106° in liquid water [3], which is smaller than the 109° of a perfect tetrahedron.) While a water molecule has no net charge, the greater electronegativity of oxygen causes the electrons to be distributed unequally, resulting in a partial positive charge on the hydrogen atoms and a partial negative charge on the oxygen atom. As a consequence, the hydrogen atom of one water molecule is attracted to the oxygen lone pairs of another water molecule:

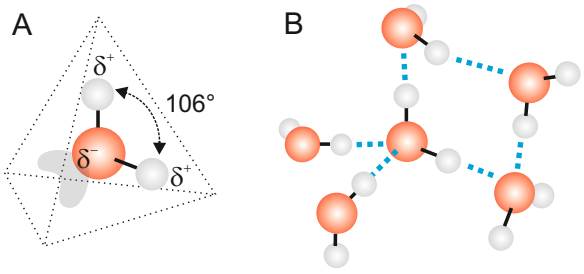

Figure 1.1. (A) Structure of a water molecule. (B) Hydrogen-bond network of water.

water forms hydrogen bonds (fig. 1.1B). A hydrogen atom can donate a single hydrogen bond, and an oxygen atom can accept two (one at each lone pair), such that each water molecule can participate in up to four hydrogen bonds. Each bond is highly directional, with the OH··O hydrogen bond being parallel to the O-H bond, leading to the formation of an interconnected tetrahedral network of water molecules. This hydrogen-bond network explains the extraordinary properties of water mentioned earlier: the strong attraction between the molecules raises the surface tension and the melting and boiling points, and the large amount of energy that can be stored in the hydrogen-bond network leads to a larger heat capacity.

In ice, each water molecule forms exactly four hydrogen bonds. In liquid water, however, the hydrogen-bond network is more disordered, with each water molecule forming on average 3.6 hydrogen bonds[4]. These hydrogen bonds are by no means static: water molecules move around on a picosecond (10^{-12} s) timescale, and hydrogen bonds are continuously being broken and reformed[5–10]. This process involves rapid switching of hydrogen-bond partners (<200 fs) and re-arrangement of the larger hydrogen-bond network[5,11–13]. As a result of these rapid motions, water can quickly adjust to changes in environment, which makes it an excellent solvent for reactions[14].

In fact, water is an excellent solvent in general. Water interacts most favorably with compounds that it can form hydrogen bonds to, that is, molecules with hydrogen atoms covalently bound to a strongly electronegative atom (O, N or F). In addition, water forms hydrogen bonds to charged species like ions and - to a lesser extent - to polar molecules in general, as a result of its large dipole moment of 1.85 D[15]. Compounds that interact favorably with water are called hydrophilic, and are easily solvated by water. In contrast, compounds that water can hardly interact with, like apolar molecules, are called hydrophobic, and tend to cluster in an aqueous environment. The unfavorable hydrophobic interaction arises from the fact that in order to accommodate apolar molecules, water needs to make room for them[16]. For small hydrophobic solutes (<1 nm) the hydrogen-bond network can fold around the solute, and the energy penalty is mainly entropic. To accommodate larger hydrophobes, hydrogen bonds need to be broken and the energy penalty is larger and mainly enthalpic, with a cost of ∼2.5 kJ/mol per hydrogen bond[17,18]. As a result, hydrophobes like to stick together: water and oil do not mix.

1.2 WATER AND BIOMOLECULES

Life as we know it takes place in liquid water; the human body, for example, contains on average 65% of water. In fact, water seems so essential for life that astrophysicists get excited whenever liquid water is found somewhere in the universe. The fact is that water is not merely a passive solvent, but plays an active role in many biological processes[19,20]. Understanding the subtle interplay between water and biomolecules is therefore crucial for understanding the mechanics and chemistry of life. A few cases, which will feature later in this

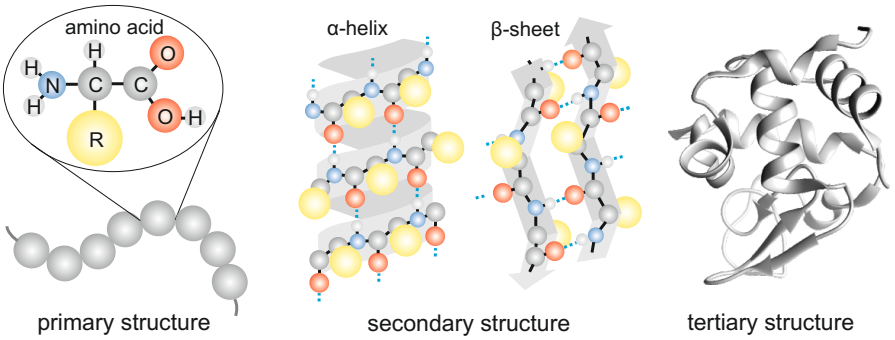

FIGURE 1.2. Structural levels of a protein. Each amino acid is defined by its side chain R. The sequence of amino acids (primary structure) determines the formation of specific hydrogen-bonded structures like α-helices and β-sheets (secondary structure), which in turn can fold into a compact shape (tertiary structure).

thesis, are highlighted here.

LIPID STRUCTURE AND ASSEMBLY

The interaction between water and phospholipids drives the self-assembly of phospholipid bilayers that make up the membrane of cells[21]. The phospholipids arrange themselves such that their hydrophilic head-groups are solvated by water, while their hydrophobic tails are clustered together, shielded away from the water. This results in an effective barrier between the inside and the outside of the cell, and enables cells to regulate in- and outward transport of materials. Another major class of lipids is the triglycerides, which are consumed as foods and constitute the main part of body fat, where they are responsible for energy supply and storage[22]. In analogy to phospholipids, it is expected that the interaction with water influences triglyceride structure, however this interaction has hardly been studied yet.

PROTEIN FOLDING AND FUNCTION

Water is crucial for the folding and function of proteins[23,24]. Proteins are components of every living cell that perform many specific tasks, ranging from catalysis to material transport and the formation of a structural framework. The specific task of a protein is determined by its three-dimensional structure: Each protein consists of a linear chain of amino acids, the primary structure, which can form particular hydrogen-bonded segments in its secondary structure, and these segments in turn can pack in a specific way to form the tertiary structure of a protein (fig. 1.2). Nature has constructed an enormous amount of proteins, each with their specific function, from just 20 types of amino acids. The molecular mechanism by which proteins adopt their functional fold remains one of the fundamental questions in biochemistry[25].

One of the main drivers of the protein folding process is the unfavorable interaction between water and hydrophobic groups of the protein[23]. Folding allows

the burial of hydrophobic groups inside the core of the protein, shielded away from the water, which is energetically favorable. In many cases, water plays a role via more specific interactions as well, for example by bridging different protein residues[24,26]. These internal water molecules can contribute to the folding speed, stability and structure of the protein.
Besides influencing the protein structure, water can also contribute to the function of a protein directly. Many proteins need a minimal amount of hydration water in order to retain their normal catalytic activity[27,28]. It has been suggested that this is due to the dynamics of hydration water driving protein motion[29–31]. In addition, water can interact more specifically with proteins, for example to assist in molecular recognition and binding, allostery, and proton conduction[32–34].

OSMOLYTES
Osmolytes are small organic molecules that enable cells to maintain a healthy amount of water[35]. These molecules can strongly affect the three-dimensional structure of proteins as well; some osmolytes unfold proteins, whereas others stabilize the folded protein structure[36,37]. Hence, many organisms use osmolytes to counteract chemical factors that might promote protein unfolding. Marine animals, for example, use trimethylamine N-oxide (TMAO) to deal with extreme deep-ocean pressures, and seeds of desert plants can survive in dry conditions due to the presence of certain sugars.
Osmolytes affect the structure of proteins by shifting the equilibrium between the folded and unfolded state. Protecting osmolytes like TMAO drive the equilibrium towards the native folded state, whereas denaturing osmolytes like urea and guanidinium favor the unfolded state. Even though this process is well understood from a thermodynamical viewpoint[37,38], a consistent picture of the molecular mechanism by which some osmolytes interact with proteins is still lacking. Proposed mechanisms include direct interactions between osmolyte and protein[39–41], as well as indirect effects, where osmolytes primarily modify the properties of the water solvent[42–45]. In both mechanisms, the effect of osmolytes on the structure of proteins cannot be understood without including the role of water.

1.3 SPECTROSCOPY OF WATER

To study the dynamics of water on the molecular scale, one can use spectroscopy: the interaction of water with light. While water is mostly transparent in the visible region, it strongly absorbs UV light due to electronic resonances, and mid-infrared light due to molecular vibrations. At room temperature, a water molecule vibrates; the hydrogen and oxygen atoms wiggle around like balls connected by springs. The vibrational resonances of water are of particular interest as they can supply information on the hydrogen-bond structure and dynamics of water. The frequencies of the main vibrational modes, the bend vibration and the OH stretch vibration, are very sensitive to hydrogen-bond strength[8,46–48] (fig. 1.3). Formation of an OH··O hydrogen bond weakens the

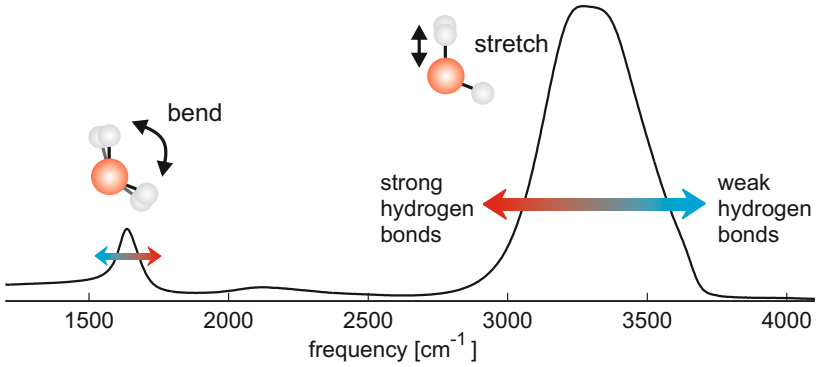

FIGURE 1.3. Infrared absorption spectrum of liquid water at 25°C in the infrared spectral region, indicating the main vibrational modes and their correlation with hydrogen-bond strength.

covalent OH bond, causing the OH stretch vibration to shift to lower frequencies. This is why the OH stretch frequency of liquid water, centered around 3404 cm^{-1}, is so much lower than the OH stretch frequency of water in the gas phase at 3657 cm^{-1} (symmetric stretch[49]); in the former case water molecules are hydrogen-bonded while in the latter case they are not.

An additional difference between the spectrum of liquid water and that of water in the gas phase, is the broad spectral width. In the liquid phase, water molecules exist in many different configurations with different hydrogen-bond strengths, and as a result, the absorption spectrum of the OH stretch vibration is the sum of many different vibrational frequencies: it is inhomogeneously broadened[9,48,50,51]. Because of the rapid movement of water molecules, these different hydrogen-bonded water molecules quickly interconvert, and the water absorption spectrum presents a time-averaged picture of the hydrogen-bond network of water. To investigate the time-evolution of the hydrogen-bond network, one has to use nonlinear spectroscopy. In this case the water molecules interact with multiple light pulses, making it possible to excite particular vibrations with one pulse and follow their behavior over time with another.

1.4 OUTLOOK

This thesis focuses on the interactions between water and different biomolecules, studied by vibrational spectroscopy. The next three chapters take a closer look at vibrational spectroscopy, with chapter 2 highlighting the theory, chapter 3 focusing on the experimental implementation, and chapter 4 describing the analysis of spectra. After that, we get to the core of the thesis. Chapter 5 describes the effect of sugars on the reorientation dynamics of water. Chapter 6 focuses on water reorientation dynamics in solutions of globular proteins. In

these solutions, a fraction of the water is strongly slowed down by the interaction with the protein surface, which we use to follow the exposure of the protein to water upon urea and temperature-induced unfolding. In chapter 7 we describe the interaction between water and a special type of protein: the antifreeze glycoprotein, which enables the survival of arctic fish by preventing the growth of ice crystals. Finally, in chapter 8 and 9, water is no longer the solvent, but a solute in a matrix of triglyceride oil, which we find to lead to specific water hydrogen-bond configurations and dynamics.

2 Vibrational spectroscopy

2.1 Vibrations and the harmonic oscillator

The simplest vibration is the harmonic oscillator. Imagine a mass suspended by a spring (fig. 2.1A). If it is displaced slightly from its equilibrium position along the spring direction, it experiences a restoring force $F = -kx$. Newton's balance of forces states

$$F(t) = m\frac{d^2x}{dt^2} = -kx \tag{2.1}$$

which has the solution

$$x(t) = x_1 \cos(\sqrt{k/m}t) \tag{2.2}$$

This means that the mass oscillates harmonically around its equilibrium position with a frequency $\omega_0 = \sqrt{k/m}$.

A polyatomic molecule can be represented by a series of masses connected by springs (fig. 2.1B), where the masses are the nuclei and the springs the forces between them (these internuclear forces depend on the electronic structure of the molecule). Since in this case the movement of a single mass will cause motion of the others, Newton's balance of forces in terms of mass displacement is more complex. Despite this complexity, the vibrations of a polyatomic molecule can be described as a sum of independent harmonic oscillators, provided all restoring forces are harmonic[52,53]. These harmonic oscillations are called normal modes. A normal mode involves the synchronous movement of several nuclei; the vibrations are delocalized. In this case, the mass is replaced by the effective mass, which is usually a complicated function of the individual nuclear masses. The number of normal modes of a molecule is always equal to the number of vibrational degrees of freedom, which is 3N-6 for a nonlinear molecule with N nuclei and 3N-5 for linear molecules.

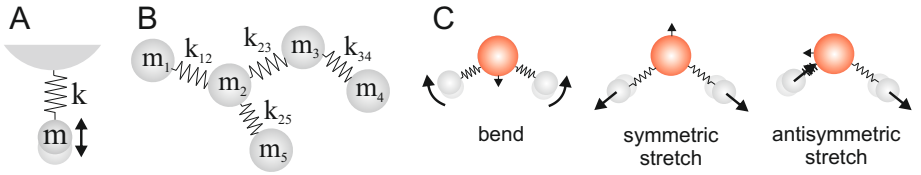

Figure 2.1. (A) Example of a harmonic oscillator: a mass suspended by a spring. (B) Representation of a polyatomic molecule as a series of masses - the nuclei - connected by springs. The spring constants depend on the electronic structure of the molecule. (C) The normal modes of a water molecule.

The normal modes of a water molecule are shown in fig. 2.1C; these are the bend, the symmetric stretch and the antisymmetric stretch vibration. The normal modes of water are not pure normal modes in the sense that the oscillations are independent. Instead the different vibrations are coupled. This originates from the restoring forces for nuclear displacement, which are not linear in x; the vibrations are anharmonic. This is, in fact, the case for all molecules, but as for water, a set of *coupled* harmonic oscillations can often still accurately describe the vibrational motion of the molecule.

2.2 The quantum harmonic oscillator

To describe oscillations on the molecular level, it is necessary to treat the molecule quantum mechanically. Since we saw in the previous section that vibrations can be described by a set of coupled harmonic oscillations, we again consider the simple case of a harmonic oscillator. The Hamiltonian of a quantum harmonic oscillator is given by

$$\hat{H}_0 = \frac{\hbar^2}{2m}\frac{d^2}{dx^2} + \frac{1}{2}k\hat{x}^2 \tag{2.3}$$

where the first term is the kinetic energy and the second term the potential energy corresponding to a linear force $\vec{F} = -k\vec{\hat{x}}$. The energy levels of the oscillator can be found by solving the time-independent Schrödinger equation

$$\hat{H}_0\psi = E\psi \tag{2.4}$$

and are

$$E_v = \left(v + \frac{1}{2}\right)\hbar\omega_0 \qquad\qquad v = 0, 1, 2... \tag{2.5}$$

with v the vibrational quantum number and $\omega_0 = \sqrt{k/m}$ the vibrational frequency. The energy is quantized, and we can speak of zeroth, first, second and higher vibrational states, which are evenly spaced by an energy separation of $\hbar\omega_0$ (fig. 2.2A). A transition from one vibrational state to another can be induced by interacting with light, which can be described by solving the time-dependent Schrödinger equation

$$\hat{H}\Psi = i\hbar\frac{\partial\Psi}{\partial t} \tag{2.6}$$

in the presence of light. We can consider the light as a time-dependent perturbation of the original Hamiltonian $\hat{H}_0$, so that the Hamiltonian is defined as

$$\hat{H}(t) = \hat{H}_0 + \hat{V}(t) \tag{2.7}$$

Since light is an electromagnetic wave, it interacts with the charges of the system, and $\hat{V}(t)$ is a function of the electric field of the light, $\vec{E}(t)$, and the electric

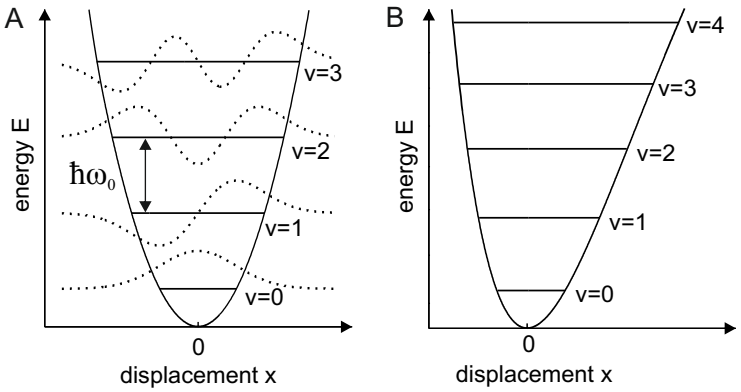

FIGURE 2.2. (A) The energy levels of a harmonic oscillator, which are evenly spaced with a separation of $\hbar\omega_0$, and the corresponding eigenstates ψ. (B) The energy levels of a Morse oscillator, which decrease in separation with increasing quantum number.

dipole moment of the system $\vec{\hat{\mu}}$. (For the moment we ignore higher order electric moments, and magnetic interactions as well, because these are much weaker than the interaction with the electric dipole moment.) The electric dipole moment depends on the positions $\vec{\hat{x}}$ of all charges q in the system:

$$\vec{\hat{\mu}} = \sum_n q_n \vec{\hat{x}}_n \tag{2.8}$$

We can consider the light as a simple oscillating electric field if we assume that the wavelength of the light is much larger than the size of the system, such that we can ignore the spatial variation of the field. This is quite reasonable for infrared light ($\lambda \sim 10^{-6}$m) interacting with molecular vibrations (bond lengths $\sim 10^{-10}$m). Then the perturbation is defined as

$$\hat{V}(t) = -\vec{\hat{\mu}} \cdot \vec{E}(t) = -\vec{\hat{\mu}} \cdot \vec{E}_0 \cos(\omega t) \tag{2.9}$$

The time-dependent Schrödinger equation (eq. 2.6) can be solved by separation of variables:

$$\Psi(\hat{x}, t) = \psi(\hat{x}) e^{-iEt/\hbar} \tag{2.10}$$

where ψ is the solution to the time-*in*dependent Schrödinger equation (eq. 2.4). The general solution to the time-dependent Schrödinger equation is thus given by

$$\Psi(\hat{x}, t) = \sum_n c_v(t) \psi_v(\hat{x}) e^{-iE_v t/\hbar} \tag{2.11}$$

which means that the system can be described at all times as a superposition of the different vibrational states ψ_v with a phase term and a time-dependent amplitude $c_v(t)$. We can calculate the time-dependent amplitudes by solving the Schrödinger equation with the perturbed Hamiltonian. From the calculation

it follows that the transition rate from a negligibly perturbed state ψ_a to state ψ_b is given to first order approximation by [54]

$$R_{a\to b} \cong \frac{d}{dt}|c_b|^2 = \frac{\pi}{2\hbar^2}|\langle\psi_b|\,\vec{\hat{\mu}}\cdot\vec{E}_0\,|\psi_a\rangle\,|^2\int\delta(\omega\pm\omega_{ab})d\omega \tag{2.12}$$

This equation is known as Fermi's golden rule. We can rewrite it as

$$R_{a\to b} \cong \frac{\pi E_0^2}{2\hbar^2}\cos^2\theta|\mu_{ab}|^2\int\delta(\omega\pm\omega_{ab})d\omega \tag{2.13}$$

where θ is the angle between the polarization direction of the light $\vec{E}_0$ and the electric dipole moment $\vec{\hat{\mu}}$, and $\mu_{ab} = \langle\psi_b|\,\hat{\mu}\,|\psi_a\rangle$ is the so-called transition dipole moment. Since we are interested in vibrations around an equilibrium position $\hat{x}_0$, we write the electric dipole moment as a Taylor expansion around $\hat{x}_0$:

$$\hat{\mu} = \hat{\mu}_0 + \frac{d\hat{\mu}}{dx}(\hat{x}-\hat{x}_0) + ... + \frac{1}{n!}\frac{d^n\hat{\mu}}{dx^n}(\hat{x}-\hat{x}_0)^n \tag{2.14}$$

Combining this expression up to first order with Fermi's golden rule finally gives

$$R_{a\to b} \cong \frac{\pi E_0^2}{2\hbar^2}\cos^2\theta\left(\frac{d\mu}{dx}\right)^2|\langle\psi_b|\,\hat{x}\,|\psi_a\rangle\,|^2\int\delta(\omega\pm\omega_{ab})d\omega \tag{2.15}$$

This equation has a few important implications:

- $R_{a\to b} \propto \int\delta(\omega\pm\omega_{ab})d\omega$: The frequency of the light, ω, has to match the frequency of the transition, $\omega_{ab} = (E_b - E_a)/\hbar$, for the transition to take place (this is basically energy conservation). For vibrational transitions, the required light is in the infrared range.

- $R_{a\to b} \propto |\frac{d\mu}{dx}|^2$: Light can only interact with vibrations that cause a change in dipole moment; these vibrations are said to be infrared active. Homonuclear diatomic molecules, for instance, are not infrared active, because a change in relative position of the nuclei does not change the net dipole moment.

- $R_{a\to b} \propto \cos^2\theta$: Light interacts most strongly with the system when it is polarized along the direction of the dipole moment. This forms the basis of polarization-resolved pump-probe spectroscopy (see section 2.6).

- $R_{a\to b} \propto |\langle\psi_b|\,\hat{x}\,|\psi_a\rangle|^2$: For a harmonic oscillator, it can be shown that $\langle\psi_b|\,\hat{x}\,|\psi_a\rangle$ is always zero unless $b = a \pm 1$, which means that transitions are only allowed between consecutive states [54]. For anharmonic oscillators this rule is lifted, though generally the transition rate is much lower for transitions involving two or more quanta.

- $R_{a\to b} = R_{b\to a}$: A transition from state ψ_a to ψ_b is just as likely as the reverse process. An upward transition corresponds to absorption: the matter absorbs energy $\hbar\omega_{ab}$ from the light. A downward transition corresponds to stimulated emission: the light gains energy $\hbar\omega_{ab}$.[a] (See fig. 2.3.)

[a] In addition to these light-driven processes the system can "spontaneously" decay to a

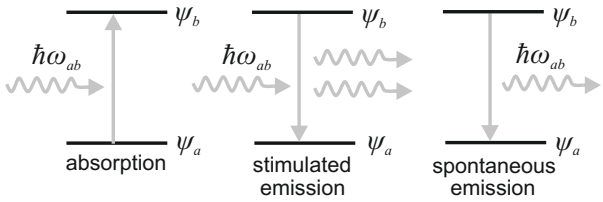

FIGURE 2.3. Illustration of absorption, stimulated emission and spontaneous emission for a two-level system. Photons are indicated as wiggly arrows and have energy $\hbar\omega_{ab}$, corresponding to the energy difference between the two states. The rate of absorption equals the rate of stimulated emission, while the rate of spontaneous emission is directly related to these by a factor of $\frac{\hbar\omega_{ab}^3}{\pi^2 c^3}$ as a consequence of energy conservation [55].

ANHARMONICITY Most molecular vibrations have some degree of anharmonicity. At high vibrational excitations, the harmonic approximation always breaks down because the molecular bond can dissociate. In this case the restoring force is no longer linear with the displacement $\hat{x}$, and the potential energy is no longer quadratic (recall that $V_0 = \frac{1}{2}k\hat{x}^2$ for the harmonic oscillator), but converges to a constant value for large distances $\hat{x}$. A potential accounting for this behavior is the Morse potential [55]

$$V_0 = D(1 - e^{-a\hat{x}})^2 \tag{2.16}$$

where D and a are the depth and curvature of the potential, respectively. The energy levels of the Morse oscillator can be found by solving the time-dependent Schrödinger equation, and are given by

$$E_v = \left(v + \frac{1}{2}\right)\hbar\omega_0 - \left(v + \frac{1}{2}\right)^2 \frac{\hbar^2\omega_0^2}{4D} \tag{2.17}$$

with $\omega_0 = a\sqrt{2D/m}$. The energy levels are spaced closer together with increasing vibrational quantum number v (see fig. 2.2B). This is generally the case for anharmonic vibrations. Aside from the Morse potential, many other potentials have been put forward to describe the energy landscape of molecular vibrations. Lippincott and Schroeder, for instance, developed an emperical potential for water and other hydrogen-bonding materials that explicitly takes into account the anharmonicity arising from hydrogen-bond formation [56].

Besides these modifications of the potential, which are referred to as mechanical anharmonicity, vibrational transitions can be modified by a nonlinear dependence of the electric dipole moment on the position $\hat{x}$: this is referred to as electrical anharmonicity. In this case quadratic and higher order terms in eq. 2.14 significantly contribute to the transition rate, enabling Δv>1 transitions.

---

lower energy state by spontaneous emission. This process happens even in the absence of external light, because the electromagnetic field is never truly zero due to the zero-point energy of vacuum.

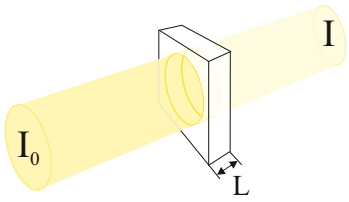

FIGURE 2.4. In linear spectroscopy, one measures the attenuation of a beam of light as it travels through a piece of material.

2.3 LINEAR SPECTROSCOPY

In linear spectroscopy, one generally measures the attenuation of a beam of light as it travels through a piece of material (fig. 2.4). Here the light has a moderate intensity, such that it excites only a very small fraction of the molecules. In this case the macroscopic response of the material is linear with the electric field of the light. This section describes how the linear spectrum is determined by the microscopic light-matter interaction described earlier.

2.3.1 ABSORPTION CROSS SECTION

At room temperature and moderate light intensities, most molecules are in the ground vibrational state, so we only observe the process of absorption. Suppose we start out with a beam of light with intensity

$$I_0 = \frac{c\epsilon_0}{2} E_0^2 \tag{2.18}$$

which is the intensity (radiated power per unit area) for a beam with an electric field of $\vec{E}_0 \cos(\omega t)$, with c the speed of light, and ϵ_0 the permittivity of vacuum. Assuming ω matches the frequency of the first vibrational transition ω_{01}, a single molecule absorbs photons with energy $\hbar\omega_{01}$ from the beam at a rate of

$$R_{0\to 1} \cong \frac{\pi I}{3c\epsilon_0\hbar^2} |\mu_{01}|^2 \tag{2.19}$$

This equation follows from eq. 2.13, under the assumption that the medium is isotropic, such that $\cos^2\theta = \frac{1}{3}$. Now suppose we have a material with C molecules per volume, then the intensity reduction after traveling through a tiny slab dL of this material is

$$dI = -\hbar\omega_{01} \frac{\pi I}{3c\epsilon_0\hbar^2} |\mu_{01}|^2 \cdot C \cdot dL \tag{2.20}$$

$$= -\sigma_{01} \cdot I \cdot C \cdot dL \qquad \sigma_{01} = \frac{\pi\omega_{01}}{3c\epsilon_0\hbar} |\mu_{01}|^2 \tag{2.21}$$

The quantity σ_{01} is called the absorption cross section; it can be interpreted as the optical area of the molecule (note that this is not the same as the actual

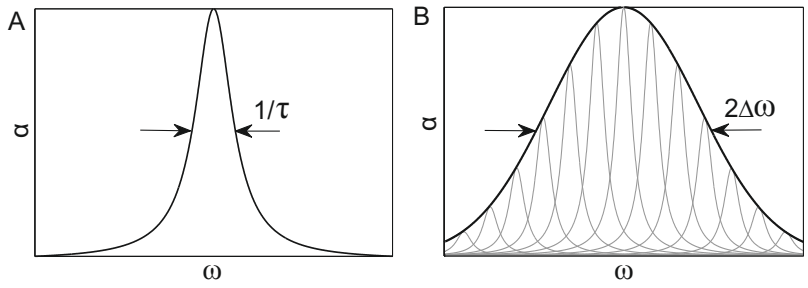

FIGURE 2.5. (A) Lorentzian or homogeneous lineshape, (B) Gaussian or inhomogeneous lineshape with underlying homogeneous lines.

area). Solving the differential equation 2.21 leads to the following expression

$$\frac{I}{I_0} = e^{-\sigma_{01} \cdot C \cdot L} \tag{2.22}$$

This equation is known as the Lambert-Beer law. It relates the macroscopic transmission I/I_0, which can be measured experimentally, to the molecular property σ_{01}. In linear spectroscopy, one usually quantifies the macroscopic absorbance, defined as

$$\alpha = \ln\left(\frac{I}{I_0}\right) = \sigma_{01} \cdot C \cdot L \tag{2.23}$$

This is a convenient measure because it is linear with all the relevant parameters.

2.3.2 ABSORPTION LINESHAPE

So far we described vibrational transitions with a single frequency, which implies that the absorption spectrum of a single resonance is infinitely narrow. However, this is not the case in reality. The absorption lineshape cannot be infinitely narrow due to the energy-time uncertainty principle:

$$\Delta E \Delta t \gtrapprox \hbar \tag{2.24}$$

which means that the energy of a state cannot be determined exactly when the state exists for a finite time. The lifetime of a state is limited by the rate of spontaneous emission. It can be deduced by Fourier transformation[57] that the spectral lineshape of a state with lifetime τ has the following form:

$$\alpha(\omega) \propto \frac{\Delta\omega}{2\pi} \frac{1}{(\omega - \omega_{01})^2 + (\Delta\omega/2)^2} \tag{2.25}$$

with $\Delta\omega = 1/\tau$. This spectral lineshape is called a Lorentzian lineshape and is shown in fig. 2.5A.

Many vibrational lines are actually much broader than the Lorentzian linewidth dictated by the vibrational lifetime. The OD stretch vibration in isotopically diluted water, for example, has a lifetime of 1.7 picoseconds, which corresponds to a linewidth of $\sim$3 cm^{-1}, but the actual spectrum is more than fifty times broader. Line-broadening processes that affect all molecules equally are called homogeneous. In the case of water, the broadening is mostly due to the pushing and pulling of the water molecules at each other: local differences in hydrogen bond strength lead to different potential energy surfaces for each OD stretch vibration, and hence to different vibrational frequencies. Broadening of this type, which originates from differences in local environment, is called inhomogeneous. In most cases the center frequency of the individual Lorentzian lineshapes is statistically distributed and the overall lineshape is Gaussian (fig. 2.5B).

Due to the dynamical nature of the hydrogen-bond network of water, the vibrational frequency of a water molecule is modulated continuously, and the spectral lineshape reflects the time-averaged frequency distribution. In general, if the frequency modulations are very small or very fast ($\Delta\omega \cdot \tau_c \ll 1$, see section 2.5.1), the average observed linewidth becomes narrower than the actual frequency distribution. This phenomenon is called motional narrowing, and is responsible for a slight narrowing of the lineshape of the water stretch vibration[58]. Additional mechanisms contribute to the lineshape of the water stretch vibration as well, such as the fact that the transition dipole moment increases strongly with increasing hydrogen-bond strength (non-Condon effect)[59]. Since the frequency of the water stretch vibration depends on the hydrogen-bond strength, with strongly hydrogen-bonded water molecules absorbing at lower frequencies, this effect leads to a relative enhancement of the absorption at lower stretch frequencies.

2.4 PUMP-PROBE SPECTROSCOPY

In vibrational pump-probe spectroscopy, vibrations are excited with an intense light pulse, the pump. These vibrations are monitored by measuring the absorption of a second, weaker probe pulse (fig. 2.6). In contrast to linear spectroscopy, which gives a time-averaged picture, pump-probe spectroscopy is sensitive to vibrational dynamics: the pump pulse perturbs the system from equilibrium,

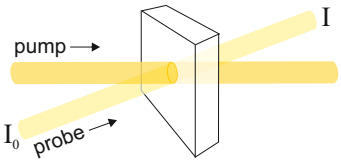

FIGURE 2.6. In pump-probe spectroscopy, an intense pump pulse excites vibrations in the sample, which are subsequently monitored by measuring the absorption of a second weaker probe pulse.

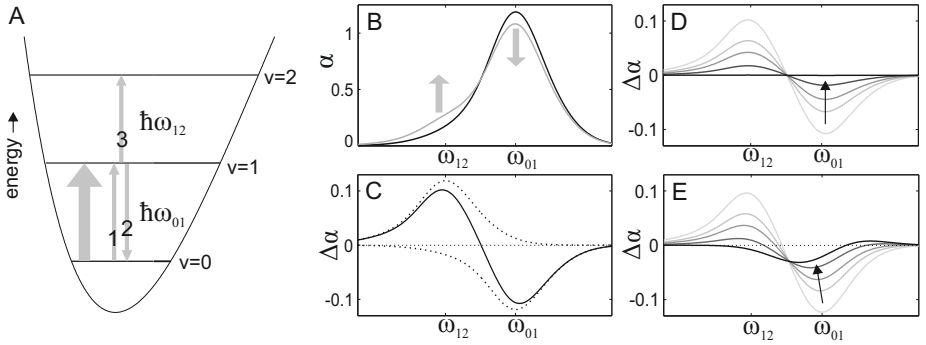

FIGURE 2.7. Illustration of pump-probe spectroscopy, with spectra that are chosen to resemble those of the OD stretch vibration of HDO molecules. (A) Energy level description: the pump (big arrow) excites vibrations from the ground state to the first excited state, which are then monitored by the probe (small arrows). (B) Probe absorption spectrum: excitation by the pump lowers the absorption around ω_{01} and increases the absorption around ω_{12}. (C) Probe differential absorption spectrum, with the positive σ_{12} and negative σ_{01} contributions shown in dotted lines. (D) Probe differential absorption spectrum at different pump-probe delay times. (E) Probe differential absorption spectrum at different pump-probe delay times, with a contribution from sample heating.

and the relaxation of the excited vibrations back to the ground state is measured with the probe pulse. As we will see later on, pump-probe spectroscopy can supply information on molecular fluctuations, coupling and reorientation dynamics.

Pump-probe spectroscopy is a form of nonlinear spectroscopy. This means that the system is perturbed from equilibrium, and as a consequence its response is no longer linear with the total electric field (pump+probe) of the light. A full description of the pump-probe signal therefore requires nonlinear response theory[60,61]. Here we limit ourselves to a mathematically simpler description that nonetheless captures the main observed features and refer the interested reader to the books by Hamm and Zanni[60] and Mukamel[61].

The absorbance of a piece of material is given by

$$\alpha_0(\omega) = \sigma_{01}(\omega) N_0 \tag{2.26}$$

where N_0 is the amount of molecules per area ($N_0 = CL$, see eq. 2.23). In case an intense pump pulse excites vibrations from the ground state to the first vibrational state, the absorbance changes due to three processes (fig. 2.7):

1. Ground state depletion: since there are less molecules in the ground state, less light is absorbed at the fundamental frequency ω_{01}.
2. Stimulated emission from the first excited state: light is emitted at the fundamental frequency ω_{01}.
3. Excited state absorption: molecules in the first excited state can be further excited to the second vibrational state, absorbing light at frequency ω_{12}.

The resulting absorbance is given by

$$\alpha(\omega,t) = \sigma_{01}(\omega)\Big(N_0 - 2N_1(t)\Big) + \sigma_{12}(\omega)N_1(t) \tag{2.27}$$

where $N_1(t)$ is the amount of excited molecules per area. The processes of ground state absorption and stimulated emission lower the absorbance equally, since the rates of absorption and stimulated emission are the same (eq. 2.15), hence the factor 2 in the above equation. By comparing the probe spectrum with and without pump excitation, we can calculate the differential absorbance

$$\begin{aligned}\Delta\alpha(\omega,t) &= \alpha(\omega,t) - \alpha_0(\omega,t) &(2.28)\\ &= -2\sigma_{01}(\omega)N_1(t) + \sigma_{12}(\omega)N_1(t) &(2.29)\\ &= \big(-2\sigma_{01}(\omega) + \sigma_{12}(\omega)\big)N_1(t) &(2.30)\end{aligned}$$

For a harmonic oscillator, the frequencies of the first and second vibrational transition overlap, and $\sigma_{12} = 2\sigma_{01}$. As a consequence, the pump-probe signal of a harmonic oscillator is zero. Luckily for spectroscopists, molecular vibrations are anharmonic. Usually, ω_{12} is lower than ω_{01}, and the differential absorbance is thus nonzero (fig. 2.7C).

Note that the differential absorbance is a function of the time delay between pump and probe pulses, since the excited vibrations relax back to the ground state (fig. 2.7 D). For this reason the differential absorbance is often referred to as the transient absorption spectrum. In the simplest case, the vibrational relaxation can be described by

$$N_1(t) = N_1(0)e^{-t/T_1} \tag{2.31}$$

where T_1 is the lifetime of the vibration. In general, a vibration relaxes by transferring energy to its environment, exciting lower-energy vibrations of the same molecule or surrounding molecules in the process[62]. The lifetime of a vibration therefore strongly depends on the coupling to its immediate surroundings. The lifetime can provide structural information: In chapter 5, for example, we will show that the vibrational response of OD stretch vibrations of water can be distinguished from the OD stretch vibrations of sugars using their difference in spectrum and vibrational lifetime. Ultimately, the energy of excited vibrations is transferred into heat. This can create an additional contribution to the transient spectrum, because the cross section of a vibration usually depends on temperature. The contribution due to sample heating has the shape of a thermal difference spectrum (fig. 2.7E), i.e. the difference between the absorption spectrum at room temperature and the absorption spectrum at an elevated temperature.

2.5 FREQUENCY-RESOLVED PUMP-PROBE SPECTROSCOPY: 2DIR

In vibrational pump-probe spectroscopy, it is often useful to pump and probe at different frequencies, such that the vibrational response of a system can be

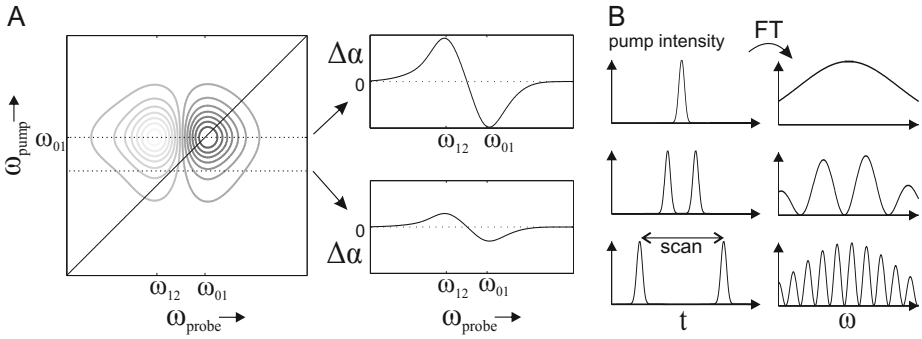

FIGURE 2.8. Two-dimensional infrared spectroscopy (2DIR). (A) Illustration of a 2DIR spectrum. Each horizontal slice of the 2D spectrum corresponds to the spectral response after excitation at a specific frequency ω_{pump}. (B) The 2D spectrum can be recorded by exciting with two broadband pump pulses with variable time delay between them. Scanning this time delay corresponds to a sinusoidal modulation of the pump pulse in the frequency domain. The 2D spectrum then can be obtained by Fourier transformation of the transient probe spectrum (recorded as usual) with respect to the scanned pump time delay.

probed after a subset of vibrations is excited. By scanning the frequency of a spectrally narrow pump pulse and recording transient spectra with a broadband probe pulse, we can construct a transient two-dimensional infrared (2DIR) spectrum, where each horizontal slice of the spectrum corresponds to the spectral response following excitation at a specific frequency (fig. 2.8A).

The 2DIR spectrum is often obtained by exciting the sample with two broadband pump pulses instead of a narrowband pump pulse. In this case different subsets of vibrations can be excited by varying the time delay between the two pump pulses, which creates a sinusoidally modulated pump spectrum with varying period (fig. 2.8B). The 2D spectrum can then be calculated by Fourier transformation: the transient probe spectrum determines the probe axis, and its modulation by the pump pulse pair after Fourier transformation yields the pump axis.

2.5.1 2D LINESHAPE

We already noted that the frequency of a vibrational mode is continuously modulated due to the mutual pushing and pulling of molecules (section 2.3.2). While the linear lineshape reflects the time-averaged frequency distribution, the 2DIR lineshape is sensitive to the frequency fluctuations. An inhomogeneous vibrational mode gives rise to a 2DIR spectrum that is elongated along the diagonal, as the excitation frequency corresponds to a particular subset of the vibrations that will show their maximum response at the same frequency. At later delays, however, the character and thus the resonance frequency of the excited subset changes (due to the molecular dynamics). The average resonance

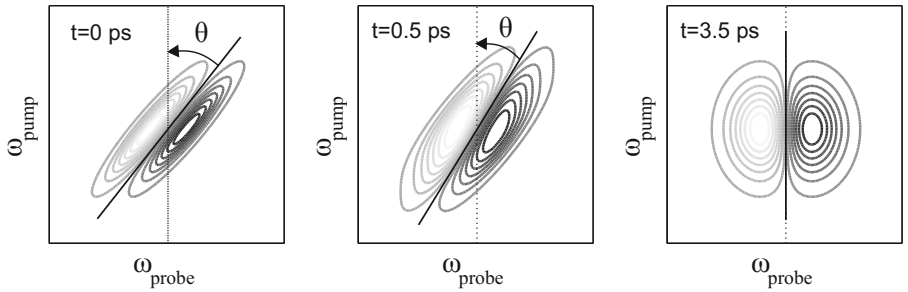

FIGURE 2.9. Illustration of a 2DIR spectrum of an inhomogeneous vibrational mode at different pump-probe delay times. The 2DIR spectrum is initially elongated along the diagonal, but acquires a more spherical shape with increasing delay time. The decay of the nodal line slope, $\sin\theta$, is a measure for the frequency-frequency correlation function.

frequency of each subset of excited vibrations tends more towards the overall average and the spectrum will acquire a more spherical shape. This phenomenon is spectral diffusion resulting from structural dynamics, and is illustrated in figure 2.9.

For a vibrational mode with overlapping peaks due to the $0 \rightarrow 1$ and $1 \rightarrow 2$ transitions, inhomogeneity results in a tilt of the nodal line between the two responses. The nodal line slope as a function of time is a measure for the spectral diffusion as expressed in the frequency-frequency correlation function (FFCF)[63]:

$$C_1(t) = \langle \delta\omega_{01}(\tau)\delta\omega_{01}(0)\rangle \tag{2.32}$$

where $\delta\omega_{01}$ is the instantaneous fluctuation away from the mean vibrational frequency ω_{01}, and $\langle ...\rangle$ denotes the ensemble average. The decay of the FFCF can often be described emperically by

$$C_1(t) = \Delta\omega^2 e^{-\tau/\tau_c} \tag{2.33}$$

where $\Delta\omega$ is the fluctuation amplitude and τ_c the characteristic timescale of the frequency fluctuations. The latter is a direct measure of how fast surrounding molecules move around the excited vibrational mode. Aside from the nodal line slope method, several other methods exist to obtain the frequency-frequency correlation function from the 2DIR spectrum[63–65].

2.5.2 CROSS PEAKS

Perhaps the most prominent feature of a 2DIR spectrum is the presence of cross peaks. Cross peaks appear off the diagonal (fig. 2.10A) and indicate that exciting a certain vibrational mode affects the vibration of another mode. Hence, cross peaks supply information on molecular coupling. The coupling in turn provides information on molecular structure, since the interaction between vibrations depends on their relative orientation and distance. We can distinguish between two types of vibrational coupling:

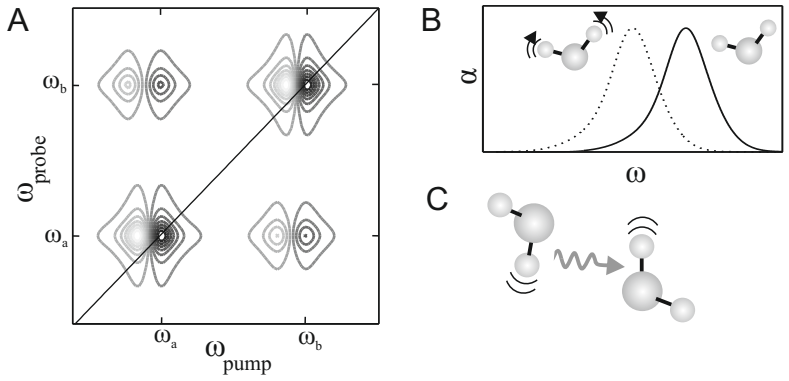

FIGURE 2.10. (A) Illustration of a 2DIR spectrum of two coupled vibrational modes with different center frequencies ω_a and ω_b. Cross peaks appear off the diagonal. (B) Illustration of anharmonic coupling for water: the spectrum of the OH stretch vibration is redshifted if the bending vibration is excited. (C) Illustration of energy transfer: the vibrational excitation transfers from one vibration to the other via the coupling of their transition dipole moments.

- Anharmonic coupling:
  Excitation of one vibrational mode alters the potential, and therefore the vibrational energy levels, of another vibrational mode (fig. 2.10B). This is the case when the two vibrations are part of the same molecule and affect each other through chemical bonds, i.e. mechanically, or when the two vibrations are coupled electrically by the interaction between their transition dipole moments. The effect of anharmonic coupling is present immediately after excitation of the vibration.

- Coupling by energy transfer:
  Coupling between the transition dipole moments of vibrational modes can also lead to transfer of the vibrational excitation of one vibrational mode to another (fig. 2.10C). Energy transfer shows up in the 2DIR spectrum as a rising cross peak, where the rise is defined by the rate of transfer. This process is usually referred to as vibrational resonant energy transfer, or Förster transfer, after Theodor Förster. The rate of Förster energy transfer is given by[66,67]

$$K_F \propto \frac{|\vec{\mu}_a|^2 |\vec{\mu}_b|^2 \kappa_{ab}^2}{|\vec{R}_{ab}|^6} \int \sigma_a(\omega)\sigma_b(\omega) d\omega \tag{2.34}$$

  where $\vec{\mu}_a$ and $\vec{\mu}_b$ are the transition dipole moments of the coupled vibrations, R_{ab} is their mutual distance, κ_{ab} is a geometrical factor, and σ is the absorption cross section. The rate of Förster transfer depends on the distance between the two coupled vibrations, the magnitude of their transition dipole moments, and their spectral overlap.

Aside from vibrational coupling, cross peaks can arise from structural dynamics, which is usually slower. This is for example the case when molecules can exist in two different hydrogen-bonded configurations that give rise to different vibrational frequencies. During the time between pump and probe pulses, the molecules can be converted from one configuration to the other, which results in cross peaks that rise with the average structural conversion time. This phenomenon is much like the spectral diffusion resulting from structural dynamics described earlier, except that the vibrational frequency distribution is bimodal in this case, instead of continuous.

2.6 Polarization-resolved pump-probe spectroscopy

We showed that light interacts most strongly with vibrations that have their transition dipole moment aligned with the polarization direction of the light (eq. 2.15):

$$R_{a\to b} \propto \cos^2\theta \tag{2.35}$$

where θ is the angle between the transition dipole moment of the vibration and the polarization direction of the light. This property can be exploited to measure molecular reorientation dynamics.

Suppose we start out with a collection of randomly oriented molecules (fig. 2.11A). A linearly polarized pump pulse creates the following normalized directional distribution of excited vibrations

$$p(\theta,\phi,t_0) = \frac{3}{4\pi}\cos^2\theta \tag{2.36}$$

If we probe the resulting absorption change with probe pulses that are polarized either parallel or perpendicular to the probe polarization, the parallel absorption change is initially higher, since more vibrations were excited in the parallel direction. With the angle definitions as shown in fig. 2.11B, the parallel and perpendicular transient absorption signals are given by:

$$\Delta\alpha_{\parallel} = 3\sigma_1 N_1 \int_0^{2\pi}\int_0^{\pi} p(\theta,\phi,t)\cos^2\theta\sin\theta d\theta d\phi \tag{2.37}$$

$$\Delta\alpha_{\perp} = 3\sigma_1 N_1 \int_0^{2\pi}\int_0^{\pi} p(\theta,\phi,t)\sin^2\theta\sin^2\phi\sin\theta d\theta d\phi \tag{2.38}$$

where σ_1 is the average isotropic cross section. Substituting $p(\theta,\phi,t_0)$ as defined by eq. 2.36, and integrating over all coordinates yields:

$$\Delta\alpha_{\parallel}(t_0) = \frac{9}{5}\sigma_1 N_1 \tag{2.39}$$

$$\Delta\alpha_{\perp}(t_0) = \frac{3}{5}\sigma_1 N_1 \tag{2.40}$$

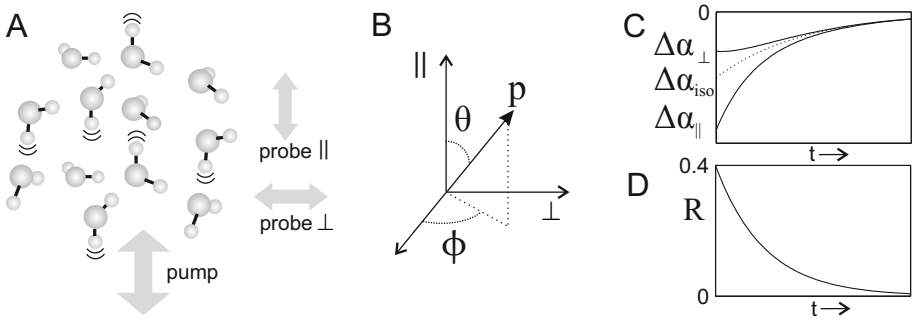

FIGURE 2.11. Polarization-resolved pump-probe spectroscopy. (A) A linearly polarized pump pulse creates an anisotropic distribution of excited vibrations, which is measured with probe pulses in parallel and perpendicular polarization configuration. (B) Angle definitions for the distribution of excited vibrations p, as mentioned in the text. (C) The transient absorption for parallel and perpendicular probe polarizations, and the isotropic signal. (D) The anisotropic signal.

It follows that the parallel signal is three times larger than the perpendicular signal. With increasing delay time between pump and probe pulses this difference will become smaller, because the excited molecules will reorient. This randomizes the directional distribution of excited vibrations until it becomes completely isotropic, at which stage the parallel and perpendicular signals are equal (fig. 2.11C). Another process that leads to directional randomization is vibrational Förster transfer, because transfer of a vibrational excitation from one vibration to another can lead to a change of the direction of the transition dipole moment of the excited vibration.

A consequence of the above described depolarization (due to molecular reorientation or Förster energy transfer) is that the transient absorption signal does not simply decay with the vibrational lifetime. It is therefore convenient to define the isotropic signal

$$\Delta\alpha_{iso} = \frac{1}{3}\left(\Delta\alpha_{\parallel} + 2\Delta\alpha_{\perp}\right) \tag{2.41}$$

which decays with the vibrational lifetime and is independent of orientational dynamics, provided the sample itself is isotropic.[b]

In addition to the isotropic signal, we can construct the anisotropic signal

$$R = \frac{\Delta\alpha_{\parallel} - \Delta\alpha_{\perp}}{\Delta\alpha_{\parallel} + 2\Delta\alpha_{\perp}} \tag{2.46}$$

which is the difference between the two absorption signals, normalized by the rate of vibrational relaxation (note the similarity between the denominator of

[b]The fact that the isotropic signal depends only on the vibrational lifetime can be shown by returning to the expressions of eq. 2.37 and 2.38, which combined with eq. 2.41 yield

$$\Delta\alpha_{iso} = \sigma_1 N_1 \int_0^{2\pi}\int_0^{\pi} p(\theta,\phi,t)\left(\cos^2\theta + 2\sin^2\theta\sin^2\phi\right)\sin\theta d\theta d\phi \tag{2.42}$$

above equation and the isotropic signal), which makes it independent of the vibrational lifetime. It can be shown that the anisotropy is directly proportional to the second order orientational correlation function of the direction of an excited vibration[68,69]:

$$R(t) = \frac{2}{5}\big\langle P_2(\cos\theta_r(t))\big\rangle \tag{2.47}$$

where $\theta_r(t)$ is the rotation of the transition dipole moment of the excited vibration as a function of time and $P_2 = \frac{1}{2}(3x^2-1)$ is the second order Legendre polynomial. Note that $R(0) = \frac{2}{5}$, which follows directly from the initial values of the parallel and perpendicular signals given in eq. 2.39 and 2.40, which in turn are a direct consequence of the $\cos^2\theta$ dependence of the excitation. Using eq. 2.47, which connects the macroscopic observable R with the molecular orientational dynamics, we can calculate the anisotropy decay for different events.

REORIENTATION In the simplest case, the molecules reorient diffusively in all directions. The distribution of excited vibrations is then described by:

$$\frac{\partial p_\theta(\theta,t)}{\partial t} = D_\theta \nabla^2 p_\theta(\theta,t) \tag{2.48}$$

with D_θ the orientational diffusion constant, ∇^2 the Laplacian operator and p_θ the distribution of excited vibrations for an isotropic sample (which is independent of the angle ϕ). The solution to the above diffusion equation is a sum of exponentially decaying Legendre polynomials P_l:

$$p_\theta(\theta,t) = \sum_{l\geq 0} c_l P_l(\cos\theta) e^{-D_\theta l(l+1)t} \tag{2.49}$$

where c_l are coefficients that are determined by the initial distribution $p_\theta(\theta,0)$. Since the anisotropy is related to the second order Legendre polynomial, it follows from above equation that the anisotropy decay due to orientational diffusion is given by

$$R(t) = \frac{2}{5} e^{-t/\tau_{reor}} \tag{2.50}$$

with $\tau_{reor} = {}^1\!/_{6D_\theta}$.

In some systems, molecules can only reorient diffusively within a limited cone angle θ_c. As a consequence, the anisotropy decays with τ_{reor} to a value of

$$R = \left({}^1\!/_2 \cos\theta_c(1+\cos\theta_c)\right)^2 \tag{2.51}$$

For an isotropic sample, the distribution p does not depend on ϕ, in which case

$$\Delta\alpha_{iso} = \sigma_1 N_1 \int_0^{2\pi}\int_0^{\pi} \frac{p_\theta(\theta,t)}{2\pi}\left(\cos^2\theta + 2\sin^2\theta\sin^2\phi\right)\sin\theta d\theta d\phi \tag{2.43}$$

$$= \sigma_1 N_1 \int_0^{\pi} p_\theta(\theta,t)\left(\cos^2\theta + \sin^2\theta\right)\sin\theta d\theta \tag{2.44}$$

$$= \sigma_1 N_1 \tag{2.45}$$

In the above calculation we have used the fact that p and p_θ are normalized distributions.

FÖRSTER TRANSFER Transfer of the vibrational energy over an angle θ_t leads to a decay of the anisotropy to a value of

$$R = \frac{1}{5}\left(3\cos^2\theta_t - 1\right) \tag{2.52}$$

If the energy transfer occurs between two vibrations with different frequencies, we can deduce the relative angle between their transition dipole moments from the anisotropy value of the corresponding cross peak in the 2DIR spectrum. In general, the anisotropy of cross peaks often differs from that of the diagonal peaks, in which case we can enhance the visibility of the cross peaks by constructing the polarization-difference signal:

$$\Delta\alpha_{diff} = \Delta\alpha_{\perp}\left(\frac{\Delta\alpha_{\parallel,max}}{\Delta\alpha_{\perp,max}}\right) - \Delta\alpha_{\parallel} \tag{2.53}$$

The above equation relies on the fact that $\Delta\alpha$ usually reaches its maximum along the diagonal. At the maximum $\Delta\alpha_{diff} = 0$, and thus the diagonal peaks are eliminated.

3 Experimental methods

The results described in this thesis are obtained with pump-probe spectroscopy experiments. The experimental setup for these experiments contains three main ingredients:

- Infrared light generation: We need intense and ultrashort light pulses in the infrared spectral region. Since there are no lasers that can directly produce these pulses, the frequency of an ultrafast near-infrared laser is converted to the infrared.
- Pump-probe configuration: The infrared pulses are used as pump and probe beams, which are overlapped in the sample. The time delay between the beams can be adjusted and every other pump pulse is blocked.
- Infrared light detection: The transmitted probe light with and without pump excitation is measured by a spectrometer in combination with an infrared array detector, for a range of different pump-probe time delays. This yields the transient absorption spectrum.

In the following we first describe the principles of optical frequency conversion processes that are used to generate infrared light pulses, followed by the details of the pump-probe setups and the studied samples.

3.1 Optical frequency conversion

Light frequency conversion processes rely on the nonlinear optical response of materials. The macroscopic optical response of a material is described by the induced polarization $\vec{P}$, which is the dipole moment per unit volume. $\vec{P}$ can be written as a power series of the applied electric field $\vec{E}$:

$$\vec{P}(t) = \epsilon_0[\chi^{(1)}\vec{E}(t) + \chi^{(2)}\vec{E}(t)^2 + \chi^{(3)}\vec{E}(t)^3 + ...\chi^{(n)}\vec{E}(t)^n] \tag{3.1}$$

where $\chi^{(n)}$ is known as the n^{th}-order optical susceptibility. In contrast to the nonlinear response mentioned in the previous chapter, we have assumed here that we are far away from any resonance. This means that no light is absorbed and that the polarization response is instantaneous, i.e. following the momentary sources. Most materials that are illuminated by everyday (weak) light are fully described by the first term of eq. 3.1, the linear response. Typically, only lasers produce high enough electric fields to induce a higher order polarization response. To illustrate how a nonlinear optical response leads to frequency conversion, we consider a planar electric field moving in direction $\vec{x}$ with two distinct frequency components ω_1 and ω_2:

$$\vec{E}(\vec{x},t) = \vec{E}_1 e^{i(\vec{k}_1\vec{x}-\omega_1 t)} + \vec{E}_2 e^{i(\vec{k}_2\vec{x}-\omega_2 t)} + c.c. \tag{3.2}$$

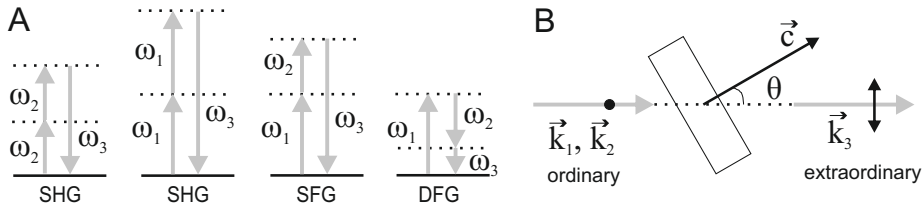

FIGURE 3.1. (A) Energy level description of second-order frequency conversion processes induced by light fields at ω_1 and ω_2: second harmonic generation (SHG), sum-frequency generation (SFG) and difference-frequency generation (DFG). Dashed lines indicate virtual states. (B) Geometry of phase-matching for sum-frequency generation in a negative ($n_e < n_o$) uniaxial crystal (type I). The dot and double-sided arrow indicate the polarization directions of the fields.

The second-order polarization response is then given by[70]

$$\vec{P}^{(2)}(\vec{x},t) = \epsilon_0 \chi^{(2)} \vec{E}(\vec{x},t)^2 \tag{3.3}$$

$$\begin{aligned} \vec{E}(\vec{x},t)^2 =& \vec{E}_1^2 e^{i(2\vec{k}_1\vec{x}-2\omega_1 t)} + c.c. && (SHG) \\ &+ \vec{E}_2^2 e^{i(2\vec{k}_2\vec{x}-2\omega_2 t)} + c.c. && (SHG) \\ &+ 2\vec{E}_1 \cdot \vec{E}_2 e^{i((\vec{k}_1+\vec{k}_2)\vec{x}-(\omega_1+\omega_2)t)} + c.c. && (SFG) \\ &+ 2\vec{E}_1 \cdot \vec{E}_2^* e^{i((\vec{k}_1-\vec{k}_2)\vec{x}-(\omega_1-\omega_2)t)} + c.c. && (DFG) \\ &+ 2|\vec{E}_1|^2 + 2|\vec{E}_2|^2 && (OR) \end{aligned} \tag{3.4}$$

The second-order polarization response contains terms with different combinations of the input frequencies ω_1 and ω_2: these correspond to the processes of frequency doubling, or second harmonic generation (SHG), sum-frequency generation (SFG), difference-frequency generation (DFG) and optical rectification (OR). These processes are illustrated in fig. 3.1A.

The efficiency of each conversion process depends on the so-called phase-matching condition. Both the input fields and generated field travel through the material at a speed given by their wavevector $\vec{k}$, where $\vec{k} = \vec{n}\omega/c$, with $\vec{n}$ the refractive index of the medium and c the speed of light. To get efficient conversion, the generated field at any point in the material must maintain a fixed phase relation with respect to the field generated earlier. Microscopically this means that the individual atomic dipoles of the material all are phased such that the field emitted by each dipole adds up constructively in the propagation direction of the field. This is the case when the following condition is fulfilled:

$$\sum \vec{k}_- = \sum \vec{k}_+ \tag{3.5}$$

where $\vec{k}_-$ and $\vec{k}_+$ refer to the wavevector(s) of the converted fields (upward arrows in fig. 3.1) and generated fields (downward arrows), respectively. In practice, phase matching is not so easy to achieve. To illustrate this, we consider

the case of sum-frequency generation, for which eq. 3.5 reduces to

$$\vec{k}_1 + \vec{k}_2 = \vec{k}_3 \tag{3.6}$$

or equivalently,

$$\vec{n}_1\omega_1 + \vec{n}_2\omega_2 = \vec{n}_3\omega_3 \tag{3.7}$$

Since for most materials the refractive index $\vec{n}$ increases with frequency, the right side of eq. 3.7 is almost always larger than the left side. A common way to solve this problem is by using birefringent crystals. The refractive index of birefringent materials depends on the polarization direction of the light. Thus the phase-matching condition can be fulfilled by a proper choice of the polarization of the input fields and the orientation of the crystal. Consider for example the case of sum-frequency generation in a uniaxial crystal illustrated in fig. 3.1B. Here the two input fields are polarized perpendicular to the plane containing their wavevector $\vec{k}$ and the optical axis $\vec{c}$ of the crystal, making them experience the so-called ordinary refractive index n_o, while the generated field is polarized in the plane spanned by $\vec{k}$ and $\vec{c}$, so it experiences the so-called extraordinary refractive index $n_e(\theta)$:

$$\frac{1}{{n_e}^2(\theta)} = \frac{\cos^2\theta}{{n_o}^2} + \frac{\sin^2\theta}{{n_e}^2} \tag{3.8}$$

The extraordinary index depends on the angle θ between $\vec{k}$ and $\vec{c}$, which makes it possible to fulfill the phase-matching condition of eq. 3.7 by choosing the appropriate angle θ. In general, depending on the type of second-order process and the crystal material, different polarization combinations can be used to acquire phase matching.

For time-resolved spectroscopy, light needs to be pulsed, and pulses are inherently not monochromatic but span a range of frequencies. In this case the phase-matching condition cannot be perfectly fulfilled for all frequencies in the pulse: at the edges of the pulse spectrum the conversion efficiency decreases, which can lead to a narrowing of the generated pulse spectrum and consequently an increase in pulse duration. For undepleted input fields, the generated intensity depends on the wavevector mismatch $\Delta\vec{k} = \sum \vec{k}_+ - \sum \vec{k}_-$ and the crystal thickness L:

$$I(\omega) = I_0 \operatorname{sinc}^2(\Delta\vec{k}(\omega)L/2) \tag{3.9}$$

The above equation shows that it is possible to achieve a higher phase matching bandwidth - meaning a higher range of $\Delta\vec{k}$ for which $I > \frac{1}{2}I_0$ - by choosing a thinner crystal (smaller L). Of course, a thinner crystal also lowers the maximum generated intensity, so an optimal crystal length must be used based on the desired spectrum, duration and intensity of the generated pulse.

OPTICAL PARAMETRIC AMPLIFICATION A specific case of difference-frequency generation is optical parametric amplification (OPA). In this case the input fields are an intense high frequency beam, called the pump, and a very weak seed beam of lower frequency ω_s. During the OPA process, the weak seed

beam is amplified. In addition a new beam is created at the frequency ω_i, with $\omega_p = \omega_s + \omega_i$. The amplified beam is called the signal and the new beam is called the idler. Usually, the weak seed beam is chosen to be broadband white light; due to the broad bandwidth, the frequencies of the amplified signal and generated idler beams mostly depend on the phase-matching condition, and can be tuned over a wide range by changing the OPA crystal angle.

3.2 Single-color infrared pump-probe setup

The single-color infrared pump-probe setup used to obtain many results described later in this thesis is shown schematically in fig. 3.2. A Ti:sapphire regenerative amplifier (Spectra-Physics Hurricane) produces 900 μJ, 100 femtosecond pulses with a central wavelength of 800 nm at a repetition rate of 1 kHz. Part of this light is used to pump a β-bariumborate (BBO)-based optical parametric amplifier (OPA, Spectra-physics). In the OPA, a small part of the 800 nm light is focused into a sapphire plate to generate a broadband white light seed, which is amplified in two steps to generate signal and idler pulses of 1.33 μm and 2 μm respectively. The idler pulses are frequency-doubled in another BBO crystal and subsequently mixed with the remaining 800 nm light in a lithiumniobate (LN) crystal to produce 10 μJ infrared pulses centered at 2500 cm^{-1}, with a bandwidth of 100 cm^{-1} and a pulse duration of 200 fs. To ensure that no other light enters the pump-probe experiment, two long wave pass filters (one after the OPA, another after the DFG stage) filter out the remaining 800 nm light, and a germanium plate after the DFG stage filters out the signal and idler beams.

The polarization of the infrared pulses is cleaned up by a polarizer and the pulses are split into pump, probe and reference beams by a wedged CaF_2 window. The pump pulse passes through a $\lambda/2$ plate to rotate the pump polarization by 45°, and is chopped at 500 Hz to block every other pulse. The probe pulse passes over a motorized delay stage. All three beams are focused into the sample by a gold-coated parabolic mirror (focal length f=100 mm). The pump and probe beams are spatially overlapped in the sample, such that the probe beam monitors the pump-induced absorption changes, while the reference beam is focused at a different spot and used to correct for pulse-to-pulse intensity fluctuations of the probe. A rotating polarizer, placed directly after the sample, selects probe and reference pulses that are polarized either parallel or perpendicular with respect to the pump polarization. After passing through the sample and rotating polarizer, the probe and reference beams are recollimated using a second parabolic mirror, sent to a grating-based spectrometer (Lot Oriel MSH302) and detected by a 3x32 mercury-cadmium-telluride (MCT) array.

In some of the experiments, a wobbler is placed into the pump path to suppress the undesired interference effects in the signal due to scattering of the pump beam into the probe detector path[71]. The wobbler consists of a CaF_2 plate at Brewster angle that is slightly rotated at a frequency of 250 Hz using a set of electromagnets. By setting the correct phase and amplitude of the

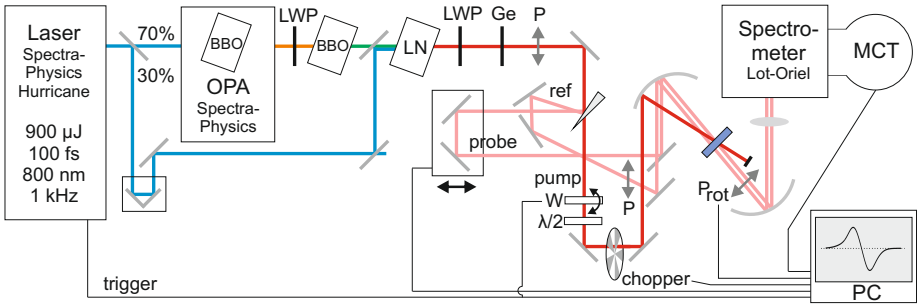

FIGURE 3.2. Schematic of the single-color pump-probe setup described in the text (not to scale). BBO: β-bariumborate crystal, LN: lithiumniobate crystal, LWP: long wave pass filter, Ge: Germanium filter, P: polarizer, P_{rot}: rotating polarizer, W: wobbler (optional), $\lambda/2$: half-wave plate, MCT: Mercury-Cadmium-Telluride detector. The colored lines indicate light beams, while the thin black lines indicate electronic signals.

rotation (via the voltage applied to the electromagnets), the pump phase can be modulated such that the unwanted interference signals average out.

3.3 DUAL-COLOR (2D) INFRARED PUMP-PROBE SETUP

The dual-color infrared pump-probe setup used for some of the experiments described in this thesis is shown schematically in fig. 3.3. It can be used in pump-probe mode, or in 2D mode by passing the pump beam through an interferometer.

A Ti:sapphire regenerative amplifier (Coherent) produces 3.3 mJ, 35 femtosecond pulses with a central wavelength of 800 nm at a repetition rate of 1 kHz. The main part of this light is used to generate the pump beam. Firstly, a white-light-seeded, three-step, β-bariumborate (BBO)-based OPA (Spectra-Physics) generates signal and idler pulses that are tunable between 1.1-1.6 μm and 1.6-2.9 μm respectively. The signal and idler pulses are difference-frequency mixed in a silver gallium disulfide ($AgGaS_2$) crystal to produce infrared pump pulses that are tunable between 1500 and 4000 cm^{-1}, with typical energies of 20 μJ, a bandwidth of 300 cm^{-1} (FWHM) and a pulse duration of 170 fs. The pump pulse passes through a $\lambda/2$ plate to rotate the pump polarization by 45°, and is then chopped at 500 Hz to block every other pulse. The probe and reference beams are generated using a similar conversion scheme: a two-step, white-light-seeded, BBO-based OPA (home-build) generates signal and idler pulses that are difference-frequency mixed in a $AgGaS_2$ crystal. This produces 4 μJ infrared pulses tunable from 1500 to 4000 cm^{-1}, with a bandwidth of 320 cm^{-1} (FWHM) and a pulse duration of 170 fs. The generated infrared light is sent through a germanium plate that blocks the signal and idler light,

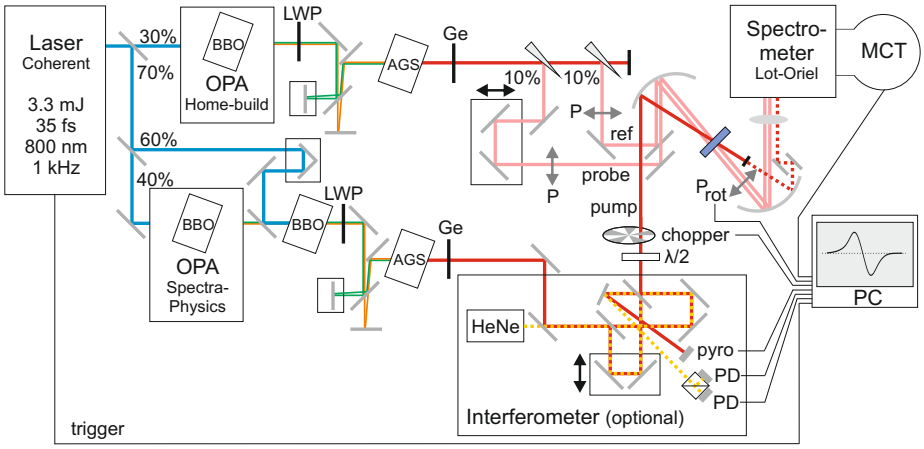

FIGURE 3.3. Schematic of the dual-color pump-probe setup described in the text (not to scale). BBO: β-bariumborate crystal, AGS: silver gallium disulfide ($AgGaS_2$) crystal, LWP: long wave pass filter, Ge: Germanium filter, P: polarizer, P_{rot}: rotating polarizer, $\lambda/2$: half-wave plate, HeNe: helium-neon laser, pyro: pyroelectric detector, PD: photodiode, MCT: Mercury-Cadmium-Telluride detector. The colored lines indicate light beams, while the thin black lines indicate electronic signals.

and reflected off two ZnSe wedges to generate probe and reference beams. The probe beam passes through a motorized delay stage, and the polarization of both probe and reference beams is cleaned up by polarizers.

Pump, probe and reference beams are focused into the sample by a gold-coated parabolic mirror (focal length f=150 mm). The pump and probe beams are spatially overlapped in the sample, so that the probe beam monitors the pump-induced absorption changes, while the reference beam is focused at a different spot. The reference is used to correct for pulse-to-pulse intensity fluctuations of the probe. A rotating polarizer, placed directly after the sample, selects probe pulses that are polarized either parallel or perpendicular with respect to the pump polarization. After passing through the sample and rotating polarizer, the pump, probe and reference beams are recollimated using a second parabolic mirror (f=100 mm), sent to a grating-based spectrometer (Lot Oriel) and detected by a 3x32 mercury-cadmium-telluride (MCT) array. The pump beam is only passed to the detector during experimental tuning and is blocked during the actual pump-probe experiment.

2D SPECTRA To obtain two-dimensional spectra, the pump pulses can be sent through a compact Mach-Zehnder interferometer[60,72]. The interferometer produces pulse pairs with variable time delay. A reference helium-neon (HeNe) laser travels a few centimeters above the infrared beam and is detected by a quadrature counter, consisting of a $\lambda/4$ plate in one of the interferometer arms and a polarizing beam splitter and two photodiodes in the output arm. This allows for an accurate determination of the interferometer delay, even when the

delay is scanned very fast. Separate beamsplitters, placed on top of each other, are used for the infrared and HeNe light. The pump interference that results from scanning the delay is directly recorded by a pyroelectric detector in one of the output arms of the interferometer, which yields the relative phase needed to calculate the 2D spectra.

3.4 SAMPLE CELL

The liquid samples under study in this thesis are held by a sample cell that consists of two infrared-transparent windows (CaF_2 or z-cut sapphire) that are separated by a 10 to 500 μm teflon spacer. CaF_2 has the advantage of being transparent down to low frequencies: it starts absorbing below 1250 cm^{-1} while sapphire absorbs below 2300 cm^{-1}. However, sapphire is much stronger, which prevents scratching and subsequent scattering of pump light into the probe detection path. The windows and liquid are held together by a 1 inch diameter aluminum cell. This cell can in turn be mounted on a temperature-controlled stage. The stage temperature is controlled by an active feedback system that consists of two water-cooled Peltier elements, a thermocouple attached to the sample cell, and a control unit (TE Technology). Alternatively, the aluminum cell can be mounted on a rotating stage, which prevents accumulated local heating of the sample.

ISOTOPICALLY DILUTED WATER The aqueous samples under study in this thesis often contain isotopically diluted water. Isotopically diluting water means mixing normal water, H_2O, with heavy water, D_2O, which has two deuterium atoms instead of hydrogen. The hydrogen and deuterium atoms exchange due to the self-ionization of water, resulting in a near-statistical mixture of HDO, H_2O and D_2O molecules[73]. Looking at isotopically diluted water has two main advantages:

- The two hydroxyl stretch vibrations of HDO are decoupled. As a consequence, there is no splitting of the water hydroxyl stretch vibration into antisymmetric and symmetric modes.
- The concentration of OD (or OH) oscillators is very low. As a consequence, intermolecular Förster energy transfer becomes negligible. In addition, the absorption per volume is smaller, so the sample thickness can be more practical (>10 μm) and the effect of sample heating is reduced since less vibrations are excited per volume.

The absence of spectral splitting and intra- and intermolecular coupling for HDO means that the interpretation of spectra is simplified: the spectrum of the hydroxyl stretch vibration directly reflects the hydrogen-bond strength, and the anisotropy measured by a polarization-resolved pump-probe experiment directly decays with the rate of molecular reorientation.

Most experiments probe the OD stretch vibration of a few percent of HDO in H_2O. The advantage of probing the OD vibration is that the vibrational

lifetime is longer compared to the OH vibration, and that most of the sample is still H_2O, which is closer to the natural situation. A disadvantage is that there is considerable background absorption of the OH stretch in the OD spectral region, so the concentration of HDO in H_2O cannot be too low (generally it is chosen to be above 4%).

4 Data modelling

4.1 Isotropic transient spectrum

The isotropic transient absorption spectrum measured by vibrational pump-probe spectroscopy reflects the dynamics of excited vibrations as they relax back to the ground state. These dynamics can be quite complicated; vibrations might relax via different intermediate states before the vibrational energy is finally converted into heat. In case the system is inhomogeneous, the dynamics are further complicated by the presence of multiple vibrational species, as each species might have a different spectral response and relaxation pathway.

To extract physical information from the transient spectrum, we usually decompose the transient spectrum into a number of different spectral components. Each spectral component can be assigned to a different state of our system, and the number of molecules in each state is proportional to the time-dependent amplitude of the spectral component. The transient absorption spectrum $\Delta\alpha_{mdl}$ is thus described as

$$\Delta\alpha_{mdl}(\omega, t) = \sum_i N_i(t) \cdot \sigma_i(\omega) \tag{4.1}$$

where $N_i(t)$ is the time-dependent amplitude, or population, of component number i and $\sigma_i(\omega)$ is its spectral signature. Note that in this notation, the subscript of σ_i does not refer to the i$^{\text{th}}$ vibrational state (as in chapter 2), but to the entire response of component number i, which includes both $0 \rightarrow 1$ and $1 \rightarrow 2$ transitions.

4.1.1 Relaxation models

The best model to describe the transient spectrum is in general based on trends that are observed in the spectrum directly, and the properties of the system (for example, knowledge of the system composition). Two models that are commonly used to describe vibrational relaxation are shown in fig. 4.1. In the cascade model, the excited vibration relaxes via an intermediate state to a thermalized ground state, and the populations are described by

$$\frac{d}{dt}N_1(t) = -k_1 N_1(t) \tag{4.2}$$

$$\frac{d}{dt}N_0^*(t) = +k_1 N_1(t) - k_h N_0^*(t) \tag{4.3}$$

$$\frac{d}{dt}N_0'(t) = +k_h N_0'(t) \tag{4.4}$$

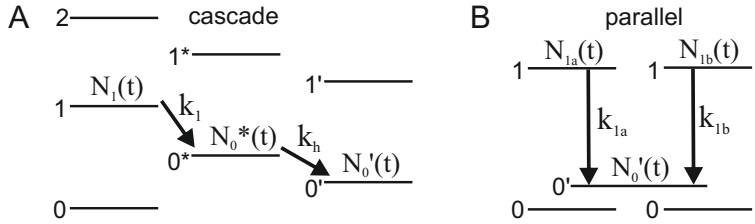

FIGURE 4.1. The energy diagram corresponding to the cascade model (A) and the parallel model (B) of vibrational relaxation.

where k_1 is the vibrational decay rate, which is the inverse of the vibrational lifetime, and k_h is the thermalization rate, i.e. the rate at which the excitation energy is converted into heat. The above set of differential equations can conveniently be written in matrix notation as

$$\frac{d}{dt}\begin{pmatrix} N_1(t) \\ N_0^*(t) \\ N_0'(t) \end{pmatrix} = \begin{pmatrix} -k_1 & 0 & 0 \\ +k_1 & -k_h & 0 \\ 0 & +k_h & 0 \end{pmatrix} \begin{pmatrix} N_1(t) \\ N_0^*(t) \\ N_0'(t) \end{pmatrix} \tag{4.5}$$

Solving these equations leads to a description of the transient signal:

$$\begin{aligned} \Delta\alpha_{mdl}(\omega,t) =& \sigma_1(\omega)N_1(0)e^{-k_1 t} \\ &+ \sigma_*(\omega)N_1(0)\left(\frac{k_1}{k_h-k_1}(e^{-k_1 t}-e^{-k_h t})\right) \\ &+ \sigma_h(\omega)N_1(0)\left(\frac{k_1}{k_h-k_1}e^{-k_h t}-\frac{k_h}{k_h-k_1}e^{-k_1 t}+1\right) \end{aligned} \tag{4.6}$$

It has been demonstrated that the vibrational relaxation of the OD stretch vibration in isotopically diluted water[74] is very well described by the cascade model. The excited OD stretch vibrations relax via an intermediate state to a thermalized ground state. This thermalized ground state accounts for the temperature rise that occurs as the energy of the excited vibrations is transferred into heat: the associated spectrum corresponds to the difference spectrum of a slightly heated sample and the original, unexcited sample. The intermediate state accounts for the fact that the thermalization is delayed, and has no spectral signature of its own ($\sigma_* = 0$), which means that the population of the intermediate state does not alter the spectral response of the OD vibration. As such, the intermediate state is unlikely to correspond to a specific vibrational mode, because the excitation of lower energy vibrational modes such as the HOD bend vibration would lead to an anharmonic shift of the OD stretch vibration. Instead, it might reflect a relatively slow adaptation of the low-energy degrees of freedom (hydrogen-bond stretch and bend) to the new equilibrium positions that correspond to the higher energy content.

For other molecular systems, the transient signal can be modelled using the parallel model, which describes the independent relaxation of two species of

excited vibrations to a common thermalized ground state. In this case

$$\begin{aligned}\Delta\alpha_{mdl}(\omega,t) =&\sigma_a(\omega)N_{1a}(0)e^{-k_{1a}t} \\ &+\sigma_b(\omega)N_{1b}(0)e^{-k_{1b}t} \\ &+\sigma_h(\omega)\left(1-N_{1a}(0)e^{-k_{1a}t}-N_{1b}(0)e^{-k_{1b}t}\right)\end{aligned} \tag{4.7}$$

This model, and variants thereof, have been used to describe the relaxation of the OD stretch vibration of HOD molecules in different mixtures [75–77]. Here the two excited states correspond to distinct water hydrogen-bond configurations. Of course, more complicated models can be defined by expanding the number of states and/or redefining the rate matrix of eq. 4.5.

4.1.2 Least-squares fit

To estimate how well a given model describes the measured transient spectrum we can calculate the error-weighted square error:

$$\chi^2 = \int\int\left(\frac{\Delta\alpha(\omega,t)-\Delta\alpha_{mdl}(\omega,t)}{\epsilon(\omega,t)}\right)^2 d\omega dt \tag{4.8}$$

where $\epsilon(\omega,t)$ is the standard deviation of the measured transient spectrum $\Delta\alpha(\omega,t)$. The model $\Delta\alpha_{mdl}$ in general contains a number of free parameters. In the formalism of the previous section, the free parameters are the vibrational relaxation rates $\mathbf{k}$ and the spectral signatures of each state σ_i. To find the optimal parameter values, we have to minimize the square error

$$\chi^2(\mathbf{k}) = \int\int\left(\frac{\Delta\alpha(\omega,t)-\sum_i N_i(\mathbf{k},t)\sigma_i(\omega)}{\epsilon(\omega,t)}\right)^2 d\omega dt \tag{4.9}$$

The minimization can be carried out numerically using an automated fitting routine: starting out with an estimate for the vibrational decay rates $\mathbf{k}$, the best-fitting spectra are obtained analytically by calculating the minimum of χ^2 with respect to the spectrum σ_i at every measured frequency ω_j (singular value decomposition):

$$\frac{d}{d\sigma_i(\omega_j)}\int\left(\frac{\Delta\alpha(\omega_j,t)-\sum_i N_i(\mathbf{k},t)\sigma_i(\omega_j)}{\epsilon(\omega_j,t)}\right)^2 dt = 0 \tag{4.10}$$

after which the square error is calculated using eq. 4.9. The loop is iterated using different values of $\mathbf{k}$ until the optimal $\mathbf{k}$ is reached.

4.2 Anisotropy dynamics

The anisotropy of the transient spectrum reflects the depolarization dynamics of excited vibrations as they reorient or transfer their energy to other vibrations by resonant Förster energy transfer. However, if the transient spectrum

contains multiple spectral components, as discussed in the previous section, the anisotropy decay of the total spectral response is not so easy to interpret. This is due to the fact that the different spectral components do not contribute equally to the anisotropy at all times. Short-lived components contribute mostly at early time delays, while long-lived components dominate at later time delays.

In the case of isotopically diluted water, the OD stretch vibration decays via a dark intermediate state to a thermalized ground state[74]. To calculate the anisotropy associated with the OD stretch vibration, the transient spectra have to be corrected for the isotropic heating contribution:

$$\Delta\alpha_{\parallel,corr}(\omega,t) = \Delta\alpha_{\parallel}(\omega,t) - N_h(t)\sigma_h(\omega) \tag{4.11}$$

$$\Delta\alpha_{\perp,corr}(\omega,t) = \Delta\alpha_{\perp}(\omega,t) - N_h(t)\sigma_h(\omega) \tag{4.12}$$

before calculating the anisotropy according to

$$R(\omega,t) = \frac{\Delta\alpha_{\parallel,corr}(\omega,t) - \Delta\alpha_{\perp,corr}(\omega,t)}{\Delta\alpha_{\parallel,corr}(\omega,t) + 2\Delta\alpha_{\perp,corr}(\omega,t)} \tag{4.13}$$

In case two species of excited vibrations relax to a common thermalized ground state, as described by eq. 4.7, we do not only want to correct for the isotropic heating contribution, but wish to extract the component-specific anisotropy decays as well. If we know the spectral signatures σ_i of each component from a fit to the isotropic data, we can calculate the component-specific anisotropy decays R_i by singular value decomposition of the parallel and perpendicular absorption signals. This means describing the parallel and perpendicular signals as

$$\Delta\alpha_{mdl,\parallel}(\omega,t) = \sum_i N_{i,\parallel}(t)\cdot\sigma_i(\omega) \tag{4.14}$$

$$\Delta\alpha_{mdl,\perp}(\omega,t) = \sum_i N_{i,\perp}(t)\cdot\sigma_i(\omega) \tag{4.15}$$

and solving for each measured delay time t_j

$$\frac{d}{dN_{i,\parallel}(t_j)}\int\left(\frac{\Delta\alpha_{\parallel}(\omega,t_j) - \sum_i N_{i,\parallel}(t_j)\sigma_i(\omega)}{\epsilon(\omega,t_j)}\right)^2 d\omega = 0 \tag{4.16}$$

$$\frac{d}{dN_{i,\perp}(t_j)}\int\left(\frac{\Delta\alpha_{\perp}(\omega,t_j) - \sum_i N_{i,\perp}(t_j)\sigma_i(\omega)}{\epsilon(\omega,t_j)}\right)^2 d\omega = 0 \tag{4.17}$$

This yields the time-dependent amplitudes $N_{i,\parallel}$ and $N_{i,\perp}$ of each component, after which the component-specific anisotropy can be calculated according to

$$R_i(t) = \frac{N_{i,\parallel} - N_{i,\perp}}{N_{i,\parallel} + 2N_{i,\perp}} \tag{4.18}$$

5 Water dynamics in aqueous sugar solutions

Sugars are an important class of biological molecules. In living organisms, they fulfill a wide range of functions, serving for example as an energy source or signaling group (when part of a glycoprotein or glycolipid), or acting as a stabilizing osmolyte of proteins under environmental stress conditions[78,79]. This latter property is still not fully understood, though it has been hypothesized that sugars stabilize proteins against unfolding indirectly, via the water solvent. In this chapter we study the effect of the sugars glucose, trehalose and sorbitol on the reorientation dynamics of water molecules. We find that at all sugar concentrations the water dynamics can be described by a single reorientation time constant. With increasing carbohydrate concentration, the water reorientation time constant increases from 2.5 picoseconds to a value of about 15 picoseconds. The slowing down of the water dynamics is strongest for trehalose, followed by glucose and sorbitol. Compared to other small amphiphilic solutes, the influence of sugars on the dynamics of water is relatively long-ranged, and involves collective structural effects. These results are in line with an indirect protection mechanism of sugars via the water solvent.

5.1 INTRODUCTION

Sugars are known to stabilize proteins against unfolding under extremely cold and dry conditions. Even though this latter property is widely used in industry and in biochemistry labs, the exact mechanism by which sugars stabilize proteins against unfolding is still not fully understood [78–80].

Since sugars are preferentially excluded from protein surfaces [78,79], it has been hypothesized that they protect proteins indirectly by modifying the properties of the water solvent. For this reason, people have extensively investigated the properties of water in solutions of sugars, using a wide range of techniques. With Raman spectroscopy [81–83], neutron scattering [83], neutron diffraction [84–86] and THz absorption experiments [87,88], it was found that the water structure around sugars is changed in comparison to the structure of neat water. However, the observed structural changes tend to be quite small [86]. A more pronounced effect is found with techniques that probe the dynamics of the water molecules. Dielectric relaxation [89], NMR [90], time-resolved fluorescence [91] and dynamic light scattering [92,93] studies all show that the dynamics of water slows down significantly near sugar molecules. A similar slowing down effect is seen with molecular dynamics simulations [81,94–96]. However, the different studies do not agree on the magnitude and the spatial extent of the effects of sugar molecules on the dynamics of water. For trehalose, for example, which is the sugar with the highest degree of bioprotectability, different techniques give different results. With NMR measurements of the spin relaxation rate of water ^{17}O in dilute trehalose solutions, a modest retardation factor of 1.6 was found, assuming that the hydration shell consists of 47 water molecules [90]. In dynamic light scattering measurements [92], a much larger retardation factor of 5 to 6 was found, for a hydration shell consisting of 25 water molecules. Finally, time-dependent fluorescence Stokes shift measurements of a small THz probe covalently attached to trehalose [91], indicate that trehalose retards the dynamics of more than 150 surrounding water molecules by a factor of $\sim$2.

In this chapter we investigate the effect of glucose, trehalose and sorbitol on water reorientation dynamics. To this end, we use polarization-resolved pump-probe spectroscopy, which directly measures the reorientation dynamics of both water and solute. The selected sugars are all commonly used as stabilizing osmolyte, and have some interesting properties of their own: glucose is the main monosaccharide unit and energy source in biological systems, trehalose is known to be the most bioprotective sugar [80], and sorbitol is a linear form of glucose, and the comparison with glucose allows us to study the effect of the sugar conformation on the water reorientation dynamics.

5.2 EXPERIMENTAL

SPECTROSCOPY The measurements described in this chapter are performed with the single-color setup described in section 3.2. The pump and probe pulses are centered around 2500 cm^{-1}, in resonance with the OD stretch vibration.

To probe the dynamics of the rise in sample temperature, the dual-color setup described in section 3.3 is used as well, with a modified pump generation scheme: a BBO-based OPA (TOPAS, LightConversion) creates signal and idler pulses of 1.33 μm and 2 μm respectively. The idler pulses are subsequently doubled in a 4 mm BBO crystal and mixed with 800 nm light in a 10 mm lithiumniobate crystal, to generate 24 μJ pump pulses centered at 2500 cm^{-1} with a bandwidth of 100 cm^{-1} (FWHM). The crystals are chosen to be relatively thick, to generate a pump spectrum that has the same bandwidth as the single-color setup. The probe pulses of the dual-color setup are centered at 2950 cm^{-1}, in resonance with the low-frequency tail of the OH stretch vibration.

SAMPLE PREPARATION Glucose, trehalose and sorbitol were purchased from Sigma-Aldrich (purity >98%) and mixed with H_2O and D_2O, such that the percentage of deuterated hydroxyl groups in the sample was always 4%. After mixing, we stirred and heated the solutions to about 50°C to promote dissolution. Upon cooling back to room temperature, the carbohydrates stayed well dissolved.

5.3 RESULTS

5.3.1 LINEAR SPECTRA

Figure 5.1 presents linear spectra of solutions of glucose in isotopically diluted water. The spectra show a broad absorption band centered at 2500 cm^{-1} due to the OD stretch vibrations of water and glucose. With increasing glucose concentration, the center frequency and spectral shape show little change. The absorption around 2500 cm^{-1} slightly decreases, due to the decrease of the concentration of OD oscillators, and the absorption at frequencies above 2600 cm^{-1} increases, due to the absorption of the CH stretch vibrations of glucose. The same trends are observed for solutions of trehalose and sorbitol in isotopically diluted water.

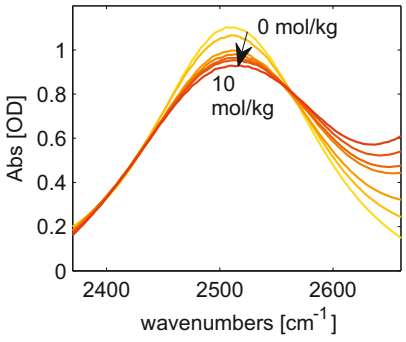

FIGURE 5.1. Linear spectra of aqueous glucose solutions (0, 1, 2, 3, 5, 7, 10 mol/kg), with 4%D:H. The spectra are corrected for H_2O background.

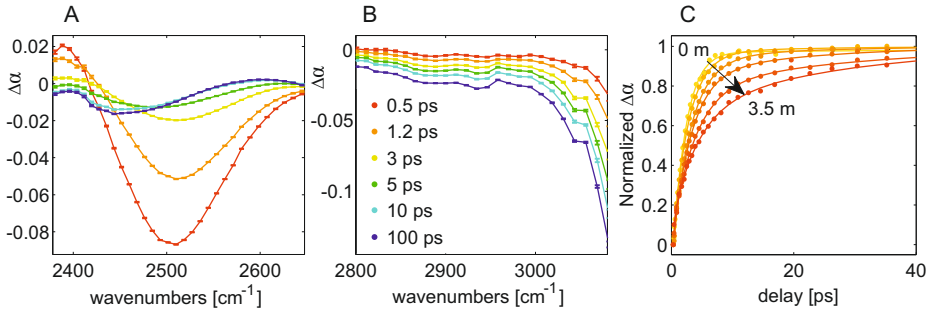

FIGURE 5.2. Isotropic absorption change for solutions of trehalose in water at different picosecond delay times after excitation with a 2500 cm^{-1} pump pulse. (A) Absorption change between 2400 and 2600 cm^{-1}(OD stretch vibration) for 3.5 molal trehalose. (B) Absorption change between 2800 and 3100 cm^{-1} (tail of OH stretch vibration, heating signal) for 3.5 molal trehalose. (C) Absorption change between 2800 and 3100 cm^{-1}, normalized at 100 picoseconds, for different concentrations of trehalose (0, 0.5, 1, 1.5, 2.5 and 3.5 molal). The lines represent empirical triple-exponential fits.

5.3.2 ISOTROPIC AND ANISOTROPIC SIGNALS

In figure 5.2 we present isotropic transient absorption signals measured for solutions of trehalose after exciting the sample with a pump pulse at 2500 cm^{-1}. Figure 5.2A presents the isotropic absorption signal between 2400 and 2600 cm^{-1} for a solution of 3.5 molal trehalose. At early delay times, we observe a bleach at the fundamental transition of the OD stretch vibration around 2500 cm^{-1}, and an induced absorption at frequencies below 2420 cm^{-1}. At later delay times, these signals have decayed and the transient spectral response is formed by a thermal difference spectrum. Figure 5.2B presents the isotropic absorption signal between 2800 and 3100 cm^{-1} for the same solution. The bleaching signal (negative absorption change) slowly rises with increasing delay time. This signal is due to the shift and decrease in cross section of the OH stretch vibrations with temperature, and directly represents the rise in sample temperature. The dynamics of the heat signal between 2800 and 3100 cm^{-1} (normalized at 100 picoseconds) for different concentrations of trehalose are shown in figure 5.2C. With increasing concentration of trehalose, the heat dynamics slow down considerably. For solutions of glucose and sorbitol we observe a similar slowing down of the heat dynamics with increasing solute concentration. Knowing the dynamics of the heat signal and its spectral response - of which the shape is given by the transient spectrum at long delays - we can correct the isotropic spectra of the OD stretch at all delay times for the heating contribution [97].

Figure 5.3 presents the isotropic transient absorption signals for water and the three studied sugars, after correcting for the heating contribution. All isotropic spectra show a strong bleaching signal around 2500 cm^{-1} due to the bleaching of the fundamental $v = 0 \rightarrow 1$ transition (ground-state bleaching and stimulated emission) and an induced absorption at frequencies below 2420 cm^{-1}

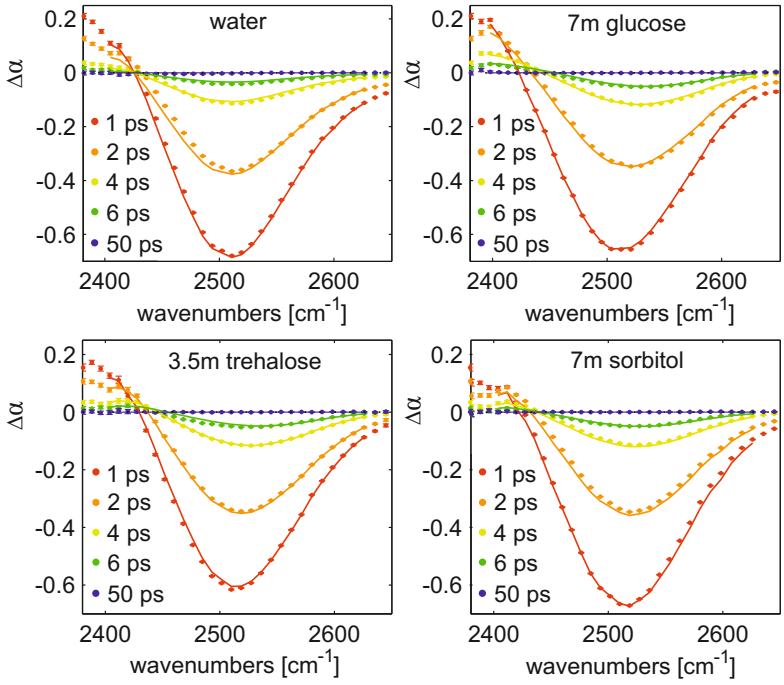

FIGURE 5.3. Isotropic absorption signals for solutions of glucose, trehalose and sorbitol in isotopically diluted water, at five different picosecond delay times after the excitation. The concentrations are given in molal (mol/kg). The solid lines represent fits using the model described in the text.

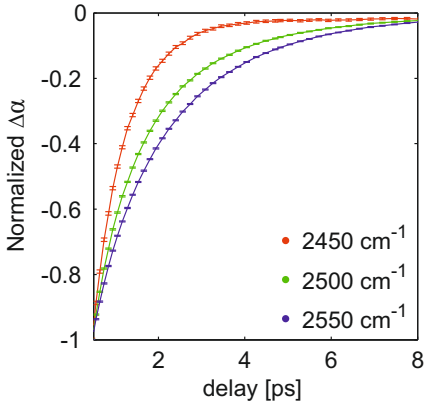

FIGURE 5.4. Isotropic absorption signal for a solution of 3.5 molal trehalose in water, shown for different probe frequencies as a function of delay time (normalized at 0.5 picoseconds).

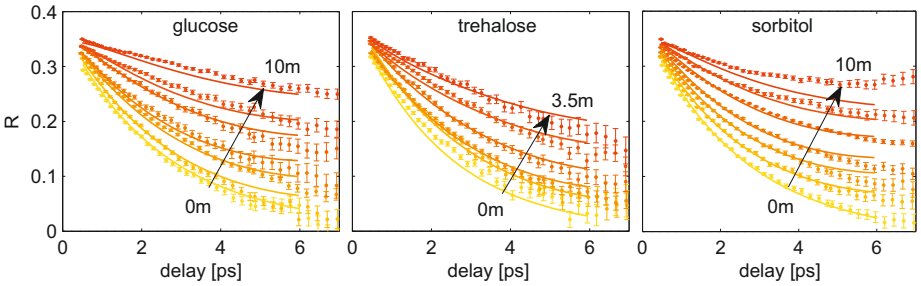

FIGURE 5.5. Anisotropic absorption signal at 2500 cm^{-1} for solutions of glucose, trehalose and sorbitol in water of different concentrations (trehalose: 0, 0.5, 1, 1.5, 2.5 and 3.5 molal). Solid lines are description with our model fit.

due to $v = 1 \rightarrow 2$ excited-state absorption. The spectral shapes are very similar for the different carbohydrates, even at high concentrations, in accordance with the linear spectra. For neat water, we find that the transient absorption signal decays with a frequency-independent time constant of 1.7 picoseconds, in agreement with earlier reports[74]. This time constant represents the vibrational lifetime of the OD stretch vibration of HDO dissolved in H_2O.

The vibrational decay becomes quite inhomogeneous upon the addition of sugar: on the red side of the OD absorption band the decay speeds up compared to neat water, while on the blue side of the OD absorption band the decay slows down in comparison with neat water. This observation is further illustrated in figure 5.4, which shows the isotropic absorption change measured for a solution of 3.5 molal trehalose as a function of delay time at different probe frequencies. The inhomogeneity of the relaxation increases with increasing sugar concentration. This inhomogeneity follows from the fact that both water and sugar contain hydroxyl groups that contribute to the transient spectral response. The frequency-dependent decay of the isotropic spectra shows that the spectral responses and lifetimes of the water and sugar hydroxyl groups differ.

Figure 5.5 presents the anisotropy of the vibrational excitation (as defined by eq. 2.46) measured at 2500 cm^{-1} for the three sugars at different concentrations. With increasing concentration of sugar, the decay of the anisotropy strongly slows down. This is the case for glucose, trehalose and sorbitol. For neat water the anisotropy decays with a timescale of 2.5 ps, in agreement with earlier reports[74].

5.3.3 REFERENCE MEASUREMENTS IN DMSO

The transient absorption signals as shown in figure 5.3, 5.4 and 5.5 contain contributions from both water and sugar hydroxyl groups. To extract the water reorientation dynamics, we need to separate these contributions. To this purpose we performed reference measurements on solutions of the studied sugars in dimethylsulfoxide (DMSO). The carbohydrates will form similar hydrogen

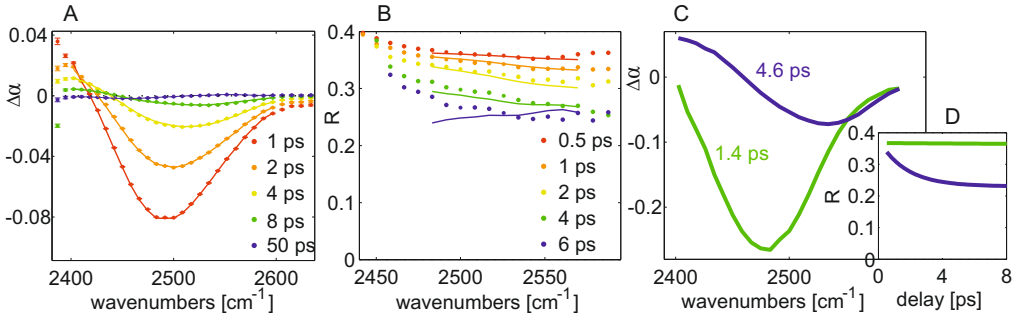

FIGURE 5.6. The isotropic absorption change (A) and the anisotropic absorption change (B) as a function of frequency for 0.4 molal 10% deuterated glucose in DMSO (solid lines are description with model fit). Spectral components (C) contributing to isotropic signal (relative amplitudes correspond to 1 ps), and anisotropy (D) of the two spectral components as a function of delay time.

bonds with DMSO as with water, but since DMSO itself does not contain hydroxyl groups, the transient absorption signals only represent the response from the OD stretch vibrations of the sugars. Figure 5.6 presents the isotropic and anisotropic signals of a solution of 0.4 molal glucose (10% deuterated) in DMSO. The decay of the isotropic absorption change is again observed to be frequency dependent: on the red side the decay is much faster than on the blue side of the OD absorption band. We find that the dynamics of the isotropic and anisotropic signals can be very well described with two spectral components, with vibrational relaxation time constants of 1.4 ± 0.2 picoseconds and 4.6 ± 0.2 picoseconds (figure 5.6C), and different associated anisotropy dynamics (figure 5.6D). The responses of trehalose and sorbitol dissolved in DMSO can also be very well described with two spectral components with different vibrational lifetimes and different associated anisotropy dynamics.

5.3.4 SPECTRAL DECOMPOSITION MODEL

Based on the findings for the sugar solutions in DMSO, we analyze the results measured for the sugar solutions in water with a model that includes two spectral components for the sugar response and one spectral component for the water response. In this model we assume that the relative amplitudes of the sugar and water components are only defined by the sugar concentration. We further assume that the spectral shape and lifetime of each component do not change with concentration, and fix the spectral shape and lifetime of the water component to the corresponding values for neat water (4% D_2O:H_2O). Each spectral component is assumed to show an associated anisotropy decay of the form:

$$R_i(t) = A_i e^{-t/\tau_i} + B_i \tag{5.1}$$

The anisotropy dynamics of the two sugar components are taken to be the same at all concentrations. Only the anisotropy decay of the water component is

allowed to vary with concentration. We fit this model to the isotropic absorption and anisotropy signals at all measured concentrations for each sugar. The fit is performed with a single fitting routine that adds the least-square errors for each concentration. During each iteration of the fit, the isotropic absorption signal is spectrally decomposed in three spectra $\sigma_i(\nu)$ for a given set of mono-exponentially decaying populations $N_i(t)$. The error is then determined by comparing the isotropic transient spectral response at all frequencies and delay times to the result of the spectral decomposition $\sum_i N_i(t)\sigma_i(\nu)$. The error for the anisotropic signal is determined by comparing each model anisotropy component R_j (given by A_j, B_j and τ_j) to the following quantity

$$\frac{\frac{1}{3}(\alpha_{\parallel} - \alpha_{\perp}) - \sum_{i \neq j} R_i N_i \sigma_i}{N_j \sigma_j} \tag{5.2}$$

Here $\alpha_{\parallel}$ and $\alpha_{\perp}$ are the measured parallel and perpendicular transient spectra, respectively. Equation (5.2) is based on the following expression, which follows from eqs. 2.41 and 2.46:

$$\frac{1}{3}(\alpha_{\parallel} - \alpha_{\perp}) = \sum_i R_i N_i \sigma_i \tag{5.3}$$

The result of the fits is displayed with solid lines in figure 5.3 and 5.5. The fits are in good agreement with the data for all sugars. The spectral components resulting from the fits are shown in the top row of figure 5.7. For all three sugars, the two components originating from the sugar hydroxyl groups are red-shifted and blue-shifted with respect to the water band, and have lifetimes around 0.4 ps and 3.8 ps respectively. The spectral shapes are very similar to what is found for the sugars in DMSO. For sorbitol the center frequencies of the two sugar hydroxyl bands are slightly closer together than for glucose and trehalose.

The anisotropy dynamics of the three spectral components are shown in the bottom row of figure 5.7. It is seen that the anisotropy of the two sugar hydroxyl components decays very slowly. The anisotropy dynamics of the water hydroxyl band are faster, but strongly slow down with increasing sugar concentration. We find that the final value of the anisotropy (coefficient B in eq. 5.1) of the water component stays within ± 0.015 for all sugars at all concentrations. Hence, the anisotropy decay of the water component can be well characterized by a single reorientation time constant τ_w of which the value depends on the nature of the sugar and its concentration. This reorientation time constant is presented in figure 5.8 for each sugar as a function of concentration.

5.3.5 MODELING WATER REORIENTATION OF SUGAR HYDRATION SHELLS

We measure the reorientation dynamics of water in sugar solutions up to very high concentrations. At the highest concentrations, only 5 to 6 water molecules (and 15 in the case of trehalose) are available per sugar molecule. As a result, the hydration shells of the sugar molecules will overlap, which implies

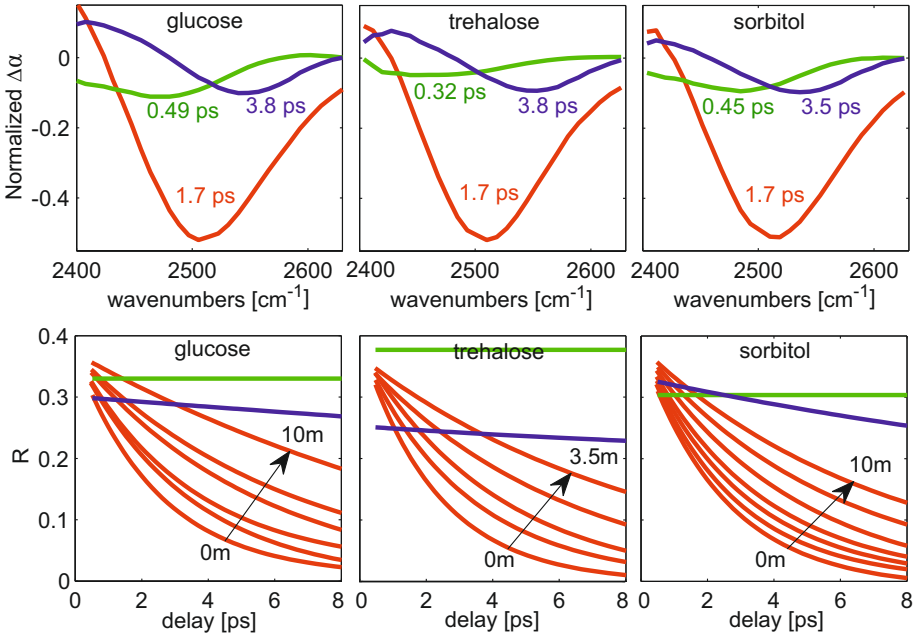

FIGURE 5.7. Top: Spectral components of the transient spectral response of aqueous sugar solutions. The spectral components decay with different vibrational lifetimes (indicated as legends). The three panels present the amplitudes of the spectral components at 1 ps after the excitation for the same sugar concentrations that are shown in figure 5.3). Bottom: Anisotropy as a function of delay time for the two sugar hydroxyl bands (green and blue) and the water hydroxyl band (red), at different sugar concentrations.

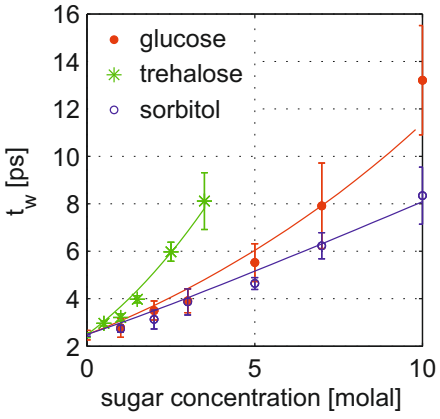

FIGURE 5.8. Water reorientation time constant as a function of sugar concentration. Solid lines represent the description with overlapping hydration shell model described in the text.

that the reorientation dynamics of the water molecules will be affected by the nearby presence of multiple sugar molecules. It is to be expected that the reorientation dynamics of water will be become slower when the number of nearby sugar molecules increases. To account for this effect, we calculate the probabilities that a water molecule is located in zero, one, two or more sugar hydration shells. We assume the sugars to be randomly distributed, which is a reasonable assumption according to neutron diffraction experiments[84,85] and MD simulations[85,98]. The water molecules are largely randomly distributed as well, except for the fact that we do not allow a water molecule to belong to more than two hydration shells. The distribution depends on the sugar molar concentration C_M (calculated from the sugar molal concentration c_m with $C_M = c_m \cdot \rho/(1000 + c_m \cdot M_{sugar})$) and the size of the hydration shell, which is the number of water molecules dynamically perturbed by each carbohydrate. The calculation of the distribution of probabilities of the number of hydration shells to which a water molecule belongs is described in detail in the appendix of this chapter. To translate the distribution to the dynamics of water, we assign increasingly slow reorientation rates to water in zero, one, or two hydration shells. A single retardation factor x relates the reorientation rates, such that the rate decreases a factor x when going from zero to one hydration shell, and x^2 when going from one to two hydration shells. This model yields a triple exponential anisotropy decay R_{mdl} at each sugar concentration:

$$R_{mdl} = 0.4\left(P_c(0)e^{-k_0 t} + P_c(1)e^{-k_0 x t} + P_c(2)e^{-k_0 x^2 t}\right) \tag{5.4}$$

where $P_c(i)$ is the probability that a water molecule belongs to i hydration shells, as calculated from the sugar concentration and the size of the hydration shell, and $k_0 = {}^1/_{2.5}$ is the reorientation rate of unperturbed water. We can approximate eq. 5.4 well with a single time constant (in the interval of 0-8 picoseconds) to allow for a comparison with the time constant coming from the experiment at the same sugar concentration. Only two parameters, the retardation factor and the hydration shell size, are varied until the calculated water reorientation time constant is in accordance with the experimentally determined values, shown in figure 5.8. The calculated values are shown as solid lines in the same figure. We find an optimal retardation factor of 1.65 ± 0.15, independently of the type of sugar, and hydration numbers of 24 ± 3, 46 ± 5 and 22 ± 3 for glucose, trehalose and sorbitol, respectively.

5.4 DISCUSSION

5.4.1 SOLUTE DYNAMICS

For all investigated sugar solutions, the nonlinear vibrational response of the hydroxyl vibrations can be well described with three spectral components, each with its own vibrational relaxation time constant and associated anisotropy decay. The two components associated with the sugar hydroxyl groups probably do not represent two distinct species of sugar hydroxyl groups but rather

a continuous distribution of vibrational relaxation time constants across the inhomogeneously broadened sugar hydroxyl absorption band. The vibrational lifetime is observed to be significantly shorter in the red wing than in the blue wing of the absorption band. This is a quite general observation [77,99,100] that follows from the fact that both the hydroxyl stretch frequency and the vibrational lifetime decrease with increasing strength of the hydrogen bond donated by the hydroxyl group. The shape and vibrational lifetime of the sugar hydroxyl components are very similar for glucose, trehalose and sorbitol. For sorbitol the two bands are slightly closer in frequency, which suggests that for sorbitol, the relaxation of the OD stretch vibrations is less inhomogeneous than for glucose and trehalose. This might be due to the lower chemical heterogeneity and the greater flexibility of the sorbitol molecule [98] compared to trehalose and glucose.

For all sugars, the anisotropy of the vibrational excitation of the hydroxyl stretch vibrations decays only partially within the experimental time window of ~10 ps. The partial decay indicates that the reorientation of the sugar hydroxyl groups occurs within a finite cone angle. The complete decay of the anisotropy requires the molecular reorientation of the entire sugar molecule, which takes tens of picoseconds [90,92]. The sugar hydroxyl band at lower frequencies (green band in figure 5.7) has a higher and more persistent anisotropy value than the band at higher frequencies. This difference can be explained from the fact that the band at lower frequencies corresponds to more strongly hydrogen bonded hydroxyl groups for which the cone angle will be smaller. The anisotropy decay of the sugar components is not very different for sorbitol compared to glucose and trehalose, which indicates that the flexibility of the backbone of the sugar does not play a role for the hydroxyl reorientation dynamics occurring on a 10 ps time scale. The reorientation on this time scale is thus only governed by the strength of the local hydrogen-bond interaction.

5.4.2 WATER DYNAMICS

For all three sugars we observe a superlinear increase of the water reorientation time with sugar concentration. Based on our modeling of the water reorientation in the sugar hydration shells, we explain this superlinear behavior from a combination of two effects. The first is that the probability for a water molecule to belong to two or more hydration shells strongly increases with concentration. The second is that the reorientation of water molecules belonging to two or more hydration shells is slower than for water molecules belonging to a single hydration shell. In an NMR study of a solution of trehalose in water a similar superlinear increase of the reorientation time with concentration has been observed [90]. This observation was interpreted as the result of water molecules interacting with multiple trehalose molecules, in agreement with our interpretation. A similar trend has been observed with dielectric relaxation (DR) measurements of solutions of glucose in water [89]. In the NMR and the DR measurements the water dynamics are observed to slow down even more strongly with increasing concentration than in our measurements. A possible explanation may be that the NMR and DR results are more sensitive to col-

lective effects on the spin relaxation and the polarization response, whereas the femtosecond infrared experiments probe the reorientation of single hydroxyl groups.

We find that we can describe the increase in average water reorientation time with a model that assigns increasingly slow reorientation times to water molecules in zero, one or two carbohydrate hydration shells. From the model we extract a retardation factor of 1.65 ± 0.15. This retardation factor implies that water molecules that are located within the hydration shell of one sugar molecule reorient 1.65 ± 0.15 times slower compared to water molecules in bulk water, while water molecules within the hydration shell of two sugar molecules reorient 2.7 ± 0.3 times slower again. Obviously, this discrete description of the water reorientation in the vicinity of sugars is an approximation of the actual, more diffuse, water reorientation, but it nonetheless indicates the magnitude and extent of the effect of sugars on the water dynamics in concentrated sugar solutions. Interestingly, the retardation is very similar for the different types of sugars. A similar observation was made using dynamic light scattering measurements[92].

For all investigated sugars, the water reorientation in a solution with a particular sugar concentration can be described with a single reorientation time constant. This time constant increases strongly with increasing sugar concentration, reflecting an overall slowing down of the water reorientation. In contrast to the water dynamics around small amphiphilic molecules[101,102] and salts[77,99], we do not observe a clear distinction between bulk-like water and hydration water. For these solutions, it was found that the reorientation of a fraction of the water molecules is strongly retarded, while the remaining water molecules were observed to reorient with the same time constant as observed for neat water, even at high solute concentrations. For the sugar solutions we do not observe such a bimodal distribution of the reorientation time of the water molecules. This finding indicates that the hydration layer in which the water dynamics are affected is far more diffuse around carbohydrates than around ions or hydrophobic molecular groups. The effect on the dynamics of water thus appears to be longer ranged for sugars than for ions or hydrophobic molecular groups.

The long-range character of sugar molecules on the dynamics of water may find its origin in their large number of hydrophilic hydroxyl groups. These hydroxyl groups will form strong hydrogen bonds with nearby water molecules[94], and thus it has been proposed that the effect of sugars on the dynamics of water scales with the number of hydrogen bonds between the sugar and water[88], or alternatively, with the number of sugar hydroxyl groups[92]. Following this idea, we plotted the water reorientation time constant against the number of sugar hydroxyl groups in figure 5.9A. It is apparent from the figure that the water reorientation time constants we measure do not follow the suggested scaling behavior. Trehalose has a comparatively strong effect on the water dynamics per hydroxyl group, while the effect of sorbitol is relatively weak. This is most apparent at sugar concentrations above 1 molal (trehalose) and 2 molal (glucose, sorbitol).

At higher concentrations, the effect of the overlapping hydration shells be-

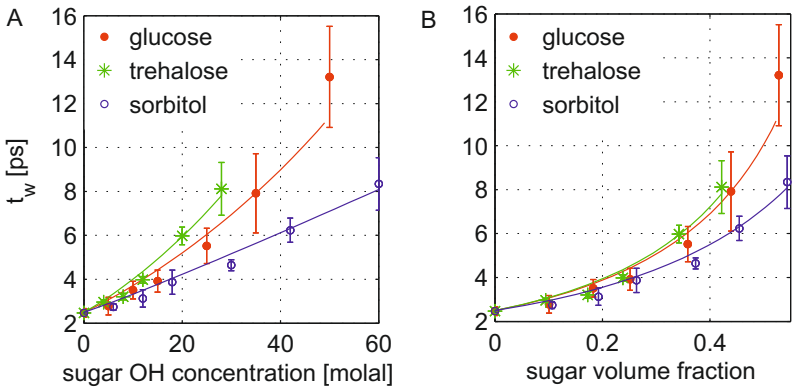

FIGURE 5.9. Water reorientation time constant as a function of (A) concentration of sugar hydroxyl groups and (B) sugar volume fraction.

comes important. In this regime the water dynamics are not only influenced by the hydrogen-bond interactions between the sugar molecules and water, but also by the volume that is left for water in between the sugar solutes. In this limit the volume occupied by the sugar solutes starts to play a role. The molecular weight and volume taken by trehalose are almost 2 times as large as for glucose. If we plot the water reorientation time against the sugar volume fraction, as determined from density measurements (figure 5.9B), we find that the water reorientation time constants in solutions of glucose and trehalose follow almost the same trend up to the highest concentrations.

For sorbitol the effect on the water dynamics is lower than for glucose and trehalose. In modeling the effect of sorbitol on the reorientation, we found that the hydration shell of sorbitol is somewhat smaller than for glucose, in spite of the fact that the molecular masses are nearly the same and sorbitol has 6 hydroxyl groups instead of 5. However, the molecular structure of sorbitol strongly differs from that of glucose and trehalose. The linear flexible structure of sorbitol allows for the formation of intramolecular hydrogen bonds[98], thus reducing the effect on the surrounding water molecules. The less strong effect of sorbitol on the water reorientation dynamics compared to glucose and trehalose thus likely finds its origin in their difference in molecular structure. For sugar molecules of similar structure like glucose and trehalose, the effect appears to scale quite well with the molecular volume, and surprisingly, less well with the number of hydroxyl groups. These findings suggest that the influence of sugars on the dynamics of the surrounding water involves collective structural effects in which the shape and size of the sugar molecule play important roles.

The long-range effects of sugars on the dynamics of water may in turn play a role in their influence on the conformation of proteins. Experiments show that trehalose is the most effective in preserving biomolecules, compared to other sugars, and most notably for concentrations above 1 M.[80] This is the concentration range for which we observe a larger effect of trehalose on the water

dynamics compared to glucose and sorbitol. The present results are therefore in line with an indirect protection mechanism of sugars via the water solvent.

5.5 CONCLUSIONS

We have investigated the molecular reorientation dynamics of water molecules in aqueous solutions of glucose, trehalose and sorbitol. With increasing sugar concentration, the decay of the OD stretch vibration becomes more inhomogeneous, due to an increasing contribution of sugar hydroxyl groups. We separate the contributions of sugar and water hydroxyl groups to the nonlinear vibrational signals using a spectral decomposition model. This allows us to observe the dynamics of water and sugar separately.

We find that the sugar hydroxyl groups only move in a restricted cone angle on the timescale of our experiment. The water reorientation is faster, but strongly slows down with increasing sugar concentration. Interestingly, the water reorientation can be characterized with a single reorientation time constant. We find that the water reorientation time τ_w increases from 2.5 $\pm$ 0.3 to 13 $\pm$ 2 ps for a solution with a glucose concentration of 10 molal, to 8 $\pm$ 1 ps for a solution with a trehalose concentration of 3.5 molal, and to 8 $\pm$ 1 ps for a solution with a sorbitol concentration of 10 molal. The fact that we do not observe a bimodal distribution of the reorientation time of the water molecules, as for aqueous solutions of small amphiphiles and salts, indicates that the hydration layer of sugars is more diffuse and extents over a longer range.

For all three sugars, the water reorientation time increases superlinearly with sugar concentration. We explain this superlinear dependence with the effect of overlapping hydration shells, and describe the water reorientation time with a model that assigns increasingly slower reorientation times to water molecules in zero, one, two or three carbohydrate hydration shells. From the model, we find that for all three studied sugars the retardation factor is 1.65 $\pm$ 0.15. From the model we also find that the hydration shells of glucose, trehalose and sorbitol comprise approximately 24 $\pm$ 3, 46 $\pm$ 5, and 21 $\pm$ 3 water molecules, respectively. A comparison of the effects of the different sugars, suggests that the influence of sugars on the dynamics of the surrounding water involves collective structural effects in which the shape and size of the sugar molecule play important roles.

5.6 APPENDIX: HYDRATION SHELL MODEL

To calculate the probabilities that water molecules belong to 1, 2, 3, or even more hydration shells of sugar molecules, we consider a system containing N_s solute molecules. For each solute molecule the fully filled solvation shell has a volume x (x does not include the volume of the solute) of the total volume, and thus the total volume of the solvation shells in case the shells would not overlap is equal to $N_s x$. The volume x is given by $x = N_h v_w$, where N_h is the number of water molecules in the hydration shell and v_w is the volume of a water molecule

($0.018/N_A$ liter, with N_A Avogadro's number). N_s is equal to N_A times C_M, the solute molar concentration.

To determine the probabilities that a water molecule belongs to a particular number of hydration shells we consider picking N_s times a volume x out of 1 liter of the solution and calculate the probability that a molecule is within at least one of the picked volumes x. We define $a^{(1)} = N_s x$. At every selection a molecule has a chance of x to be chosen, and a chance of $1-x$ not to be chosen. The probability that a molecule is not chosen after choosing N_s times a volume fraction x is equal to $(1-x)^{N_s} = (1-x)^{a^{(1)}/x}$. We arrive at the following probabilities of molecules belonging to 0, 1, 2, 3 solvation shells:

$$\begin{aligned} P^{(1)}(0) &= (1-x)^{N_s} = (1-x)^{a^{(1)}/x} = e^{-a^{(1)}} \\ P^{(1)}(1) &= N_s x(1-x)^{N_s-1} = a^{(1)} e^{-a^{(1)}} \\ P^{(1)}(2) &= \frac{N_s(N_s-1)}{2} x^2 (1-x)^{N_s-2} = \frac{[a^{(1)}]^2}{2} e^{-a^{(1)}} \\ P^{(1)}(3) &= \frac{N_s(N_s-1)(N_s-2)}{6} x^3 (1-x)^{N_s-3} = \frac{[a^{(1)}]^3}{6} e^{-a^{(1)}}, \end{aligned} \tag{5.5}$$

where we used that $x \ll 0$. In general:

$$P^{(j)}(i) = \frac{[a^{(j)}]^i}{i!} e^{-a^{(j)}}, \tag{5.6}$$

where we changed the superscript (1) for the more general superscript (j), indicating the number of the iteration. It should be noted that $a^{(j)} = \sum_{i=0}^{\infty} i P^{(j)}(i)$.

For geometric reasons, a water molecule can only belong to a maximum number of solvation shells, which we define as k. To account for this fact, we redistribute the probabilities of molecules belonging to more than k shells over molecules belonging to less than k shells. This redistribution is performed with a statistical approach, and will again yield non-zero probabilities of molecules belonging to more than k shells. However, the sum of these probabilities will be smaller than in the first calculation. The procedure is repeated until there are only probabilities of molecules belonging to k shells or less. We define an excess volume $a_{ex}^{(j)}$ of $a^{(j)}$ that is contained in molecules belonging to $k+1$ and even more solvation shells. For $j = 1$ the excess volume $a_{ex}^{(1)}$ is given by:

$$a_{ex}^{(1)} = \sum_{i=k+1}^{\infty} (i-k) P^{(1)}(i), \tag{5.7}$$

where the term $(i-k)$ is introduced to account for the fact that a molecule belonging to $i > k$ shells has been chosen $i-k$ times too much. The excess volume $a_{ex}^{(j)}$ has to be redistributed over molecules that belong to less than k solvation shells. As we will calculate the final distribution with an iterative procedure, applying several subsequent calculations of the redistribution of excess volumes $a_{ex}^{(j)}$, we define the distribution $P_c^{(j)}(i)$ as the distribution that results after the j'th iteration. Obviously $P_c^{(1)}(i) = P^{(1)}(i)$.

To calculate the probability distribution of the redistribution of $a_{ex}^{(j)}$ we account for the fact that only molecules belonging to less than k shells can be selected. Hence, we renormalize $a_{ex}^{(j)}$ to the volume from which molecules can be selected in the next $j+1$ selection round:

$$a^{(j+1)} = \frac{a_{ex}^{(j)}}{\sum_{i=0}^{k-1} P_c^{(j)}(i)} \tag{5.8}$$

Substitution of $a^{(j+1)}$ in equation (5.6) yields the distribution function $P^{(j+1)}(i)$ of the excess volume $a_{ex}^{(j)}$. The division by $\sum_{i=0}^{k-1} P_c^{(j)}(i)$ accounts for the fact that the total volume from which molecules can be selected in the $(j+1)$'th round corresponds to the volume of the molecules that have only been selected $k-1$ or less times after the j'th round. The volume taken by these molecules is smaller than the original volume by a factor $\sum_{i=0}^{k-1} P_c^{(j)}(i)$. This means that the probability that a particular molecule is selected from this volume is larger than in the case that the excess volume $a_{ex}^{(j)}$ could have been picked from all molecules. This larger selection probability is expressed in the fact that $a^{(j+1)} > a_{ex}^{(j)}$. The distribution function $P^{(j+1)}(i)$ is used to determine the corrections to the total probability function $P_c^{(j)}(i)$.

Selection of molecules that belong to $P_c^{(j)}(i)$ in the $(j+1)$'th round will lead to a decrease of $P_c(i)$, i.e. of the fraction of molecules belonging to i solvation shells, irrespective of whether these molecules are chosen 1, 2 or more times. On the other hand, $P_c(i)$ will increase if a molecule belonging to $P_c^{(j)}(i-l)$ is selected l times. The probability of selecting a molecule l times from a particular $P_c^{(j)}(i)$ is given by $P^{(j+1)}(l)P_c^{(j)}(i)$. Hence, the redistribution leads to the following expression for the new, corrected fraction $P_c^{(j+1)}(i)$ of molecules belonging to i solvation shells:

$$P_c^{(j+1)}(i) = P_c^{(j)}(i) - P_c^{(j)}(i)\sum_{l=1}^{\infty} P^{(j+1)}(l) + \sum_{l=1}^{i} P_c^{(j)}(i-l)P^{(j+1)}(l), i \leq k \tag{5.9}$$

In case molecules from $P_c^{(j)}(i)$ $(i < k)$ are selected two or more times $(P^{(j+1)}(i \geq 2) \neq 0)$, the redistribution also leads to a non-zero probability of molecules belonging to $i > k$ solvation shells. As the maximum number of solvation shells to which a molecule can belong is defined by k, the probability of belonging to to $i > k$ solvation shells needs to be redistributed over $P_c(i)$ $(i < k)$. This is done in the following manner. First the probability of molecules of belonging to $i > k$ solvation shells is added to $P_c^{(j+1)}(k)$:

$$P_c^{(j+1)}(k) = P_c^{(j+1)}(k) + \sum_{i=0}^{k-1} P_c^{(j)}(i) \sum_{l=k-i+1}^{\infty} P^{(j+1)}(l) \tag{5.10}$$

The excess selections $i > k$ define a new excess volume $a_{ex}^{(j+1)}$ with a magnitude

given by:

$$a_{ex}^{(j+1)} = \sum_{l=2}^{\infty} P^{(j+1)}(l) \sum_{i=k-l+1}^{k-1} (i-k+l) P_c^{(j)}(i) \tag{5.11}$$

The case of $a_{ex}^{(1)}$, as expressed in equation (5.7), applies to the case before any selection was made, i.e. to $P_c^0(0) = 1$ and $P_c^0(i > 0) = 0$. The value of $a_{ex}^{(j+1)}$ evaluated with equation (5.11) is used in equation (5.8) to transfer $a_{ex}^{(j+1)}$ and $P_c^{(j+1)}(i)$ to $a^{(j+2)}$. Next, equation (5.6) is used to calculate the normalized distribution function $P^{(j+2)}(i)$, and equation (5.9) to calculate $P_c^{(j+2)}(i)$. The calculation is repeated until the probability of molecules belonging to $i > k$ solvation shells has become negligibly small ($\sum_i P_c(i > k) \approx 0$) or until all molecules are at least k times selected, meaning that $\forall P_c(i < k) = 0$.

6 Water dynamics in aqueous protein solutions

Proteins perform specific biological functions that strongly depend on their three-dimensional structure that results from the folding of the polypeptide chain. A crucial factor for protein folding is the interaction between the protein and the water solvent. In this chapter, we study the dynamics of water in aqueous solutions of several globular proteins in their native state and at different degrees of temperature and urea-induced unfolding. We observe that a fraction of the water molecules is strongly slowed down by their interaction with the protein surface. The slow water fraction is a measure of the amount of water-exposed surface. In the case of urea-denatured proteins, we observe that the wetted protein surface increases by almost 50%, while the secondary structure is still intact. This finding indicates that protein unfolding starts with the protein structure becoming less tight, thereby allowing water to enter.

6.1 INTRODUCTION

The interaction between proteins and water is crucial for protein folding and stability[23]. However, what happens locally at the protein-water interface at different degrees of unfolding remains largely unexplored. A common technique to observe the process of unfolding is circular dichroism (CD), which is sensitive to the macromolecular structure of the protein[103]. The macromolecular structure of proteins can also be probed with magnetic relaxation dispersion of water ^{17}O, as this technique is very sensitive to the dynamics of the internal water molecules that are released upon unfolding[104,105]. These methods show that the unfolding of globular proteins constitutes a sharp cooperative transition, a property which sets them apart from non-functional random polypeptides. It is unclear, however, what happens at the protein-water interface during unfolding, in particular whether the macromolecular structural transition corresponds to a similarly sharp change in the intermolecular interactions between the water molecules and the protein surface.

The dynamics of water near protein surfaces has been studied with several theoretical and experimental techniques. MD calculations predict that the dynamics of water slow down near protein surfaces, and that the amount of slowing down strongly depends on the protein surface topology[106–109]. NMR studies also find a slowdown effect[104,105,110], but cannot determine the number of slow water molecules and their reorientation rates independently[105]. Time-resolved fluorescence[111,112] and Nuclear Overhauser Effect[113,114] studies find a wide distribution of water reorientation times in the protein hydration layer, but both techniques require the embedding of specific probes in the protein (or protein encapsulation[114]). The experimental information on the properties of the hydration shell of proteins thus remains limited, in particular regarding the number and dynamics of the water molecules that are in direct contact with the protein surface.

In this chapter we study the dynamics of water in aqueous solutions of bovine α-lactalbumin, hen egg-white lysozyme, bovine β-lactoglobulin and bovine serum albumin at different degrees of unfolding, using polarization-resolved femtosecond infrared spectroscopy. We (partially) unfold the proteins by increasing the temperature or adding the denaturant urea.

6.2 EXPERIMENTAL

SPECTROSCOPY The measurements described in this chapter are performed with the single-color setup described in section 3.2. The pump and probe pulses are centered around 2500 cm^{-1}, in resonance with the OD stretch vibration.

SAMPLE PREPARATION Bovine α-lactalbumin (purity >90%, Davisco foods), bovine β-lactoglobulin (purity >90%, mixture of type A and B, Davisco foods), bovine serum albumin (purity >96%, Sigma) and hen egg-white lysozyme (70000 U/mg, Fluka) are used without further purification. Each protein is

dissolved in isotopically diluted water, consisting of 4% D_2O in H_2O. The protein concentrations are determined using their molar extinction coefficient (ϵ) at 280 nm: ϵ=2.01 $g^{-1}cm^{-1}$, 0.958 $g^{-1}cm^{-1}$, 0.6606 $g^{-1}cm^{-1}$ and 2.67 $g^{-1}cm^{-1}$ for α-lactalbumin, β-lactoglobulin, serum albumin and lysozyme respectively. In the experiments with urea, the proteins are dissolved with urea (purity>98%, Sigma-Aldrich) in isotopically diluted water. The solution pH is left unadjusted and ranges between 7.0 and 7.2 for α-lactalbumin and β-lactoglobulin, between 6.6 and 6.8 for serum albumin and between 4.2 and 4.8 for lysozyme, depending on the urea concentration. Control experiments with small added amounts of NaOH or HCl showed that there is no dependence of the water dynamics on pH within this range. All measurements are conducted at 24 °C unless stated otherwise.

6.3 Results and discussion

6.3.1 Vibrational relaxation

Figure 6.1A presents the isotropic transient absorption spectra at different delay times for a concentrated solution of α-lactalbumin in isotopically diluted water. At early delay times, the transient response shows a bleach around 2500 cm^{-1}, due to the fundamental transition of the OD stretch vibration, and an induced absorption at frequencies below 2420 cm^{-1}. These signals decay to the spectral response of a thermal difference spectrum, indicative of a heated ground state. To calculate the anisotropy decay that exclusively represents the reorientation of excited OD stretch vibrations, the transient spectra have to be corrected for the time-dependent heating contribution.

For isotopically diluted water, the vibrational decay and subsequent rise of the heat signal are well described with the cascade model (eq. 4.6), which describes the relaxation of the OD stretch vibrations via an intermediate state to a thermalized, heated ground state[74]. Applying this model to solutions of α-lactalbumin in isotopically diluted water, we find that it very well describes the transient spectral response (solid lines in fig. 6.1A). The extracted vibrational lifetime, T_1, and the thermalization time, T^*, are shown in fig. 6.1D as a function of protein concentration. It can be seen that both times depend only weakly on the concentration of α-lactalbumin. The spectral signatures of the OD vibration and the thermalized ground state do not change with protein concentration.

In case the temperature is increased, the isotropic transient absorption spectrum of α-lactalbumin in isotopically diluted water shifts to higher wavenumbers (fig. 6.1B), reflecting a weakening of the water hydrogen-bond network. Nonetheless, we find that the vibrational relaxation can be described with the cascade model at all temperatures. The temperature-dependent vibrational lifetime and thermalization time are presented in figure 6.1E for a concentrated solution of α-lactalbumin. With increasing temperature, the vibrational lifetime increases, while the thermalization time decreases. This is in agreement with

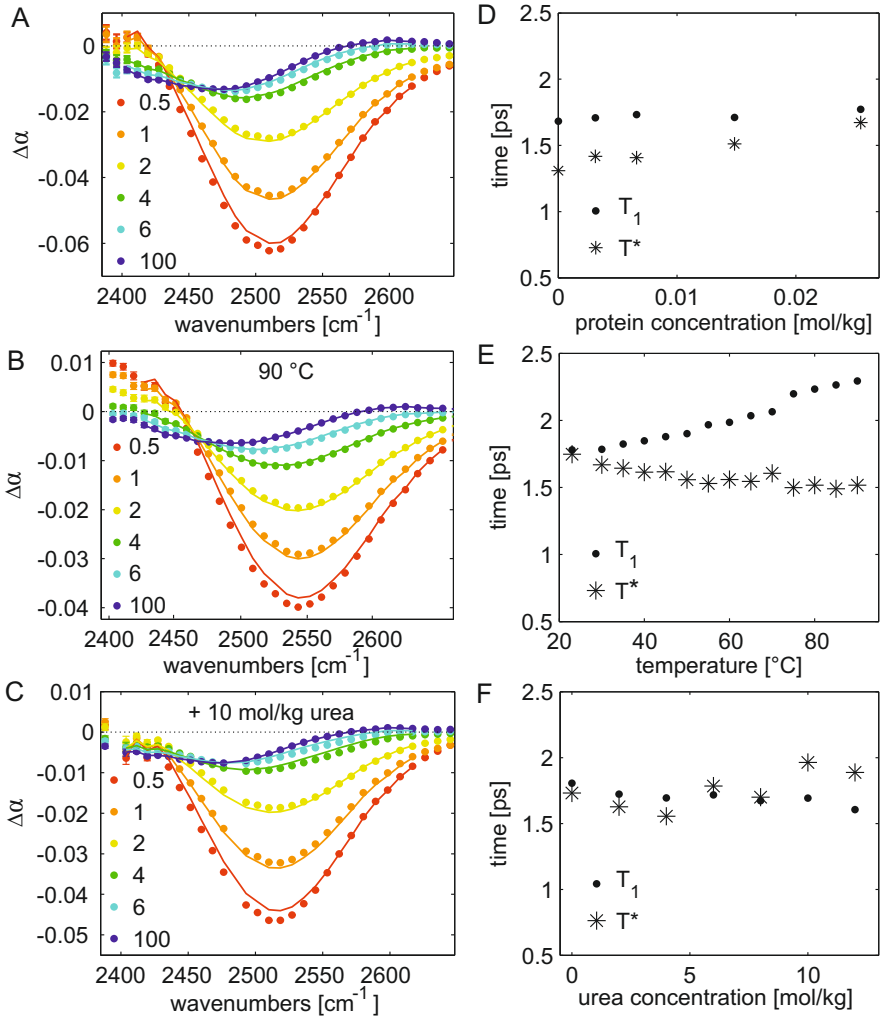

FIGURE 6.1. (A-C) Isotropic absorption change as a function of frequency at different picosecond delay times, for a solution of 0.0255 mol/kg α-lactalbumin in isotopically diluted water (A), for the same solution at 90 °C (B), and for a solution of 0.0255 mol/kg α-lactalbumin in 10 mol/kg urea (C). The solid lines represent the result of a model fit (see text). (D-F) Vibrational lifetimes T_1 and T^* as a function of α-lactalbumin concentration (D), temperature (E), and urea concentration (F).

previous studies on the temperature dependence of the OD stretch vibrational relaxation in neat isotopically diluted water (HOD in H_2O)[115] and in solutions of 1.5 mol/kg tetramethylurea[116]. The increase of the vibrational lifetime likely originates from the blueshift of the OD stretch vibration, which increases the energy gap between the OD stretch vibration and the lower energy vibrational modes to which the OD stretch vibration relaxes.

In case urea is added to a concentrated solution of α-lactalbumin in isotopically diluted water (fig. 6.1C), the spectral signature of the isotropic spectrum stays unchanged. We find that the vibrational relaxation can be described quite well with the cascade model at all urea concentrations. The extracted vibrational lifetime and thermalization time are presented in figure 6.1F. The vibrational lifetime is independent of the urea concentration, in good agreement with results reported earlier on solutions of urea in isotopically diluted water[117]. The thermalization time has a slight tendency to increase with urea concentration, but stays nearly constant as well.

For solutions of lysozyme, β-lactoglobulin and serum albumin in isotopically diluted water we observe similar trends for the vibrational relaxation of the OD stretch vibration. In all cases the relaxation is well described by the cascade model, which allows for an accurate subtraction of the time-dependent heat signal, and subsequent calculation of the OD anisotropy decay.

6.3.2 NATIVE PROTEINS

Figure 6.2A presents the anisotropy decay as a function of delay time for different concentrations of native α-lactalbumin in isotopically diluted water. The presented curve represents an average over the frequency range 2450-2600 cm^{-1}. For water without added protein, the anisotropy decays exponentially with a time constant of 2.45 $\pm$ 0.1 picoseconds. This means that in neat HDO in H_2O, water molecules reorient with this time constant, in good agreement with the value of 2.5 $\pm$ 0.1 picoseconds reported earlier[74]. Addition of α-lactalbumin leads to a slow reorientation component of which the amplitude increases with concentration. The time constant of this slow component is >10 ps. As the experimental time window amounts to 8 picoseconds, this component can be modeled well as an offset in the anisotropy decay. We thus fit the decay of the anisotropy $R(t)$ of the vibrational excitation to a single exponential decay plus an offset: $R(t) = R_0 e^{-t/\tau_r} + R_{slow}$. The fitted reorientation time constant τ_r is 2.45 $\pm$ 0.15 picoseconds for all protein concentrations. The fact that τ_r does not change with protein concentration shows that a fraction of the water molecules reorients as in neat water, even for highly concentrated protein solutions.

Figure 6.3A shows the slow water fraction, given by the offset R_{slow}, as a function of α-lactalbumin concentration. The slow water fraction increases linearly with the protein concentration in mol/kg. Hence, we can calculate the number of slowly reorienting water molecules per protein molecule from the slope of R_{slow} against the protein concentration c, multiplied by the number of

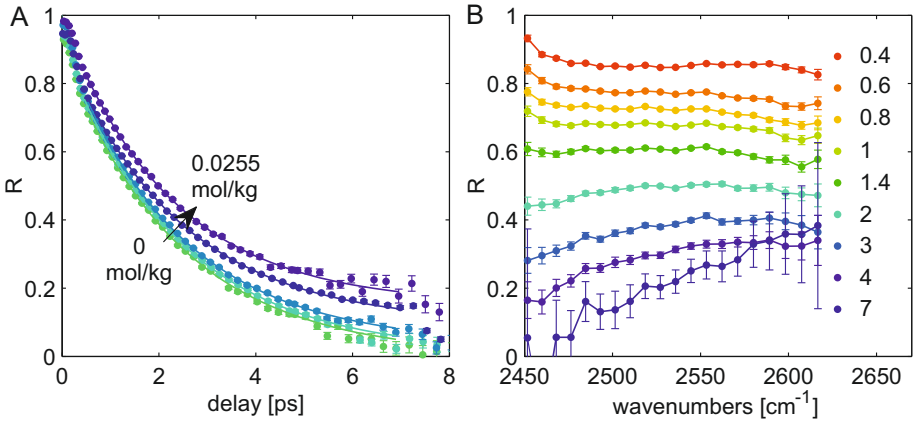

FIGURE 6.2. (A) Anisotropy decay of the OD stretch vibration for solutions of α-lactalbumin in isotopically diluted water with concentrations up to 0.0255 mol/kg, averaged over the frequency range 2450-2600 cm^{-1}. The solid lines are fits to a single exponential decay plus an offset R_{slow}. (B) Anisotropy decay for 0.0255 mol/kg α-lactalbumin in isotopically diluted water as a function of frequency at different picosecond delay times. All curves are divided by 0.4.

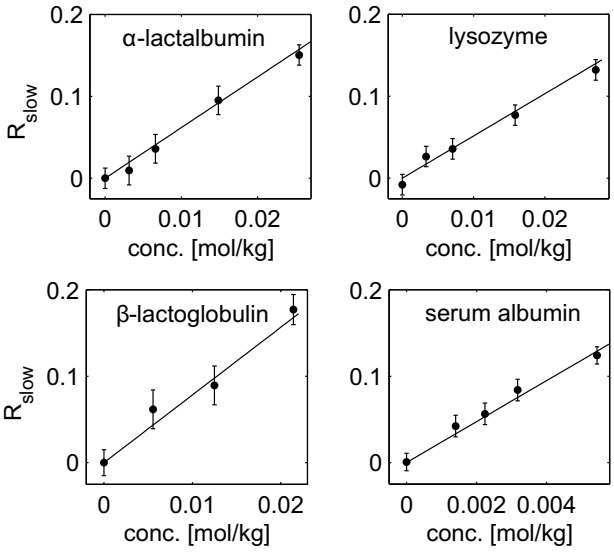

FIGURE 6.3. Slow water fraction R_{slow} obtained from the fit to the anisotropy decay, as a function of the protein concentration, for the proteins α-lactalbumin, lysozyme, β-lactoglobulin and serum albumin.

moles of water in a kilogram (which is 55.257 for 4% D_2O in H_2O):

$$N_{slow} = \frac{R_{slow}}{c} \cdot 55.257 \tag{6.1}$$

It follows that on average 342 ± 20 water molecules are strongly slowed down in their reorientation per α-lactalbumin molecule. For solutions of lysozyme, β-lactoglobulin and serum albumin in isotopically diluted water we observe a distinct slow component in the anisotropy dynamics as well, that corresponds to the slow water fractions as shown in fig. 6.3. From the slow water fraction, we calculate that 292 ± 20, 433 ± 20 and 1310 ± 150 water molecules are slowed down per lysozyme, β-lactoglobulin and serum albumin molecule, respectively.

The slow component of the anisotropy decay will also contain a small contribution of protein hydroxyl groups. The number of protein OH groups can be exactly calculated from the protein sequence and amounts to 38, 29, 45 and 180 for α-lactalbumin, lysozyme, β-lactoglobulin and serum albumin, respectively. This is a small amount compared to the measured number of slow waters, which correspond to 684 ± 40, 584 ± 40, 866 ± 40, and 2620 ± 300 slow OD groups. Assuming that all protein hydrogens can exchange with water, and that the anisotropy decay of these groups is infinitely slow, we can thus calculate the maximum contribution of the protein OH groups to the slow fraction R_{slow} of the anisotropy decay: this is about 5% for all studied proteins, which is smaller than the error bar of the amplitude of R_{slow}.

The number of slowly reorienting water molecules per protein molecule is proportional to the number of water molecules in the first hydration layer of the protein. This hydration number can be estimated by computing the solvent accessible surface area of the protein (with a probe radius of 1.7 Å)[118], where the protein structure is obtained with crystallography, and dividing this surface by 10.75 $Å^2$ (the mean surface area per water molecule)[90,119]. With this approach, we calculate hydration numbers of 629, 610, 769 and 2335 for α-lactalbumin, lysozyme, β-lactoglobulin and serum albumin, respectively (see table I). This implies that the number of slow water molecules corresponds to about half the water molecules in the first hydration layer of the protein, which suggest that the effect of the proteins on the reorientation dynamics of water is quite local.

The hydration layer can be subdivided into water molecules hydrating hydrophilic and hydrophobic groups (table I). Previous femtosecond infrared and

TABLE I. Number of slowly reorienting water molecules N_{slow} and the number of water molecules in the first hydration layer of the protein N_h (calculated according to refs[118,119]).

	N_{slow}	N_h (N_h hydrophobic)
bovine α-lactalbumin	342 ± 20	629 (367)
hen egg-white lysozyme	292 ± 20	610 (335)
bovine β-lactoglobulin	433 ± 20	769 (476)
bovine serum albumin	1310 ± 150	2335 (1560)

dielectric relaxation experiments on small amphiphilic molecules showed that hydrophobic methyl groups have a stronger slowing down effect on the reorientation of nearby water molecules than hydrophilic groups [101,102]. One can therefore expect that the local water reorientation dynamics are mainly governed by the exposed hydrophobic part of the protein surface. This agrees well with the present observations. Comparing the hydration numbers for lysozyme and α-lactalbumin, two proteins with very similar secondary and tertiary structures [120], the difference in the number of slow water molecules (292 ± 20 versus 342 ± 20) agrees within error bars with the calculated number of waters hydrating hydrophobic groups of the protein (335 versus 367).

To further investigate the nature of the slow water molecules hydrating the protein, we measure the frequency dependence of the anisotropy decay, which is shown in fig. 6.2B for a concentrated solution of α-lactalbumin in isotopically diluted water. It is seen that the anisotropy decays slower at high frequencies than at low frequencies. This frequency dependence is absent for neat water and becomes more apparent with increasing protein concentration. We observe a similar frequency dependence of the anisotropy decay for solutions of lysozyme, β-lactoglobulin and serum albumin. Since this frequency dependence is not observed for solutions of small amphiphilic solutes [101,102], it likely originates from the three-dimensional folded protein structure. A higher vibrational frequency of the water OD stretch vibration corresponds to a weaker donated water hydrogen bond. Thus, the water molecules that are most strongly slowed down by the protein form on average weaker hydrogen bonds. This combination of weak hydrogen bonding and slow reorientation is characteristic for confined water molecules. It was demonstrated by Laage and Hynes that water molecules reorient by rapidly switching hydrogen-bond partners [13]. The reorientation rate of a water molecule is thus strongly determined by the rate at which a bifurcated hydrogen-bond configuration can be formed, since this configuration forms the transition state for reorientation. The formation of this configuration requires the approach of another water molecule which will be hindered near surfaces and in nanoconfinement, thus leading to a slowing down of the reorientation compared to bulk water. This indicates that the slow water is located in nanopockets of the protein and in grooves on the protein surface, in agreement with the results of MD simulations [106–109].

6.3.3 HEAT-DENATURED PROTEINS

As we have established that a fraction of the water is slowed down by interacting with the surface of native proteins, we can study how this fraction changes upon protein unfolding. We first unfold the proteins by increasing the temperature. Figure 6.4 presents the anisotropy decay for concentrated solutions of α-lactalbumin and lysozyme in isotopically diluted water at different temperatures (we did not record temperature-dependent spectra for the other proteins). With increasing temperature, the anisotropy decay speeds up and the slow water fraction decreases. To quantify this trend, we again fit the anisotropy decay to a single exponential with an offset. The result is shown as solid lines in figure

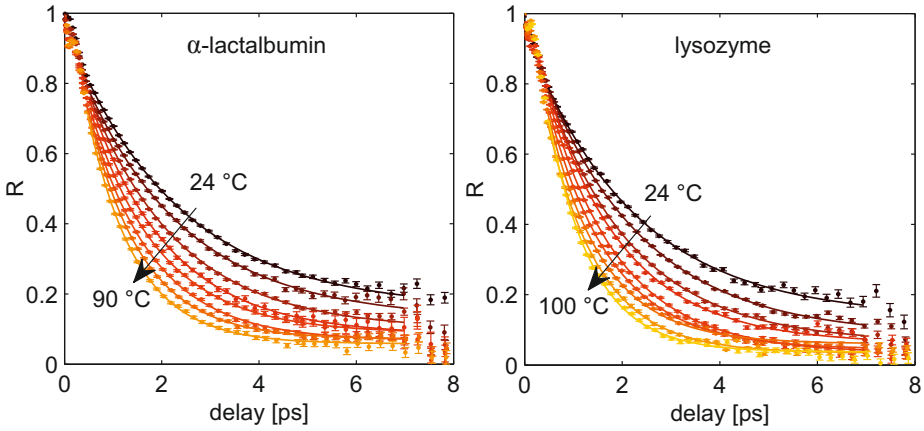

FIGURE 6.4. Anisotropy decay of the OD stretch vibration for 0.0255 mol/kg α-lactalbumin and 0.0248 mol/kg lysozyme in isotopically diluted water at different temperatures, averaged over a frequency range of 150 cm^{-1}. The solid lines are fits to a single exponential decay plus an offset R_{slow}. All curves are divided by 0.4.

6.4 and the extracted parameters are presented in figure 6.5. We find that the reorientation time decreases with increasing temperature. Assuming that the water reorientation is an Arrhenius-type activated process, we can describe the temperature dependence of the reorientation by $\tau_r \propto e^{-E_{act}/k_B T}$. Here E_{act} is the activation energy for reorientation, k_B is Boltzmann's constant and T is the temperature (in Kelvins). The Arrhenius fit is indicated by the solid line in fig. 6.5A and corresponds to an activation energy of 11 $\pm$ 1 kJ/mol. This is in excellent agreement with previous results on the activation energy of bulk water reorientation [102,116]. The fact that τ_r follows the same temperature dependence as neat water confirms again that a fraction of the water molecules reorients as in neat water, even for highly concentrated protein solutions.

Figure 6.5B presents the slow water fraction as a function of temperature. With increasing temperature, the slow water fraction decreases gradually for both α-lactalbumin and lysozyme. There is no clear change of the slow water fraction at the protein denaturation temperature; in fact, even though α-lactalbumin unfolds around 65 °C and lysozyme unfolds around 80 °C [120], the temperature dependence of the slow water fraction is quite similar for both proteins. This similarity indicates that not only the protein fold changes with temperature; the effect of the protein surface on the water reorientation dynamics changes as well, and this effect might dominate. Previous dielectric relaxation and NMR experiments on small amphiphilic molecules showed that fewer water molecules are slowed down by hydrophobic groups with increasing temperature [102,119] (in the current investigated temperature range [119]). Here we observe that this is the case for α-lactalbumin and lysozyme as well.

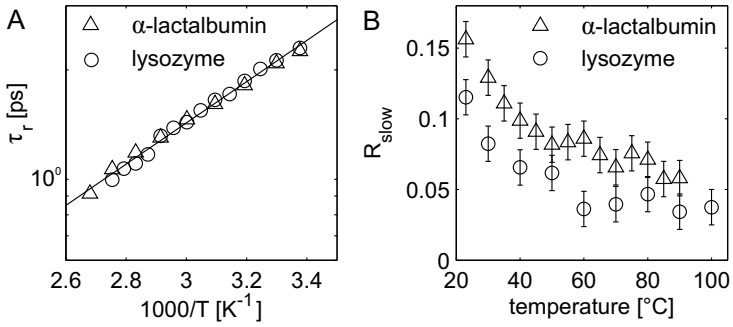

FIGURE 6.5. (A) Reorientation time and (B) slow water fraction R_{slow}, obtained from the fit to the anisotropy decay as a function of (inverse) temperature. The solid line in (A) indicates an Arrhenius-type fit.

6.3.4 UREA-DENATURED PROTEINS

Proteins can also be unfolded by adding urea, which is a well-known and widely used protein denaturant. Figure 6.6 presents the anisotropy decay for a concentrated solution of α-lactalbumin in isotopically diluted water with different amounts of added urea. With increasing concentration of urea, the fraction of slow water increases. To quantify this finding, we again fit the anisotropy to a single exponential decay plus an offset. We find that the reorientation time of the bulk-like water fraction remains 2.45 $\pm$ 0.15 picoseconds at all urea concentrations, while the amplitude of the slow water fraction increases by a maximal factor of 2.5, as shown in the inset of figure 6.6A.

Since urea itself has a very small effect on the dynamics of water[117], the increase in slow water fraction results from a change in the spatial structure of the protein that leads to higher exposure of protein surface to water. A higher exposure of the protein surface to water could also imply a higher accessibility for urea. However, the accumulation of urea at the protein interface would lower the amount of water interacting with the protein[39,42,121], which would in fact lead to a decrease of the slow water fraction. The fact that we observe an increase of the slow water fraction with urea concentration shows that there is no strong accumulation of urea at the surface of the unfolding protein.

To investigate the nature of the slow water molecules, we measured the frequency-dependence of the anisotropy decay, presented for a concentrated solution of α-lactalbumin in 10 mol/kg urea in figure 6.6B. Just as in the case without any added urea, the anisotropy decays slower at high frequencies compared to low frequencies. Comparing fig. 6.6B with fig. 6.2B, we observe that the frequency dependence is enhanced at high urea concentration, which indicates that the larger fraction of slowly reorienting water molecules has weak hydrogen bonds, which implies that these molecules are still located in nanopockets or grooves of the largely unfolded protein.

The slow water fraction shows a quite different dependence on the urea

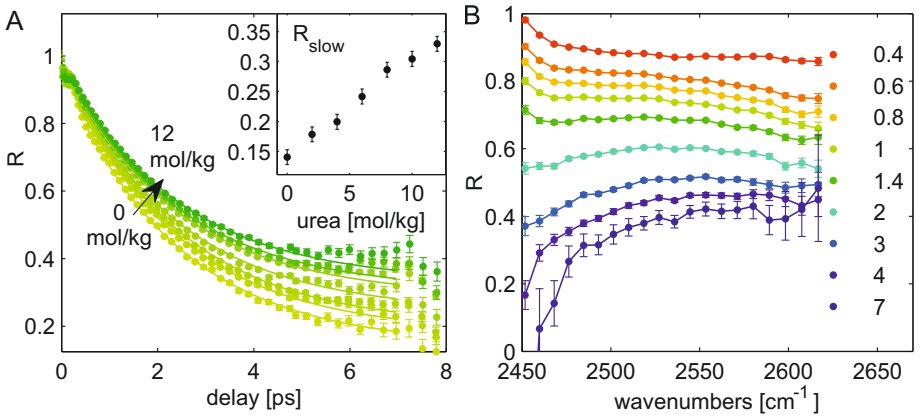

FIGURE 6.6. (A) Anisotropy decay of the OD stretch vibration for 0.0255 mol/kg α-lactalbumin in isotopically diluted water with different concentrations of added urea, averaged over the frequency range 2450-2600 cm^{-1}. The solid lines are fits to a single exponential decay plus an offset R_{slow}. The inset shows R_{slow} as a function of urea concentration. (B) Anisotropy decay for 0.0255 mol/kg α-lactalbumin in 10 mol/kg urea solution as a function of frequency at different picosecond delay times. All curves are divided by 0.4.

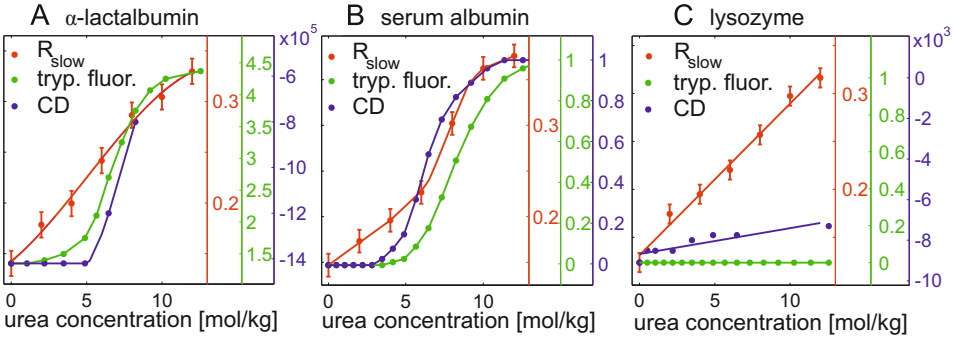

FIGURE 6.7. Comparison between different probes of unfolding. The slow water fraction, the intrinsic tryptophan fluorescence [122–124] (a.u.) and the CD signal [124–127] at 222 nm (deg·cm^2/dmol or a.u.) for (A) α-lactalbumin, (B) serum albumin and (C) lysozyme in urea solutions as a function of urea concentration.

concentration than the change in secondary structure that is characteristic for unfolding, and that is observed with CD and fluorescence techniques. This can be clearly seen in figure 6.7, where we present the slow water fraction and the CD and tryptophan fluorescence signals as a function of the urea concentration for α-lactalbumin, serum albumin and lysozyme. For all proteins, the slow water fraction increases already at low urea concentrations and continues to increase up to 12 mol/kg urea. At a urea concentration of $\sim$10 mol/kg, the slow water fraction starts to saturate for α-lactalbumin and serum albumin, indicating that the unfolding transition is almost complete. In contrast, both the CD and tryptophan fluorescence signals hardly change at low urea concentrations and then show a relatively abrupt transition at a urea concentration of $\sim$7 mol/kg (or, in the case of lysozyme, no transition at all, as lysozyme does not fully unfold even at high urea concentrations). We thus find that the exposure of the protein surface to water is a much more gradual process than the change in macromolecular structure as monitored by CD or by the fluorescence response of tryptophan residues. Hence, at mild denaturation conditions the protein is already more accessible to water, even though the secondary structure is still intact. This is illustrated schematically in fig. 6.8.

A higher accessibility of the protein to water can be either dynamical or the result of expansion of the protein. Expansion of the protein would lead to an increase of the hydrodynamic volume. For a large number of globular proteins in their native and partially unfolded states it was found that the hydrodynamic volume and secondary structure content are strictly related; they change simultaneously[128]. Pulsed field gradient NMR measurements and ion exchange chromotography show that the hydrodynamic radii of lysozyme[129,130], α-lactalbumin[131] and serum albumin[132] hardly increase at low urea concentrations, which is thus consistent with the lack of change in secondary structure as monitored by circular dichroism. These results together indicate that proteins do not show a well-defined expansion at low urea concentrations, but rather that they become less tight, showing larger conformational fluctuations and thus dynamical access to water molecules. This notion is consistent with amide hydrogen exchange studies, where very slow hydrogen exchange indicates stable protein backbone hydrogen-bonding structure and low solvent accessiblity. α-lactalbumin forms a molten globule at mild denaturing conditions[133], which is a conformational ensemble of compact states[134,135] with native-like secondary structural motifs but no specific tertiary structure. The molten globule has faster hydrogen exchange with water[134,136]. Lysozyme does not form a clear equilibrium molten globule like α-lactalbumin[137], however, in the refolding pathway of lysozyme similar states with fast hydrogen exchange are observed[138].

Previous studies showed that for many proteins, equilibrium unfolding intermediates are identical to kinetic unfolding intermediates in terms of their secondary and tertiary structure content, hydrogen exchange protection, collision cross section and stability towards unfolding[139–144]. Hence, mild denaturation conditions can be associated with earlier stages of unfolding. This means that our observation that proteins become more accessible to water at low urea con-

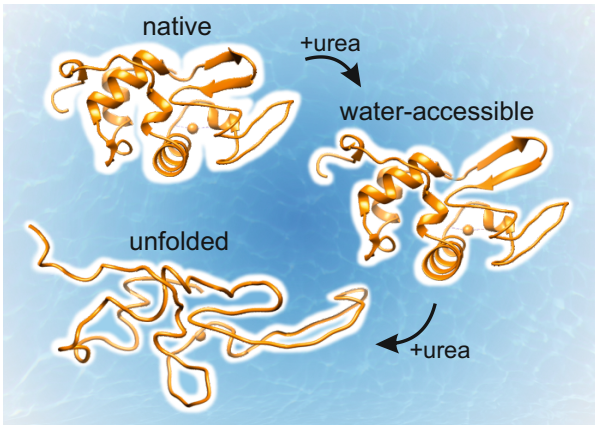

FIGURE 6.8. Schematic picture of protein unfolding, illustrating the transition from native protein (top) to protein at low urea concentration (middle), to denatured protein (bottom). At low urea concentrations, the protein is more accessible to water while the secondary structure is still intact.

centrations indicates that unfolding starts with the protein becoming less tight, allowing water to enter.

6.4 CONCLUSIONS

We have investigated the reorientation dynamics of water in solutions of globular proteins at different degrees of unfolding. A fraction of the water molecules is strongly slowed down by their interaction with the protein surface. This fraction amounts to about half of the water molecules in the first hydration shell of the protein. These slow water molecules have on average weaker hydrogen bonds, which implies that they are located in pockets or grooves on the protein surface.

With increasing temperature, the fraction of strongly slowed down water molecules gradually decreases, which can be explained from the weakening of the effect of hydrophobic groups on the dynamics of water with increasing temperature.

At a constant temperature, the slow water fraction is a measure of the amount of water-exposed surface. In the case of urea-denatured proteins, we observe that the water-exposed protein surface increases by almost 50%, while the secondary structure is still intact. This finding indicates that protein unfolding starts with the protein structure becoming less tight, thereby allowing water to enter.

7 Hydration of antifreeze glycoproteins

Antifreeze glycoproteins (AFGPs) have the ability to inhibit the growth of ice by a mechanism that is not fully understood. In this chapter we study the dynamics of water in aqueous solutions of small and large isoforms of antifreeze glycoproteins. We find that a fraction of the water molecules is strongly slowed down by the interaction with the antifreeze protein surface. The fraction of slow water molecules scales with the size and concentration of AFGP, and is similar to the fraction of slow water observed for non-antifreeze proteins, both at room temperature and close to biologically relevant working temperatures. We find that inhibiting AFGP antifreeze activity using borate buffer induces no changes in the dynamics of water hydrating the AFGP. Our findings support a local mechanism in which the sugar unit of AFGP forms the active ice-binding site.

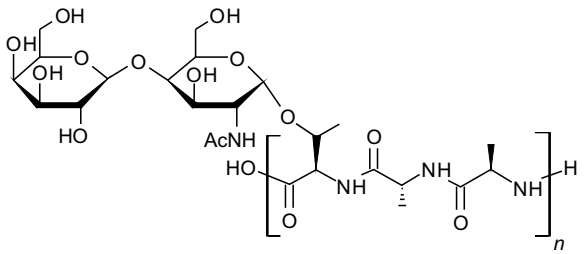

FIGURE 7.1. Chemical structure of a typical antifreeze glycoprotein (AFGP) repeat; $n = 4 - 50$.

7.1 INTRODUCTION

Antifreeze proteins (AFPs) and antifreeze glycoproteins (AFGPs) are classes of proteins that suppress ice crystal growth in organisms, thereby enabling their survival in freezing and subfreezing habitats [145,146]. The success of AF(G)Ps as an efficient protection against freezing can be witnessed by their wide distribution among biological kingdoms. AF(G)Ps from different species have evolved independently and show a great diversity in structures. Despite their structural heterogeneity, all AF(G)Ps are believed to work via an adsorption-inhibition mechanism in which the proteins recognize and irreversibly bind to embryonic ice crystals and prevent the macroscopic ice growth [145].

Among all identified AF(G)Ps, AFGPs play a unique role. AFGPs were the first antifreeze proteins discovered and are subject to considerably less structural variations than AFPs. A typical AFGP consists of the repeating tripeptide unit (alanyl-alanyl-threonyl) in which the secondary hydroxyl group of the threonine residue is glycosylated with the disaccharide β-D-galactosyl-(1,3)-α-D-N-acetylgalactosamine, as shown in figure 7.1. The molar mass of AFGPs varies between 2.6 and 33.7 kDa, which corresponds to 4 to 50 repetitions of the glycosylated tripeptide unit. The AFGP isoforms can show minor sequence variations and are typically grouped into size classes, with $AFGP_1$ representing the largest and $AFGP_8$ the smallest.

Interestingly, neither the solution structure nor the ice-binding site of AFGPs have been identified conclusively [147,148]. Another property of AFGPs that is far from being understood is their tremendous capacity to inhibit ice recrystallization (IRI), a process that is highly relevant for several industries and medical applications. AFGPs prevent the growth of large ice crystals at the expense of small ones (i.e. Ostwald ripening) several magnitudes better than any other AFP or other ice recrystallization inhibitor [149,150].

AFPs and AFGPs have a high specific affinity for the solid phase of water over the liquid form that is usually present in vast excess. It is now widely accepted that the capacity of many AFPs to bind to ice involves the hydration shell of the AFPs as an active player. Direct experimental evidence for the active involvement of water molecules in the mode of action of AFPs was found in the X-ray crystal structures of several AFPs [151,152] and in advanced spectro-

scopic studies[153], which identified preordered ice-like water layers around the active ice-binding site (IBS) of AFPs, even at room temperature. These findings are consistent with the hypothesis that some AFPs bind to ice because their hydration shell can fit into the ice lattice on a particular crystal face. Molecular dynamic simulations confirmed these findings for most classes of AFPs[154–157].

For AFGPs, the involvement of hydration water is less clear. A specialized hydration shell is not necessarily expected for the AFGPs, as the hydroxyl groups of the AFGP sugar moieties have a spatial orientation that appears to match to oxygens on the prism plane and thus bind directly to the ice lattice[158]. Early viscosity, translational diffusion, and NMR experiments showed that the amount of water affected by AFGPs is not significantly different from the amount of water affected by other glycoproteins[148]. However, terahertz spectroscopy[159] and MD simulations[160] provided evidence for a considerable long-range effect of AFGPs on the dynamics of hydration water that seems to correlate with antifreeze activity.

In this chapter, we study the hydration dynamics of large ($AFGP_{1-5}$) and small ($AFGP_{7-8}$) isoforms of antifreeze glycoproteins. To this end, we use polarization-resolved femtosecond infrared spectroscopy, which directly measures the picosecond reorientation dynamics of water molecules. We perform experiments both at room temperature and at temperatures close to the biologically relevant working temperature of the protein. We also investigate the effect of the inhibitor borate on the interaction between AFGPs and water.

7.2 EXPERIMENTAL

SAMPLE PREPARATION Antifreeze glycoprotein is purified from the blood of the antarctic notothenioid toothfish, Dissostichus mawsoni, as previously decribed[161]. Bovine α-lactalbumin (purity>90%, Davisco foods) and lactose (purity>99.5%, Sigma Aldrich) are used without further purification. The proteins and sugar are dissolved in isotopically diluted water, consisting of 4% D_2O in H_2O, or in isotopically diluted borate buffer, consisting of the same water mixture plus 0.3M boric acid (purity>99.97%) and ∼0.25M NaOH to adjust the pH to 9.0. The α-lactalbumin concentration is determined photometrically by the molar extinction coefficient at 280 nm, ϵ=2.01 $g^{-1}cm^{-1}$.

SPECTROSCOPY The measurements described in this chapter are performed with the single-color setup described in section 3.2. The pump and probe pulses are centered around 2500 cm^{-1}, in resonance with the OD stretch vibration. We measured linear infrared spectra using an FTIR spectrometer (Bruker Vertex 80v) with a single reflection diamond ATR crystal.

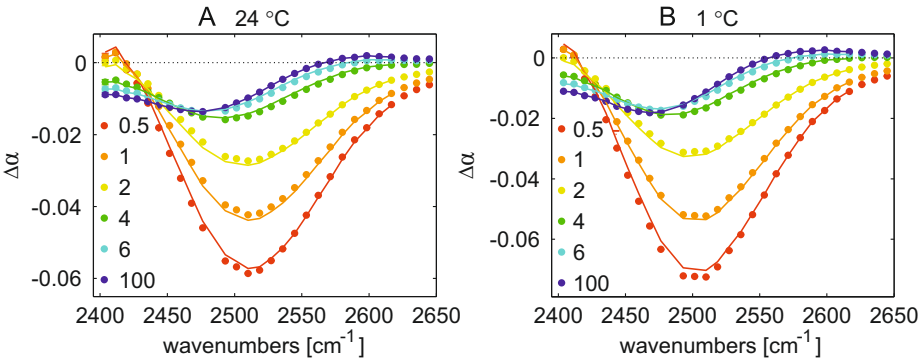

FIGURE 7.2. Isotropic absorption change as a function of frequency at different picosecond delay times, for a solution of 20 wt% $AFGP_{7-8}$ in isotopically diluted water, at (A) 24 °C and (B) 1 °C. The solid lines represent the result of a model fit (see text).

7.3 RESULTS

7.3.1 VIBRATIONAL RELAXATION

In figure 7.2A we present the isotropic absorption change at different delay times for a concentrated solution of $AFGP_{7-8}$ in isotopically diluted water. At short delay times, we observe the typical spectral response of the OD stretch vibration in isotopically diluted water: a bleach around 2500 cm^{-1} and an induced absorption below 2420 cm^{-1}. As the excited OD stretch vibrations decay back to the ground state, this signal is replaced by the thermal difference spectrum due to heating of the sample. We describe the vibrational relaxation in AFGP solutions with the same cascade model (eq. 4.6) that was used for neat isotopically diluted water[74] and for solutions of globular proteins in isotopically diluted water (chapter 6), where the excited OD vibrations relax via an intermediate state to the thermalized ground state. The result of the model fit is indicated with the solid lines in fig. 7.2, and is in good agreement with the data. The spectral signature and lifetime of the OD stretch vibration do not change with respect to neat isotopically diluted water, while the thermalization time increases slightly from a value of 1.3 ps to 1.8 ps upon addition of 20 wt% $AFGP_{7-8}$. We observe the same trends at 1 °C (fig. 7.2B), and for solutions of the larger isoform $AFGP_{1-5}$.

Having determined the time-dependence of the heat signal, we correct the transient spectra at all delay times for the isotropic heating contribution. The anisotropy decay of the corrected spectra exclusively represents the reorientation of the OD vibrations.

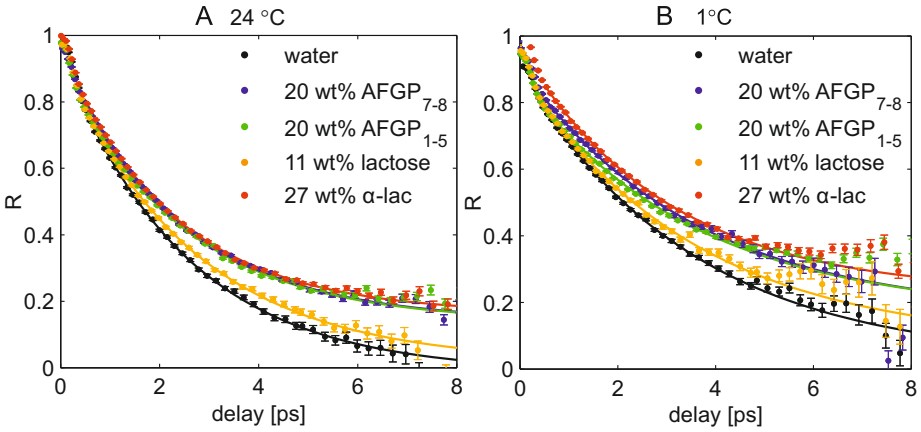

FIGURE 7.3. Anisotropy decay of the OD stretch vibration for isotopically diluted water, and for solutions of 20 wt% $AFGP_{7-8}$, 20 wt% $AFGP_{1-5}$, 11 wt% lactose and 27 wt% α-lactalbumin in isotopically diluted water, at 24 °C (A) and 1 °C (B). The anisotropy is averaged over the frequency range 2450-2600 cm^{-1} and divided by 0.4. The solid lines are fits to a single exponential with an offset R_{slow}.

7.3.2 HYDRATION DYNAMICS OF AFGPS

Figure 7.3A presents the anisotropy decay for water and aqueous solutions of $AFGP_{7-8}$, $AFGP_{1-5}$, lactose and α-lactalbumin at room temperature (24 °C). For pure water, the anisotropy decays exponentially with a time constant of 2.45 ± 0.15 ps. This means that water molecules reorient on a 2.45 ps timescale, as reported earlier[74,162]. Upon the addition of proteins to the solution, an additional slow component appears in the anisotropy decay. Since the time constant of this component is larger than our experimentally accessible time window of 8 ps, we can model this component as an offset. Hence, we fit the anisotropy decays measured for the different solutions with the following expression: $R(t) = R_0 e^{-t/\tau_r} + R_{slow}$. The results are shown as solid lines in figure 7.3.

For all AFGP solutions, we find that the time constant τ_r of the exponential component stays within 2.45 ± 0.15 ps, which means that the water molecules that are not contained in the slow component reorient with the same rate as in bulk water. Using the experimentally determined slow fraction R_{slow}, and the protein concentration c (in mol/kg), we can calculate the average number of slow hydroxyl groups per tripeptide repeat N_{slow}:

$$N_{slow} = \frac{R_{slow}}{c \cdot N} \cdot 110.514 \tag{7.1}$$

where N is the number of repeats and 110.514 is the number of moles of water hydroxyl groups in a kilogram (for 4% D_2O:H_2O). We find an average of 35 ± 6 slow hydroxyl groups per AFGP tripeptide repeat for both the smaller and larger AFGPs, indicating that the local water dynamics are similar for the

different AFGP isoforms.

The 35 ± 6 slow hydroxyl groups per AFGP repeat unit may represent water molecules being slowed down by the amino acid residues, water molecules slowed down by the sugar unit, and the response of the hydroxyl groups of the sugar unit itself. To get an estimate of the latter two contributions, we measured the water reorientation dynamics in solutions of the sugar lactose. Lactose contains the same β-D-galactopyranosyl group as the AFGP sugar moiety, and its concentration is chosen such that it matches the concentration of AFGP sugar groups by weight. As seen in figure 7.3A, the anisotropy decay for the lactose solution shows only a moderate slowdown compared to bulk water; the slow water fraction is much smaller than the slow water fraction that is observed for AFGP solutions. This observation indicates that most of the water molecules that exhibit slow reorientation dynamics in AFGP solutions are not slowed down by the AFGP sugar groups, but rather by the AFGP peptide backbone. The reorientation time for the lactose solution is 2.65 ± 0.15 ps, which means that most water molecules reorient only slightly slower than in bulk water. The anisotropy offset observed for the lactose solutions corresponds to 12 ± 4 slowly reorienting hydroxyl vibrations, which can in part be associated with slow water molecules and in part be associated with the hydroxyl groups of the lactose itself. This result implies that the 35 ± 6 slow hydroxyl groups that are slowed down in their reorientation per AFGP repeat unit largely represent water molecules that are slowed down by the three amino acid residues of this unit. We thus conclude that a total number of ∼23 hydroxyl groups are slowed down by the three amino acid residues (corresponding to ∼4 water molecules per residue), and that the remaining 12 slow hydroxyl groups are associated with water slowed down by the sugar unit and the response of the sugar unit itself. It should be noted that the above description of the effect of sugars on the reorientation dynamics of water differs from the description we presented in chapter 5. The measured anisotropy decay for solutions of lactose is very similar to the anisotropy decay for solutions of trehalose, but here we use a simpler description of the anisotropic response to enable a direct comparison of the response of the sugar unit with that of the three amino acid residues of the AFGP repeat unit.

We also compare the slow reorientation component of AFGP solutions with that of other protein solutions. For the non-glycosylated protein α-lactalbumin, we find a reorientation time constant of 2.45 ± 0.15 ps, and an offset that corresponds to 16.5 ± 1.2 slowly reorienting hydroxyl groups per 3 amino acid residues, equivalent to 2.75 ± 0.2 slow water molecules per residue for the protein in its folded state, in agreement with the findings in chapter 6. In its unfolded state, 4.6 ± 0.5 water molecules are slowed down per amino acid residue of α-lactalbumin (chapter 6). The latter number is close to the 4 water molecules per residue that are slowed down by the AFGP peptide backbone. The small difference can be explained from the somewhat larger average size of the amino acid side-chains of α-lactalbumin.

We further studied the water reorientation dynamics in the same solutions at 1 °C (fig. 7.3B), a temperature that is close to the biologically relevant working

TABLE I. Number of slowly reorienting hydroxyl groups N_{slow} per AFGP tripeptide repeat unit, per 3 amino acid residues (for α-lactalbumin) or per molecule (for lactose), at 24°C and 1°C.

	N_{slow} at 24°C	N_{slow} at 1°C
$AFGP_{7-8}$	35 ± 6	40 ± 6
$AFGP_{1-5}$	35 ± 6	38 ± 6
Lactose	12 ± 4	18 ± 6
α-lactalbumin	16.5 ± 1.2	24 ± 9
α-lactalbumin unfolded (in 12 mol/kg urea)	28 ± 3	-
$AFGP_{7-8}$ + borate	35 ± 6	37 ± 6

temperature of AFGPs. At 1 °C, the anisotropy of pure water decays with a time constant of 3.5 ± 0.3 ps for water. This reorientation time constant stays the same for all solutions. The number of slow hydroxyl groups per repeat unit, presented in table I, is clearly higher at 1 °C compared to 24 °C, but follows the same trend when comparing different protein and sugar solutions. Consequently, the effect of AFGPs on the dynamics of water depends on temperature in the same way as the effect of non-antifreeze proteins and sugars.

7.3.3 THE EFFECT OF BORATE

To investigate further whether the dynamics of hydration water are correlated with antifreeze activity, we inhibit the antifreeze activity by adding borate. Borate molecules can bind reversibly to diol-containing compounds such as sugars, and it has been suggested that borate interacts with AFGP by binding to the cis-hydroxyl groups of the β-D-galactopyranosyl group. This binding greatly reduces the antifreeze activity[163,164]. Figure 7.4 presents the anisotropy decay for solutions of the smaller isoform $AFGP_{7-8}$ in water and in 0.3 M borate buffer, at 1 °C and 24 °C. At both temperatures, we find that the addition of borate does not change the anisotropy decay within the error bars. Thus we conclude that the loss of antifreeze activity upon addition of borate is not correlated with a change in dynamics of the water molecules hydrating AFGP.

Interestingly, it was not possible to accurately measure the anisotropy decay for the larger $AFGP_{1-5}$ in a borate buffer, as these solutions formed a gel. Gel formation is a clear indication of inter-protein interactions. These interactions likely arise from the formation of borate cross links between different AFGP sugar moieties, a mechanism that is supported by linear FTIR spectra of $AFGP_{1-5}$, presented in figure 7.5A. The spectra exhibit peaks at 1645 cm^{-1} and 1555 cm^{-1} that correspond to the amide I and amide II vibrations, respectively, and that are sensitive to the hydrogen-bond configuration of the AFGP peptide backbone. These peaks do not change upon the addition of borate, indicating that the peptide conformation is similar. In contrast, the peaks associated with the vibrational modes of the sugar unit and borate change significantly. For

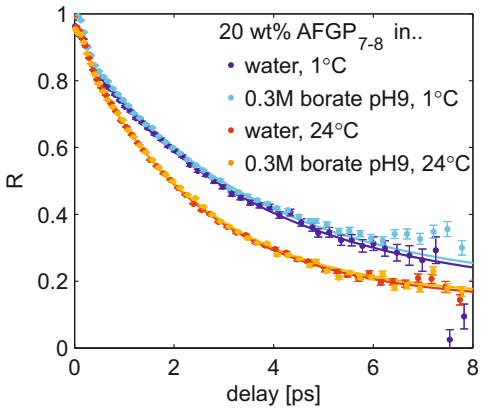

FIGURE 7.4. Anisotropy decay of the OD stretch vibration for solutions of 20 wt% $AFGP_{7-8}$ in isotopically diluted water and in isotopically diluted 0.3 M borate buffer at pH = 9.0, at 1 °C and 24 °C. The anisotropy is averaged over the frequency range 2450-2600 cm^{-1} and divided by 0.4. The solid lines are fits to a single exponential with an offset R_{slow}.

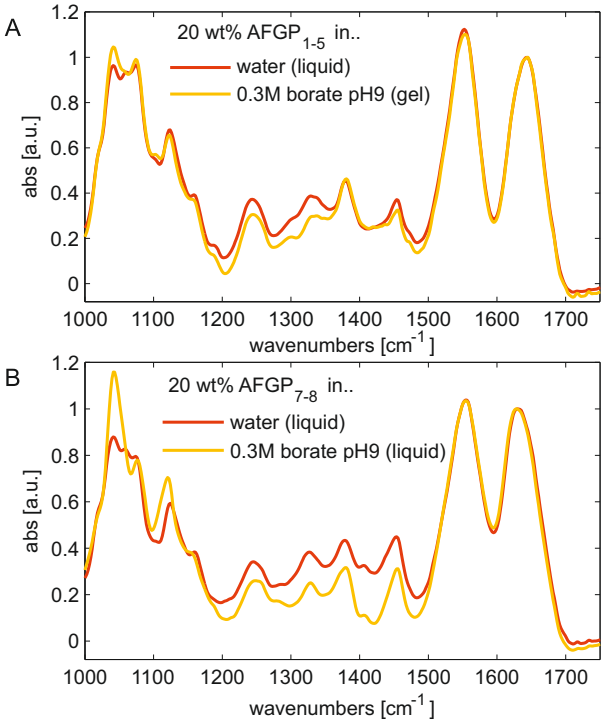

FIGURE 7.5. Linear infrared spectra for solutions of 20 wt% $AFGP_{1-5}$ (A) and 20 wt% $AFGP_{7-8}$ (B) in isotopically diluted water and in isotopically diluted 0.3 M borate buffer at pH = 9.0. The spectra are recorded at 24 °C and corrected for the water and buffer background, respectively.

$AFGP_{7-8}$ we observe a similar trend (fig. 7.5B), indicating that the smaller isoforms can form similar inter-protein cross links. We assume that the AFGP molecules in these solutions do not form a gel due to their significantly smaller size.

7.4 Discussion

Unravelling the hydration dynamics of AFGPs may provide important information on the nature of their ice-binding site and the origin of their extremely high IRI activity. Using polarization-resolved femtosecond experiments, we find that the dynamics of water near antifreeze glycoprotein surfaces are quite similar to the dynamics of water near other proteins and sugars, and that the majority of the slowly reorienting water molecules is slowed down by the AFGP peptide backbone. Our findings agree very well with early viscosity, translational diffusion, and NMR experiments, which indicate that AFGPs affect a similar amount of water as non-antifreeze glycoproteins[148]. Our findings are also consistent with vibrational surface sum-frequency generation (VSFG) spectra of aqueous solutions of AFGP that also show no indication of ice-like or unusually structured water hydrating the AFGP[165].

We find that the local hydration dynamics of the smaller and larger AFGPs are almost identical. The antifreeze activity of $AFGP_{7-8}$, however, is known to be only 60% of the activity of larger $AFGP_{1-5}$ on a weight basis[166]. The larger and smaller AFGPs also show different ice shaping properties[167]. We thus find strong indications that the hydration water of AFGP is not of significant importance for its antifreeze activity. This finding is further supported by our observation that the well-known antifreeze glycoprotein inhibitor borate does not alter the dynamics of water hydrating the AFGP.

The effects of AFPs and AFGPs on the structure and dynamics of water have also been studied with THz absorption measurements[159,168]. It was observed that the addition of AFPs and AFGPs increases the terahertz absorption, and that for AFGPs this effect diminished upon the addition of borate. Based on the present measurements of the reorientation dynamics of water molecules hydrating AFGP, we conclude that the observed THz absorption change is probably not due to a change in the reorientation dynamics of the hydrating water molecules, but due to a change of the spectrum of the low-frequency vibrations of the hydration shell, induced by a structural change of the water surrounding AFGP or by the coupling between the intermolecular water vibrations and the low-frequency modes of sugar groups and borate ions.

Inactivation of AFGP is likely caused by a direct binding between the borate and the sugar unit[163,166]. This notion agrees with the observations of the linear FTIR spectra that indeed provide evidence for borate-sugar association. The borate ions cannot only bind to one AFGP protein, but are able to form inter- and intra-protein cross links between AFGP molecules, which leads to gel formation at sufficiently high concentration. The formation of inter- and intra-protein links can also explain why the ice crystal growth behaviour of $AFGP_{1-5}$

in borate solutions is similar to that of $AFGP_{7-8}$: the binding and cross-linking by borate reduces the effective amount of sites of $AFGP_{1-5}$ that are able to interact with the ice.

Taken together, our observations are consistent with a direct ice-binding mechanism, with the AFGP sugar groups as the active binding site, as has been suggested before[163,164]. Based on the differences in activity between the smaller and larger isoforms and the effect of borate binding on the activity of both of them, the number of available ice-binding sites per AFGP seems to play an important role. The high IRI activity of AFGPs compared to AFPs might thus be related to the existence of multiple ice-binding sites, located on the same flexible protein chain[169,170], thereby making AFGPS particularly efficient in preventing the grain boundary migration that leads to the growth of large ice crystallites[171,172].

7.5 Conclusions

We have investigated the water reorientation dynamics in solutions of antifreeze glycoproteins, both at room temperature and close to biologically relevant working temperatures. We find that a fraction of the water molecules is strongly slowed down by the interaction with the antifreeze protein surface. The fraction of slow water molecules scales with the size and concentration of AFGP, and is comparable to the fraction of slow water molecules observed for non-antifreeze proteins. Inhibiting the AFGP antifreeze activity using borate buffer induces no changes in the reorientation dynamics of water hydrating the AFGP. Addition of borate does change the infrared absorption associated with vibrational modes of AFGPs sugar unit, which points at the formation of cross links between borate and AFGPs sugar units. Our findings support a local mechanism in which the sugar unit of AFGP forms the active binding site.

8 Structure and dynamics of water in triglyceride oils

It is commonly known that a small amount of water can be present in triglyceride oil, but a molecular picture of the structure and dynamics of these water molecules is lacking. In this chapter, we study the hydrogen-bond configuration and dynamics of water in triacetin, tributyrin and trioctanoin. We identify water molecules with a single strong hydrogen bond to the triglyceride, waters with two weaker hydrogen bonds to the triglycerides, and water clusters. These species do not interconvert on the 20 ps timescale of the experiment. The water molecules with two weaker hydrogen bonds to the triglyceride correspond to a single, specific hydrogen-bond configuration; these molecules likely bridge the carbonyl groups of adjacent triglyceride molecules, which can have a large influence on the properties of triglyceride oils.

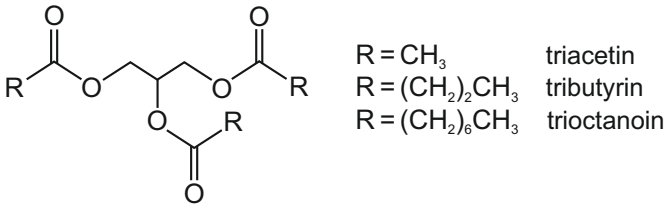

FIGURE 8.1. Triglycerides used in this study.

8.1 INTRODUCTION

Water is known to actively influence the structure and functioning of biological molecules like proteins[19,20,24,173,174], DNA[175,176], and phospholipid membranes[21,177]. However, the influence of water has been hardly studied for a major class of biomolecules: the triglycerides. Triglycerides are responsible for energy supply and storage needed for metabolic functions and are widely used in daily life as foods, pharmaceuticals, cosmetics and raw material for biodiesel[22].

Due to the hydrophobic nature of triglycerides, water is only soluble up to small amounts, but is nonetheless expected to have considerable influence on properties like the disorder of fatty acid chains, fluidity and molecular packing[22,178–180], in analogy with the effect of small amounts of water on phospholipids[21]. The presence of water in triglycerides can also be very important for crystallization of oil soluble bioactive molecules and the types of crystals that are formed[181–183]. The solubility of water in triglycerides can be critically important for stability of water-in-oil emulsions as well, as the diffusion of water can cause instabilities due to Ostwald ripening[184]. Additionally, water decreases the long-term stability of triglyceride oils by promoting hydrolysis and auto-oxidation reactions[185–187].

In this chapter we study the hydrogen-bond configuration and dynamics of water in triglyceride oils, using linear infrared and 2DIR spectroscopy of the water hydroxyl stretch vibrations. We studied three saturated triglycerides that are widely used in industry and have different fatty acid chain lengths: triacetin, tributyrin, and trioctanoin (figure 8.1). By varying the fatty acid chain length, we effectively tune the hydrophobicity of the oil.

8.2 EXPERIMENTAL

SAMPLE PREPARATION Triacetin, tributyrin and trioctanoin are purchased from Sigma-Aldrich (purity >99%), and carefully dried. Even though the triglyceride oils are mostly hydrophobic, they do absorb small amounts of water (∼0.5 ml/l) under atmospheric conditions. This water is removed using 4 Å molecular sieves (Sigma-Aldrich). After drying, solutions are prepared by adding controlled amounts of water (H_2O, D_2O, or 1:9 D_2O:H_2O) to the triglycerides. The ratio of 1:9 D_2O:H_2O is chosen as a compromise between having

mostly HDO molecules (instead of D_2O), and still maintaining a sufficient concentration of OD oscillators and signal-to-noise to record 2DIR spectra. To ensure a homogeneous distribution of water in the oil phase, the solutions are left to equilibrate for at least five days. A long equilibration time is especially important for trioctanoin, in which water diffusion is very slow.

Spectroscopy We measure linear infrared spectra using a FTIR spectrometer (Bruker Vertex 80v). Each spectrum is background-corrected with an equivalent concentration of H_2O in triglyceride (for solutions with D_2O and 1:9 D_2O:H_2O) or with D_2O in triglyceride (for solutions with H_2O). This correction is more accurate than subtracting the spectrum of pure triglyceride only, since it takes into account the replacement of triglyceride volume by water.
We measure 2DIR spectra using the dual-color setup described in section 3.3. The pump and probe pulses are centered at $\sim$2640 cm^{-1}, in resonance with the OD stretch vibration of HDO molecules in triglyceride oil.

8.3 Results

8.3.1 Linear spectra

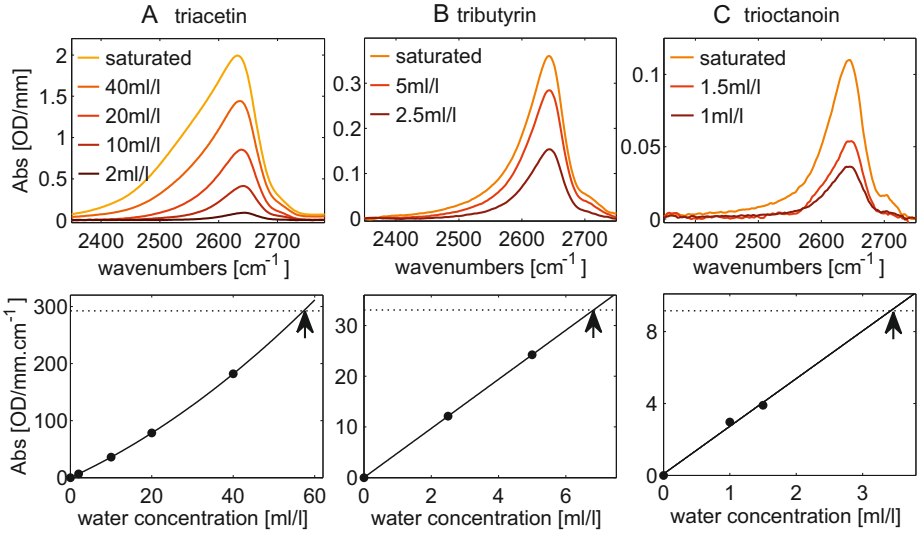

Figure 8.2. Linear absorption spectra of the OD stretch vibrations of 1:9 D_2O:H_2O in triacetin (A), tributyrin (B), and trioctanoin (C), for different water concentrations. The spectra are corrected for the response of H_2O in triglyceride at the same water concentration. The integrated infrared absorption (bottom row) can be related to the water concentration by an empirical second order polynomial fit (solid lines). The water concentration at which the fit reaches the integrated OD stretch absorption of a saturated solution (dotted lines), indicated with arrows, is then an estimate for the water concentration of a saturated solution.

Figure 8.2 presents the linear absorption spectra of isotopically diluted water in the different triglycerides as a function of the water concentration. The OD stretch absorption increases gradually with increasing water concentration, until the saturation limit is reached and adding more water does not increase the OD stretch intensity further. This allows us to determine the water solubility, which is 57±2 ml/l, 6.8±1 ml/l and 3.4±1 ml/l for triacetin, tributyrin, and trioctanoin respectively, corresponding to molar water to lipid ratios of 1:1.7, 1:9, and 1:11. The low water to lipid ratio for triglycerides with longer fatty acid chains directly reflects the lower solubility of water in these triglyceride oils.

Figure 8.3 presents the infrared absorption spectra of saturated solutions of water in the different triglycerides, for different water isotope compositions. All spectra are background-corrected and normalized to their peak intensity. For isotopically diluted water (fig. 8.3A), the infrared absorption spectrum reports on the hydrogen-bond strength, without the influence of intra- and intermolecular coupling of the hydroxyl stretch vibrations. We find we can decompose the spectra into three Gaussian bands; a broad band at lower frequencies (∼2600 cm^{-1}), a narrower band at intermediate frequencies (∼2640 cm^{-1}) and a small shoulder around 2715 cm^{-1}. The small shoulder corresponds to non-hydrogen-bonded OD groups[188].

With increasing fatty acid chain length, the broad band at low frequencies decreases in amplitude and shifts to higher frequencies by about 45 cm^{-1}, the narrow band at intermediate frequencies blueshifts by 13 cm^{-1}, and the amplitude of the small shoulder corresponding to non-hydrogen-bonded OD groups increases. This shows that the distribution of hydrogen-bond strengths shifts towards weaker hydrogen bonds for water in triglycerides with longer fatty acid chains. In addition the different spectral bands become narrower, which indicates that the distribution of hydrogen-bond strengths becomes more narrow.

Replacing isotopically diluted water by pure H_2O or D_2O (fig. 8.3B,C) leads to a splitting of the band at intermediate frequencies. The resulting two bands are assigned to delocalized symmetric and antisymmetric stretching modes that result from the intramolecular coupling of the hydroxyl stretch vibrations of H_2O and D_2O. The broad band at low frequencies does not show this behavior, which indicates that for these water molecules the two stretch vibrations do not or weakly interact, probably as result of a strong difference in hydrogen bond strength. Hence, the low frequency band likely arises from water molecules with one OH/OD group strongly hydrogen-bonded to the lipid and the other OH/OD group being free (giving rise to the small shoulder at 2715 cm^{-1}). The intermediate frequency band corresponds to water molecules that have both hydroxyl groups weakly hydrogen bonded to the lipid, or more specifically, to the C=O groups, considering that the frequency of this intermediate band matches very well with hydroxyl groups hydrogen-bonded to the C=O of acetone molecules[75,188].

The band positions resulting from the Gaussian fit are summarized in figure 8.4 for the different triglycerides and isotopic compositions. For H_2O, the relative separation between the delocalized symmetric and antisymmetric stretching

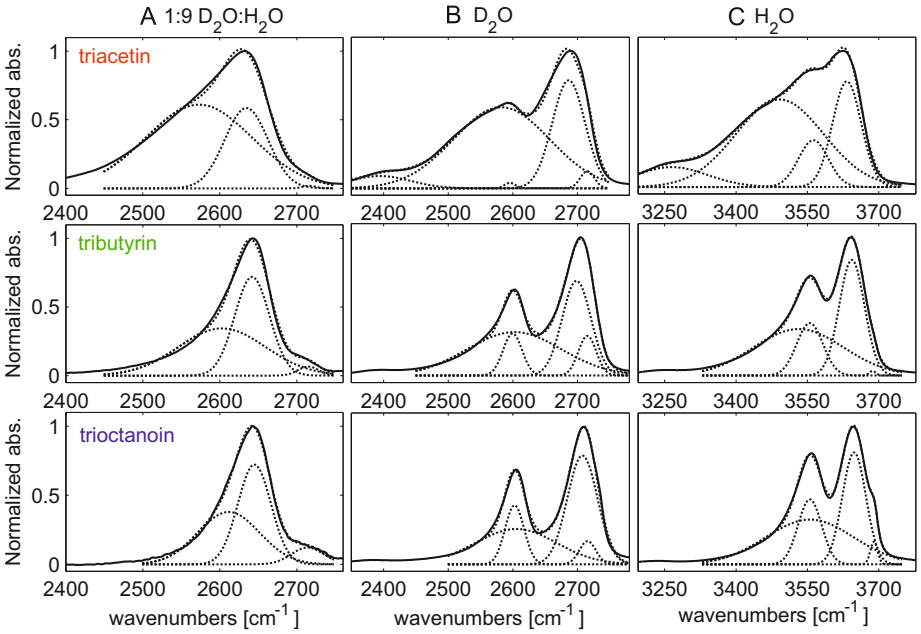

FIGURE 8.3. Linear absorption spectra of saturated solutions of water in triacetin, tributyrin and trioctanoin. A: 1:9 D_2O:H_2O, B: D_2O, C: H_2O. The spectra are corrected for the response of H_2O in triglyceride (A,B) or D_2O in triglyceride (C), and normalized on peak intensity. The dotted lines represent a Gaussian fit to the spectra.

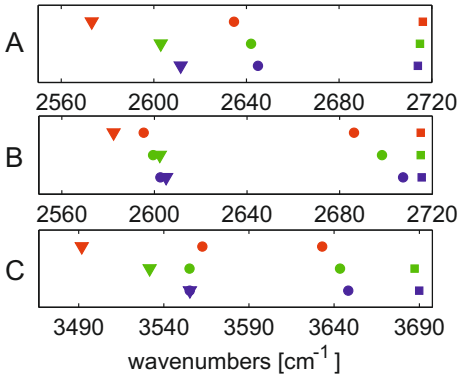

FIGURE 8.4. Center frequencies of the Gaussian bands that constitute the spectra (fig. 8.3) of saturated solutions of water in triacetin (red), tributyrin (green) and trioctanoin (blue). A: 1:9 D_2O:H_2O, B: D_2O, C: H_2O. Triangles: broad band (FWHM 90-220 cm^{-1}), circles: narrow band (FWHM 50-65 cm^{-1}), squares: small shoulder (FWHM 30 cm^{-1}).

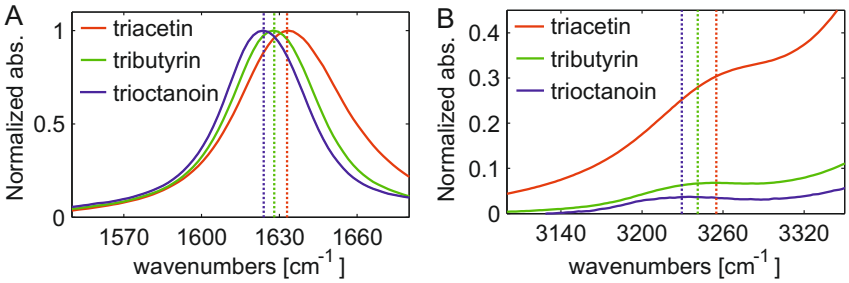

FIGURE 8.5. Linear absorption spectra of saturated solutions of H_2O in triacetin, tributyrin and trioctanoin in the water bend region (A) and at approximately twice the frequency (B). The spectra are corrected for the response of D_2O in triglyceride and normalized on peak intensity between 1580 and 1680 cm^{-1}. The dotted lines indicate peak positions.

modes is slightly smaller than the separation observed for D_2O, in accordance with their gas phase frequencies[189,190]. The spectra for D_2O and H_2O show a small peak around 2385/3240 cm^{-1} as well. The frequency of this peak is approximately twice the bend frequency, and follows the shift of the bend vibration with increasing fatty acid chain length, as can be seen in figure 8.5 (note this is in opposite direction of the OH stretch vibration). Hence, we assign this peak to the overtone of the bend vibration.

Besides a major contribution from OD stretch vibrations that are strongly hydrogen-bonded to the oil, the broad band at lower frequencies probably contains a contribution from small water clusters. Water molecules hydrogen-bonded to other water molecules give rise to a broad band centered at 2500 cm^{-1}.[46,47] To determine the contribution of water clusters, we return to the linear spectra of isotopically diluted water in the triglycerides as a function of water concentration. These spectra were presented in fig. 8.2, but for clarity we normalize them on peak intensity and present them in fig. 8.6 as well. It can be seen that the shape of the spectrum changes considerably with water concentration for solutions of water in triacetin. A Gaussian fit (see fig. 8.7) shows that with increasing water concentration, the broad band at low frequencies increases in relative amplitude and shifts from 2620 cm^{-1} to 2572 cm^{-1}, becoming more similar to the OD stretch absorption spectrum of bulk water. This observation indicates that this band contains a significant contribution of water clusters that increases with increasing water concentration. For tributyrin and trioctanoin we do not observe significant changes in spectral shape with increasing water concentration, so for these triglycerides the contribution of water clusters appears to be negligible, even at the solubility limit. Hence, for these triglycerides we can consider all water molecules to be isolated.

For low concentrations of isotopically diluted water (<4 ml/l), the OD stretch spectra of the three triglycerides are identical, so at low water concentrations the hydrogen-bond strengths and the relative contributions of each water species are the same. Hence, the differences between the water spectra

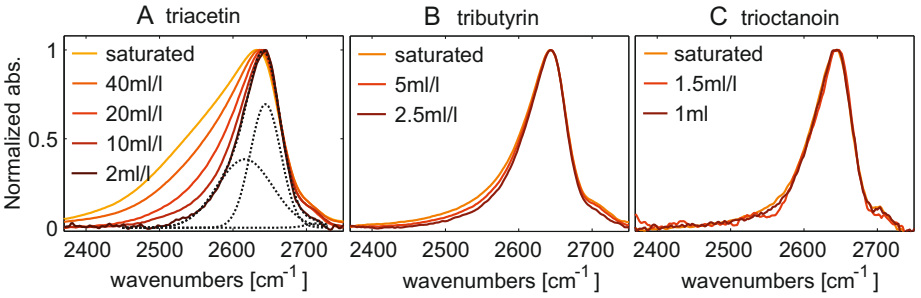

FIGURE 8.6. Linear absorption spectra of 1:9 D_2O:H_2O in triacetin (A), tributyrin (B), and trioctanoin (C), for different water concentrations. The spectra are corrected for the response of H_2O in triglyceride at the same water concentration, and normalized on peak intensity. The dotted lines represent a Gaussian fit to the spectrum.

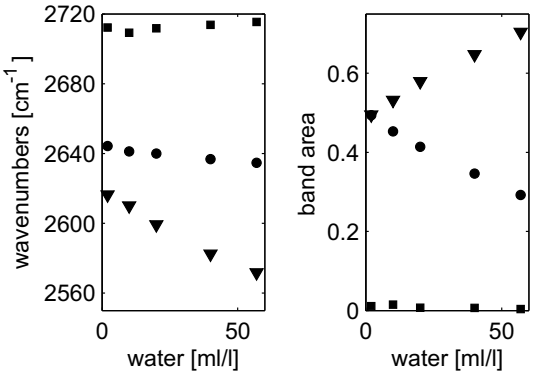

FIGURE 8.7. Center frequencies and areas of the Gaussian bands that constitute the spectra of water in triacetin at different water concentrations (fig. 8.6A). Triangles: broad band (FWHM 90-160 cm^{-1}), circles: narrow band (FWHM 50-65 cm^{-1}), squares: small shoulder (FWHM $\sim$30 cm^{-1}).

for the different oils, as shown in fig. 8.3, are mostly due to differences in water concentration. There are still subtle differences: at low water concentrations, the water bend vibration still shows a significant redshift with increasing fatty acid chain length ($\sim$ 6 cm^{-1} from triacetin to trioctanoin). The redshift of the bend vibration is also responsible for small changes of the H_2O and D_2O hydroxyl stretch spectra with fatty acid chain length, due the coupling of the water bend and hydroxyl stretch vibrations for non-isotopically diluted water.

8.3.2 2DIR SPECTRA

To investigate the dynamics of the different hydrogen-bonded water molecules and their possible interconversion, we measured time-resolved 2DIR spectra. We recorded spectra for water in triacetin and tributyrin. Unfortunately, for trioctanoin the water concentration was too low to measure 2DIR spectra with sufficient signal-to-noise.

Figure 8.8 presents the 2DIR spectra of saturated solutions of water in triacetin at 0.4 picoseconds after the excitation. The top row shows the isotropic (rotation-free) 2DIR spectra. For isotopically diluted water, the isotropic 2DIR spectrum shows a negative absorption feature along the diagonal, corresponding to the bleaching of the 0→1 vibrational transition, and a positive absorption feature corresponding to the 1→2 vibrational transition, which is redshifted along the probe axis by about 100 cm^{-1} due to the anharmonicity of the OD stretch vibration. We find the spectrum of isotopically diluted water in triacetin at 0.4 ps to be very inhomogeneous: the spectrum shows an almost perfect correlation between excitation and detection frequency (nodal line slope of ∼1). In comparison, for isotopically diluted bulk water this correlation is largely lost at 0.4 ps, as a result of rapid spectral diffusion [191]. This indicates that the hydrogen-bond strength of water molecules confined in triglyceride oil is modulated on a much longer timescale than in bulk water, reflecting much slower water dynamics.

For pure D_2O in triacetin, we observe two negative features along the diagonal corresponding to the symmetric and antisymmetric OD stretch vibration (and corresponding peaks due to the 1→2 transition). In addition, off-diagonal features (cross-peaks) appear at all delay times due to the vibrational coupling between the symmetric and antisymmetric stretch vibrations. Note that the symmetric to antisymmetric cross-peak appears around $\omega_{pump,probe}$=2580, 2680 cm^{-1}, while the corresponding diagonal signal is centered at a lower frequency of ∼2550 cm^{-1}. This lower frequency is the result of the contribution of OD stretch vibrations of singly hydrogen-bonded water molecules and water clusters; these vibrations absorb at lower frequencies compared to doubly hydrogen-bonded water molecules. For these water molecules, the hydrogen-bond configuration is asymmetric, and the OD vibrations do not form symmetric and antisymmetric vibrations. Hence, these water molecules only contribute to the diagonal signal and not to the cross-peaks of the symmetric and antisymmetric OD vibrations of the D_2O molecules with two weak hydrogen bonds of similar strength. The non-hydrogen-bonded OD stretch vibrations are not observed in the 2DIR spectra, because their cross section is very low and the diagonal 2DIR signal depends quadratically on the cross section.

The bottom row of figure 8.8 presents the polarization-difference 2DIR spectra. In the polarization-difference spectrum the diagonal signals are eliminated, and the cross-peaks become more visible, provided that the cross-peaks have an anisotropy value that differs from that of the diagonal peaks [60]. The polarization-difference spectra reveal that the spectrum of isotopically diluted water contains weak cross-peaks as well. These have a similar position and shape as the cross-peaks measured for D_2O, but much lower intensity (∼ $^1/_{100}$).

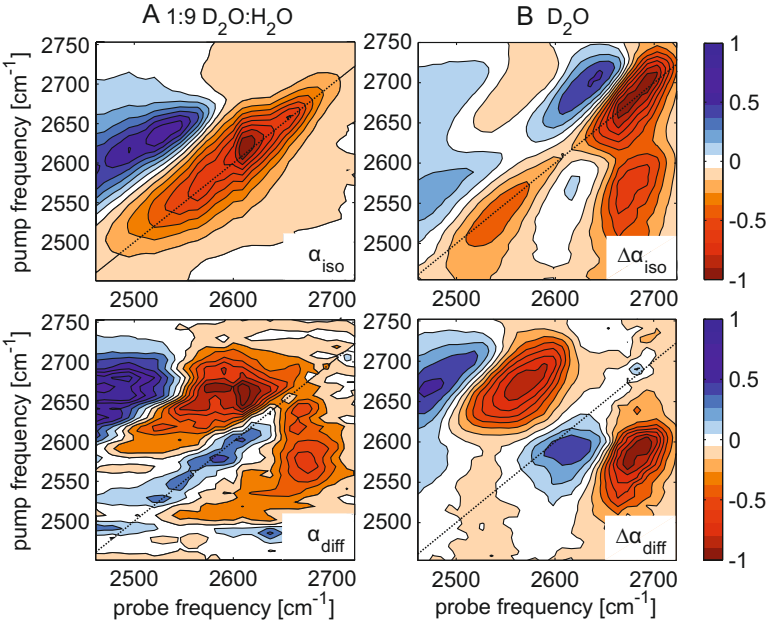

Figure 8.8. 2DIR spectra of saturated solutions of 1:9 D_2O:H_2O (A) and D_2O (B) in triacetin, at 0.4 picoseconds after excitation. The top row shows the isotropic 2DIR spectrum (eq. 2.41, rotation free) and the bottom row the polarization-difference 2DIR spectrum (eq. 2.53, cross-peaks enhanced). The spectra are normalized on peak intensity.

This indicates that these cross-peaks are due to vibrational coupling between the symmetric and antisymmetric stretch vibrations of the 1% of D_2O molecules that are left in the isotopically diluted mixture. At all time delays, only cross-peaks arising from the coupling between the symmetric and antisymmetric stretch vibrations are observed, both for water in triacetin and tributyrin. The absence of other cross-peaks indicates that the different hydrogen-bonded water species do not interconvert on the 20 picosecond timescale of the experiment.

To study the vibrational dynamics of the different hydrogen-bonded water species in more detail, we analyze slices of the isotropic 2DIR spectra at different excitation frequencies. Figure 8.9 presents these slices for isotopically diluted water in triacetin and tributyrin. For each excitation frequency, the vibrational response decays within several picoseconds, reflecting the decay of the excited vibrations back to the vibrational ground state. Based on the linear spectra, we expect at least two spectral components to contribute to the vibrational response; a component corresponding to the OD stretch vibrations of water molecules with a single strong hydrogen bond to the triglyceride, and a component corresponding to OD stretch vibrations of water molecules with two weaker hydrogen bonds to the triglyceride. We therefore analyze the spectra using a spectral decomposition model with two components that decay independently

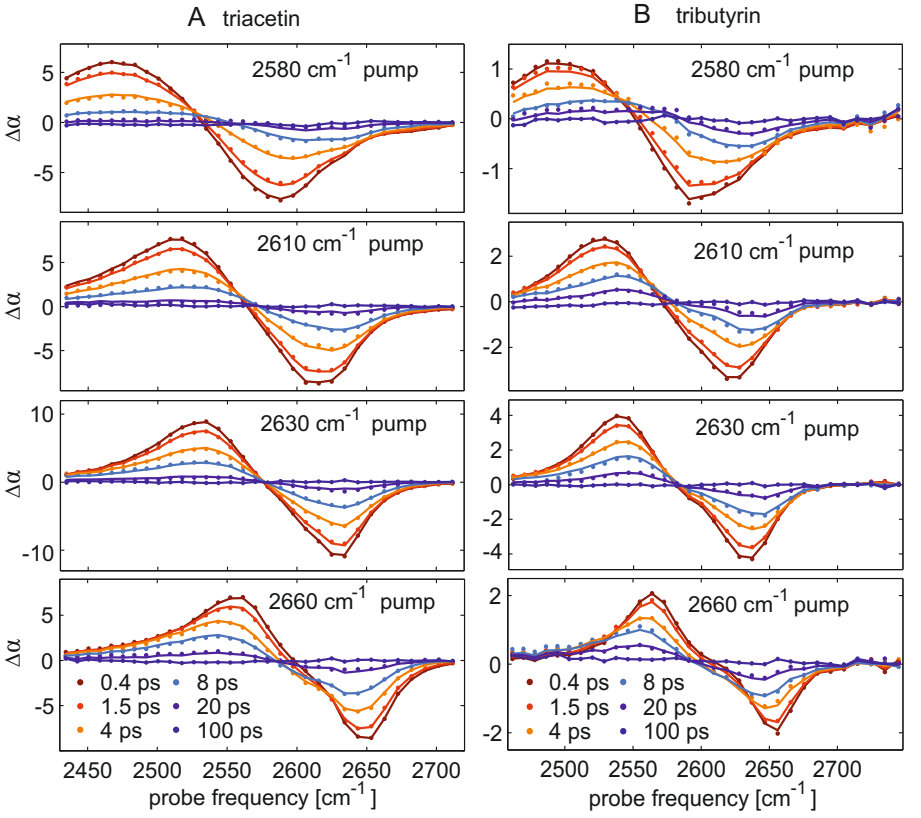

FIGURE 8.9. Slices of the 2DIR spectrum at different excitation frequencies, for saturated solutions of 1:9 D_2O:H_2O in triacetin (A) and tributyrin (B) (solid lines are description with spectral decomposition fit).

to a heated ground state (eq. 4.7). This state is included to account for the small residual signal due to heating of the sample. The vibrational lifetimes of each component, $T_{1,1}$ and $T_{1,2}$, are the primary fit parameters, while the spectral components σ_1 and σ_2 are calculated using a singular value decomposition. The spectrum of the heated ground state is taken directly from the data at 100 ps. The results of the least-squares fit are presented in figure 8.9 and describe the data well. In this analysis, we did not consider spectral diffusion effects, which are expected to lead to a slight broadening of the bands with time.

Figure 8.10 presents the spectral components. Spectral component 2, corresponding to OD vibrations of water molecules with two weak hydrogen bonds to the triglyceride, varies in amplitude, but hardly in shape, with the excitation frequency. This finding indicates that the absorption band of the water molecules with two weak hydrogen bonds is close to homogeneously broadened. In contrast, the spectral signature of component 1, corresponding to the OD vibrations of water molecules with a single strong hydrogen bond to the triglyc-

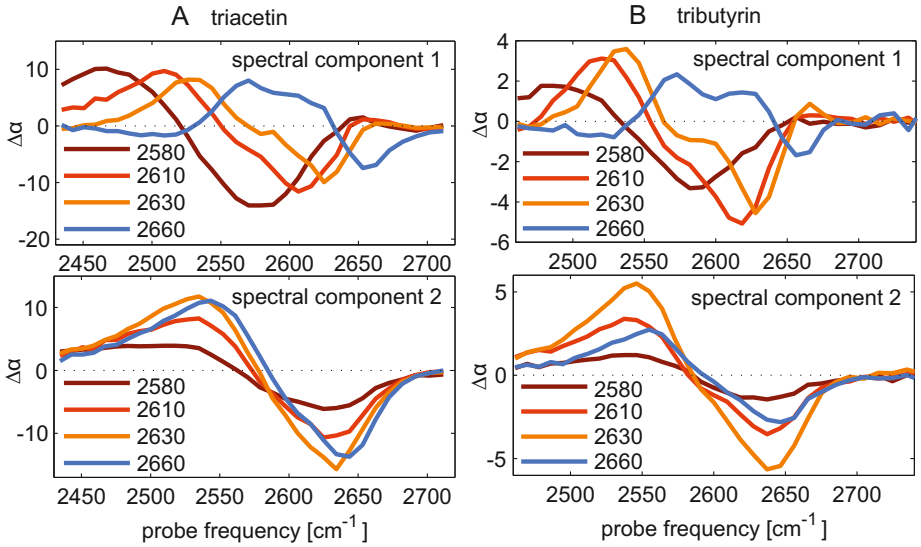

Figure 8.10. Spectral components of the 2DIR spectral slices (fig. 8.9) for saturated solutions of 1:9 D_2O:H_2O in triacetin (A) and tributyrin (B).

eride, varies strongly with the excitation frequency. This indicates that the absorption band of the singly hydrogen-bonded water molecules is inhomogeneously broadened and respresents a heterogeneous ensemble of water molecules with different hydrogen-bond strengths. This heterogeneity likely arises from the fact that water molecules are hydrogen-bonded to different groups of the triglyceride (carbonyl or ether oxygen), and from the presence of different local conformations of the glycerol backbone and fatty acid chains of the triglyceride surrounding the hydrogen-bonded water molecules. In the case of triacetin, there is an additional contribution of water clusters to the spectrum as well. This contribution manifests itself as a broadening and increase in amplitude of spectral component 1.

The vibrational lifetimes of the OD stretch vibration of water in triacetin are 2.0 ± 0.6 ps and 11 ± 1 ps, for component 1 and 2, respectively. For water in tributyrin the lifetimes are comparable: 2.3 ± 0.7 ps for component 1 and 17 ± 3 ps for component 2. The lifetime of component 2, corresponding to OD vibrations of doubly hydrogen-bonded water molecules, is quite long compared to the 1.8 ps lifetime of the OD stretch vibration observed for HDO molecules in bulk isotopically diluted water[74]. This longer lifetime points at a weaker anharmonic coupling of the excited OD vibration and low-frequency accepting modes of the triglyceride solvent, which can be explained from the weak hydrogen bonds. In this perspective, the lifetime of spectral component 1 is remarkably short, especially when it is excited at high frequencies (corresponding to weak hydrogen bonds).

Finally, we measure the anisotropic spectrum of the water molecules confined

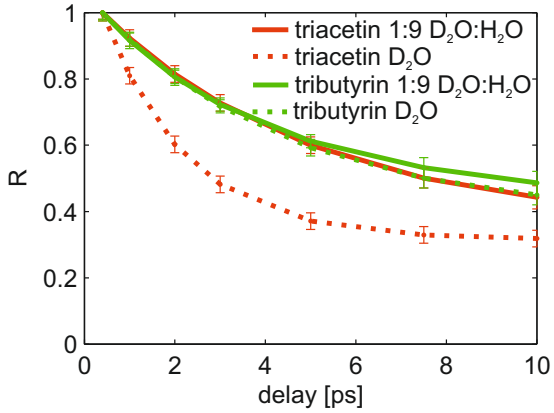

FIGURE 8.11. Anisotropy of the 2DIR spectra for saturated solutions of water in triacetin and tributyrin. The anisotropy is obtained by averaging over a frequency interval of 20 cm^{-1} around 2640 cm^{-1} (OD vibration of doubly hydrogen-bonded HDO of 1:9 D_2O:H_2O) or around 2690 cm^{-1} (antisymmetric OD stretch vibration of D_2O), and normalized at 0.4 picoseconds.

in the triglycerides. The anisotropy is directly proportional to the second order rotational correlation function, and decays due to molecular reorientation and resonant (Förster) energy transfer. Figure 8.11 presents the anisotropy decay of the vibrational excitation for saturated solutions of water in triacetin and tributyrin, obtained by averaging over a frequency range of 20 cm^{-1} around the main diagonal peak of the 2DIR spectrum. For isotopically diluted water, the anisotropy decays only partially within the time window of the experiment. This indicates that the water molecules do not fully reorient on this timescale, but instead sample a limited angular space. We can describe the partial decay of the anisotropy using a single exponential with an offset: $R = R_1 e^{-t/\tau_r} + R_0$. This yields a reorientation time τ_r of about 4 ps (τ_r=4.0 $\pm$ 0.5 ps for triacetin, and 3.8 $\pm$ 0.5 ps for tributyrin) and an offset of 0.14 $\pm$ 0.04, which corresponds to reorientation within a cone angle of 46° (see eq. 2.51).

In bulk liquid water, water molecules fully reorient on a 2.5 picosecond timescale[74] by a mechanism which involves the switching of hydrogen-bond partners[13]. The transition state for reorientation requires the approach of another water molecule. For water molecules confined in triglycerides the situation is very different, as there are no water molecules to switch to (or very few, in the case of water clusters). This lack of potential new hydrogen-bonded partners explains why the reorientation only occurs within a limited cone angle: without the possibility of forming a new hydrogen bond, the hydrogen bond to the triglyceride is maintained, which limits the angular space of the reorientation.

For D_2O, we only average the anisotropy decay over the diagonal peak that corresponds to the antisymmetric stretch vibration. By doing so, the effect of intramolecular coupling is eliminated: the antisymmetric stretch vibrations that transfer energy to the symmetric mode show up in another part of the spec-

trum (the cross-peak) and thus do not contribute to the anisotropy decay of the diagonal peak. However, intermolecular coupling due to coupling between antisymmetric vibrations located on neighboring water molecules, can still contribute to the anisotropy decay. It can be seen in fig. 8.11 that the anisotropy decay for D_2O in tributyrin is very similar to the decay for isotopically diluted water in the same triglyceride, while the anisotropy decay for D_2O in triacetin is clearly faster than its isotopically diluted counterpart. This is in line with our earlier observation that triacetin contains a significant amount of water clusters, that also contribute to the absorption at 2690 cm^{-1}. Within a water cluster, intermolecular energy transfer is possible, while in tributyrin all water molecules are isolated and intermolecular energy transfer does not happen.

Water clusters are likely only present in triacetin due to the higher concentration of hydrophilic groups versus hydrophobic groups for this triglyceride, as a result of the shorter hydrophobic fatty acid chain. This makes it more likely for a water molecule that is hydrogen-bonded to the hydrophilic carbonyl group of the triglyceride to be in the vicinity of a water molecule that is hydrogen-bonded to the carbonyl group of another triacetin. As a result, it may become favorable for other water molecules to accumulate in between and in the vicinity these hydrogen-bonded water molecules, thus leading to the formation of water clusters.

8.4 Discussion

The spectra of water molecules confined in the triglyceride oils are similar to the spectra of water molecules confined in other solvents. Studies on mixtures of water and acetone[75,188], acetonitrile[192], DMSO[75,193], poly-ether[194] and dioxane[195] showed a strong narrowing and blueshift of the water hydroxyl stretch vibrations when the water concentration was decreased. For all these solvents, a decrease of the water fraction leads to a replacement of the interconnected water hydrogen-bond network by specific hydrogen-bond configurations involving water and hydrophilic groups of the solvent. Arguably the most closely related system is water in acetone clusters[188]. Infrared spectra of the water OH stretch vibration showed that water molecules in acetone clusters form either a single strong hydrogen bond to an acetone carbonyl group, or two weaker hydrogen bonds to two acetone carbonyl groups, which is similar to what we currently observe for water molecules in the triglycerides. The main difference is that water in acetone clusters can more easily switch hydrogen-bond partners: on a 1.3 picosecond timescale, water molecules change between a single strong hydrogen bond and two weaker hydrogen bonds to the acetone carbonyl groups. Most likely, this difference is due to the much higher density of carbonyl groups in acetone, and due to the much higher mobility of the light acetone molecules compared to the bulky triglyceride molecules.

The 2DIR spectra showed that water molecules with two hydrogen bonds to the triglyceride constitute a single species, which indicates that these water molecules have a specific hydrogen-bond configuration. Considering the posi-

tioning of the carbonyl groups of the triglyceride, the most likely hydrogen-bond configuration is one where the water molecule bridges two adjacent triglyceride molecules. Below the melting point triglycerides adopt different polycrystalline phases that are thought to persist in the liquid [22]. Different models have been proposed for the liquid ordering; a smectic phase with triglycerides in a chair-like conformation [178], a nematic phase with triglycerides in the same conformation but with twisted chains [179] and a stacked-disk ordering where each disk consists of a single y-shaped triglyceride molecule [180]. Each of these structures would allow bridging water molecules between carbonyl groups of adjacent triglyceride molecules, while intramolecular bridging is unlikely. As such, water is expected to have a large influence on the liquid triglyceride properties such as viscosity and molecular ordering during crystallization, which is of great importance for many biological and industrial systems.

8.5 CONCLUSIONS

We have investigated the hydrogen-bond structure and vibrational dynamics of water in triglyceride oils, using linear infrared and time-resolved 2DIR spectroscopy. From the linear spectra of the water hydroxyl stretch vibrations measured at different isotopic dilutions, we identify several water species: waters with a single strong hydrogen bond to the triglyceride, waters with two weaker hydrogen bonds to the triglycerides, and water clusters. The latter species is only present in triacetin, the triglyceride with the shortest fatty acid chains. For tributyrin and trioctanoin the amount of clusters is negligible, and all water molecules can considered to be isolated.

The 2DIR spectra of the OD stretch vibration of D_2O in triacetin and tributyrin contains cross-peaks between the symmetric and antisymmetric stretch vibrations of D_2O. The absence of other cross-peaks shows that the different water species do not interconvert on the 20 picosecond timescale of the experiment.

The vibrational lifetimes of the OD stretch vibration of HDO in triacetin are 2.0 $\pm$ 0.6 ps for HDO molecules with a single strong hydrogen bond, and 11 $\pm$ 1 ps for HDO molecules with two weak hydrogen bonds. For tributyrin the lifetimes are 2.3 $\pm$ 0.7 ps and 17 $\pm$ 3 ps, for the singly and doubly hydrogen-bonded water molecules, respectively. Within the experimental time window, the anisotropy of the vibrational response decays only partially; the decay corresponds to reorientation on a 4 picosecond timescale within a limited cone angle of 46°. The transient spectral response of water molecules with a single strong hydrogen bond to the triglyceride depends strongly on the excitation frequency, revealing the presence of different subspecies of singly-bound water molecules with different hydrogen-bond strengths. In contrast, the water molecules with two weaker hydrogen bonds to the triglyceride correspond to a single, specific hydrogen-bond configuration. Considering the structure of the triglycerides, these water molecules likely bridge adjacent triglyceride molecules. As such, water is expected to have a large influence on liquid triglyceride properties.

9 Water in triglyceride oils: the C=O stretch vibration

In the previous chapter, we studied the hydrogen-bond configuration of water molecules confined in triglyceride oil and identified several stable hydrogen-bonded water species. Here we investigate the water-triglyceride interaction in more detail, by studying the transient response of the carbonyl stretch vibration of the triglycerides with and without added water. We find that hydrogen-bond formation between a water molecule and the carbonyl group of the triglyceride leads to a frequency downshift of the absorption of the carbonyl stretch vibration from $\sim$1745 cm^{-1} to $\sim$1728 cm^{-1}. This hydrogen-bond formation affects the transient spectral response of the carbonyl stretch vibration, and speeds up the vibrational relaxation, which we find to be strongly inhomogeneous. We further observe that the anisotropy of excited carbonyl stretch vibrations decays via vibrational (Förster) energy transfer between carbonyl stretch vibrations, and determine the Förster radii to be 2.6 $\pm$ 0.1 Å for triacetin and 2.5 $\pm$ 0.1 Å for tributyrin, independent of the water content.

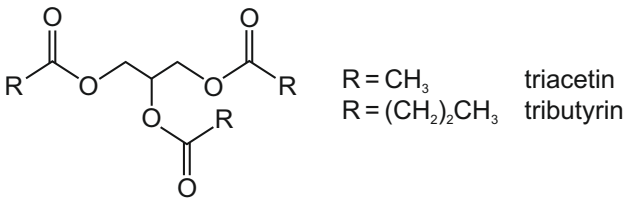

FIGURE 9.1. Triglycerides used in this study.

9.1 INTRODUCTION

Water plays an active role in many biological systems, and is known to influence the structure and functioning of for example proteins[19,20,24,173,174], DNA[175,176] and phospholipids[21,177]. One major class of biological molecules that has hardly been studied so far in terms of its interaction with water is the triglycerides. Triglycerides are important for metabolism, serving as a source of energy, and are also commonly used in daily life in, for example, foods, pharmaceuticals and cosmetics[22]. Even though triglycerides are mostly hydrophobic, small amounts of water dissolve in triglyceride oil, which can have considerable influence on triglyceride properties[183–186].

In chapter 8, we studied the hydrogen-bond structure and dynamics of water molecules in triglyceride oils, by probing the (transient) infrared absorption of the water OD stretch vibration. We identified water molecules forming a single strong hydrogen bond to the triglyceride, water molecules forming two weaker hydrogen bonds to the triglycerides, and, in the case of the triglyceride triacetin, water clusters. Based on the OD stretch vibrational frequency and the molecular structure of the triglycerides, we hypothesized that the singly- and doubly-hydrogen-bonded water molecules form hydrogen bonds with the carbonyl groups of the triglyceride. To confirm this, and to obtain more detailed information on the interaction between water molecules and triglycerides, we study the response of the carbonyl stretch vibration of the triglycerides.

In this chapter, we study the carbonyl stretch vibrations of triacetin and tributyrin (fig. 9.1), both with and without added water, using linear infrared and polarization-resolved femtosecond infrared spectroscopy. Both triglycerides have been extensively characterized in the OD spectral region in chapter 8.

9.2 EXPERIMENTAL

Triacetin and tributyrin are purchased from Sigma-Aldrich (purity >99%), and carefully dried. Even though the triglyceride oils are mostly hydrophobic, they do absorb small amounts of water (∼0.5 ml/l) under atmospheric conditions. This water is removed using 4 Å molecular sieves (Sigma-Aldrich). After drying, part of the triglyceride oil is hydrated again by adding an excess amount of heavy water (D_2O). To ensure a homogeneous distribution of water in the oil

phase, the mixtures are left to equilibrate for at least five days. The final water concentrations in hydrated triglyceride oils are 57 ± 2 ml and 6.8 ± 1 ml for triacetin and tributyrin, respectively, which corresponds to molar water to lipid ratios of 1:1.7 and 1:9 (see fig. 8.2).

We measure linear and time-resolved infrared spectra of the carbonyl stretch vibrations of the triglycerides. Since the absorption cross section of the carbonyl stretch vibration is quite high, we need to work with ultrathin samples (∼1 μm) to maintain sufficient light intensity at the detector. Ultrathin samples are prepared by sandwiching a small volume of triglyceride oil (∼2 μl) between two CaF_2 windows, and wrapping the window edges with parafilm, which prevents oil from leaking out and H_2O from leaking in, for at least a day.

The linear infrared spectra described in this chapter are recorded with a FTIR spectrometer (Bruker Vertex 80v). The time-resolved spectra are acquired with the dual-color pump-probe setup described in ref. 196. The pump and probe pulses are centered around 1745 cm^{-1}, in resonance with the carbonyl stretch vibrations of the triglycerides.

9.3 Results

9.3.1 Linear spectra

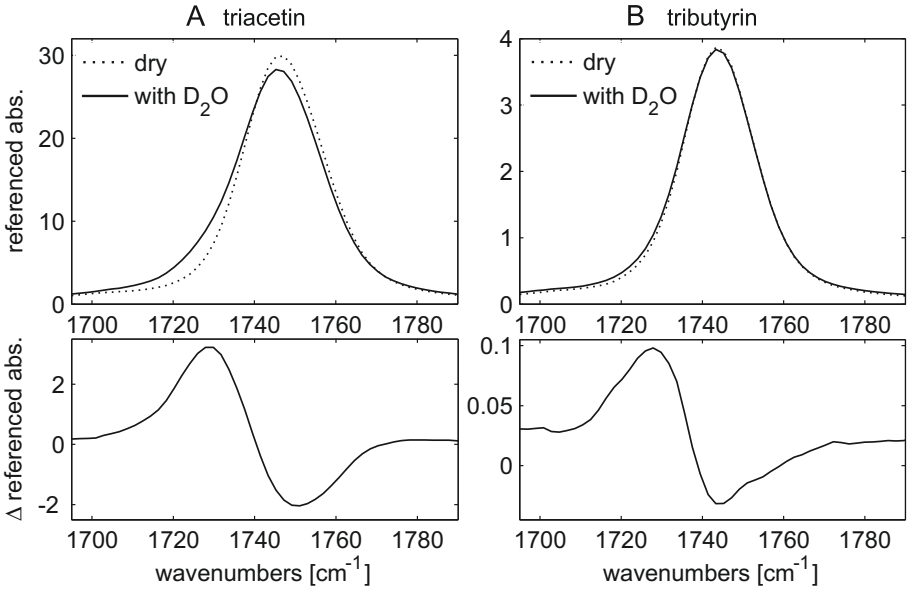

Figure 9.2. Linear absorption spectra of triacetin (A) and tributyrin (B), with and without added D_2O. The spectra are referenced to the intensity of the CH stretch modes around 2960 cm^{-1}. The bottom row shows the absorption difference between the referenced spectra with and without added D_2O.

Figure 9.2 presents the linear absorption spectra of triacetin and tributyrin with and without added water, in the spectral region of the carbonyl stretch vibration. In the absence of water, the absorption of the carbonyl stretch vibration is centered around 1746 cm^{-1} or 1743 cm^{-1}, for triacetin and tributyrin, respectively. Addition of water leads to a decrease of the amplitude of the absorption band and the appearance of an additional absorption feature around 1728 cm^{-1}. This additional feature arises from the formation of hydrogen bonds between water molecules and the carbonyl groups of the triglyceride. Since hydrogen-bond formation weakens the covalent bond between the carbon and oxygen atoms of the carbonyl group, the carbonyl stretch vibrational frequency is lowered. The vibrational frequency we observe for the hydrogen-bonded carbonyl groups corresponds very well to what has been previously observed for the carbonyl groups of methyl acetate forming a single hydrogen bond to a water molecule [197,198]. Carbonyl groups of methyl acetate that were hydrogen-bonded to two water molecules were found to absorb at 1703 cm^{-1}. [197,198] This finding indicates that the carbonyl groups absorbing at 1728 cm^{-1} are hydrogen-bonded to a single water molecule, which agrees with the fact that the water concentration is low.

9.3.2 TIME-RESOLVED SPECTRA

Figure 9.3 presents the isotropic transient absorption spectra at different delay times for triacetin and tributyrin, after excitation of the carbonyl stretch vibration. At early delay times, we observe a bleach of the fundamental transition of the carbonyl stretch vibration, centered around 1748 cm^{-1}, and an induced absorption around 1725 cm^{-1}, corresponding to the excited state absorption associated with the 1→2 vibrational transition. These signals decay on a picosecond timescale to a thermal difference spectrum, which reflects the heating of the sample following the dissipation of the energy of the vibrational excitation. For all triglyceride samples, we observe the vibrational relaxation of the carbonyl stretch vibration to be quite inhomogeneous. This can be seen clearly in figure 9.4, which presents the isotropic absorption change for dry triacetin at different probe frequencies. At low frequencies, the vibrations decay much faster than at high frequencies.

To analyze the inhomogeneous vibrational relaxation in more detail, we fit the transient spectra to a spectral decomposition model that includes three spectral components that decay independently to the thermalized ground state:

$$S(\omega,t) = \sum_{i=1}^{3} \sigma_{CO,i}(\omega) N_i(0) e^{-t/T_{1,i}} + \sigma_{end}(\omega) \left(1 - \sum_{i=1}^{3} N_i(0) e^{-t/T_{1,i}} \right) \quad (9.1)$$

Here the vibrational lifetimes of each component, $T_{1,i}$, are the primary fit parameters, while the spectral components $\sigma_{CO,i}$ are calculated using singular value decomposition. The spectrum σ_{end} of the thermalized ground state is taken directly from the transient spectrum at 220 picoseconds. We use three components as we found this to be the minimum amount of components that is needed to accurately describe the inhomogeneous vibrational decay; two components

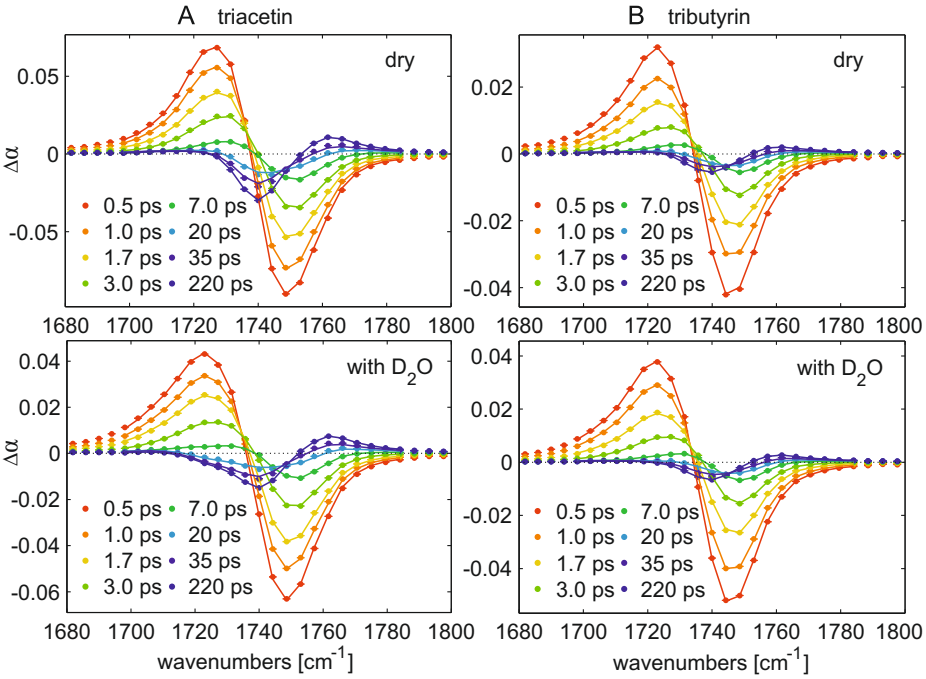

FIGURE 9.3. Isotropic absorption change as a function of frequency for different picosecond delay times, after excitation of the carbonyl stretch vibrations of triacetin (A) and tributyrin (B) with and without added D_2O. The solid lines represent fits using the model described in the text.

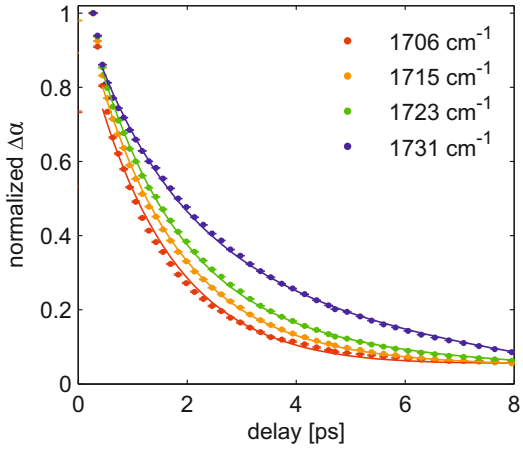

FIGURE 9.4. Isotropic absorption change after excitation of the carbonyl stretch vibrations of dry triacetin, as a function of delay time for different probe frequencies (normalized at 0.3 picoseconds). The solid lines represent fits using the model described in the text.

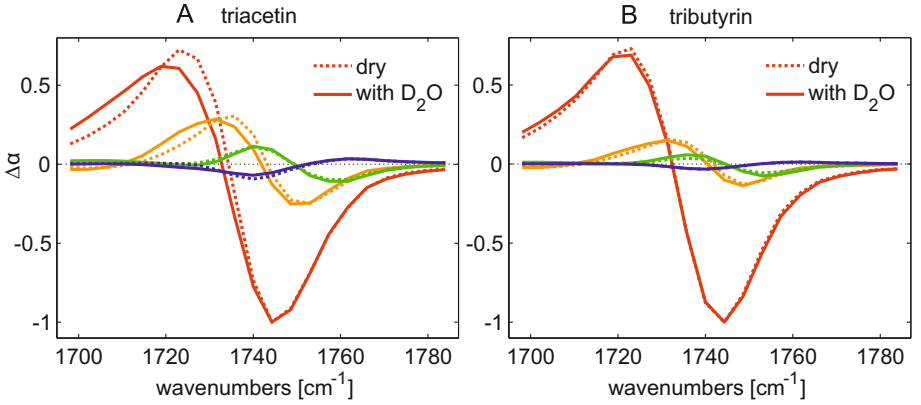

FIGURE 9.5. Spectral components that describe the isotropic absorption change (fig. 9.3) for triacetin (A) and tributyrin (B) with and without D_2O. The components are normalized on the intensity of the first component (shown in red).

fail to fully capture the dynamics beyond 15 picoseconds after the excitation, while introducing a fourth component does not significantly reduce the least-squares error of the fit. The result of the triple component fit is displayed with solid lines in figure 9.3 and 9.4, and is in good agreement with the data at all frequencies and delay times.

The spectral components resulting from the fit are displayed in figure 9.5. For all samples, each consecutive spectral component increases in center frequency, with the first and main component exhibiting a bleaching signal centered around $\sim$1745 cm^{-1}, the second component around $\sim$1750 cm^{-1} and the third around $\sim$1760 cm^{-1} or $\sim$1755 cm^{-1}, for triacetin and tributyrin, respectively. The lifetimes associated with each component are presented in table I, and range from about 1.5 picoseconds for the lowest-frequency component to about 40 picoseconds for the highest-frequency component. The large range of lifetimes directly reflects the strong inhomogeneity of the vibrational relaxation of the carbonyl vibrations.

Addition of water to the triglycerides affects the isotropic transient spectrum, as can be seen most clearly by inspection of the spectral components (fig. 9.5). For the triglycerides with water, all spectral components show a redshift,

TABLE I. Lifetimes of the spectral components (fig. 9.5) that describe the isotropic absorption change for triacetin and tributyrin with and without added D_2O.

	$T_{1,1}$ [ps]	$T_{1,2}$ [ps]	$T_{1,3}$ [ps]
Triacetin	1.6 ± 0.1	7.4 ± 0.5	43 ± 3
Triacetin with D_2O	1.6 ± 0.1	7.3 ± 0.5	32 ± 3
Tributyrin	1.4 ± 0.1	6.8 ± 0.5	40 ± 4
Tributyrin with D_2O	1.3 ± 0.1	6.2 ± 0.5	32 ± 5

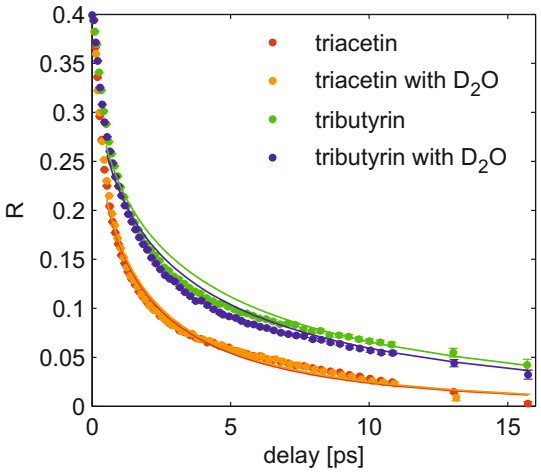

FIGURE 9.6. Anisotropy decay of the carbonyl stretch vibrations of triacetin and tributyrin with and without added D_2O, averaged over the frequency range 1700-1785 cm^{-1}. The solid lines represent fits to a Förster transfer formula (eq. 9.2).

as was observed for the linear absorption spectra. This redshift results from the response of carbonyl groups that are hydrogen-bonded to water and that absorb at lower frequencies.

The addition of water lowers the vibrational lifetime. The lifetime decreases most strongly for the third component, which has an associated lifetime of 43 $\pm$ 3 or 40 $\pm$ 4 ps for dry triacetin and tributyrin, respectively, and a lifetime of 32 $\pm$ 5 ps for triacetin and tributyrin with water. This indicates that the vibrational lifetime of carbonyl groups that are hydrogen-bonded to water is on average shorter than the vibrational lifetime of non-hydrogen-bonded carbonyl groups.

9.3.3 ANISOTROPIC RESPONSE

To further characterize the interaction between water molecules and the triglycerides, we measured the anisotropic response of the carbonyl stretch vibrations. The anisotropy is directly proportional to the second-order rotational correlation function, and decays due to molecular reorientation and vibrational (Förster) energy transfer. Figure 9.6 presents the anisotropy decay for triacetin and tributyrin with and without added water (the anisotropy is corrected for the isotropic heating contribution). For both triglycerides, the anisotropy decays almost to zero in about 15 picoseconds. Since triglyceride molecules are expected to reorient on a much slower timescale, considering their large size, and librations would lead only to partial anisotropy decay, the anisotropy likely decays as a result of vibrational energy transfer between carbonyl groups. The anisotropy decay as a result of energy transfer between the same type of oscil-

lators can be described by[66,199].

$$R(t) = \frac{2}{5} e^{-\frac{4}{3}\pi^{3/2} c \sqrt{r_o t / T_1}} \tag{9.2}$$

where c is the concentration of oscillators, in this case carbonyl groups, T_1 is the vibrational lifetime and r_o the Förster radius. The Förster radius denotes the distance between oscillators at which the rate of energy transfer between them is 50% within the vibrational lifetime. This distance depends on the transition dipole moment of the vibration and the homogeneous versus inhomogeneous linewidth (see eq. 2.34). In writing eq. 9.2, it is assumed that the distance between the oscillators is statistically distributed, and that the orientation of oscillators is independent of this distance[199]. This is not the case for the carbonyl groups of triglycerides, where the three carbonyl groups of each molecule sample a limited amount of distances and orientations with respect to each other. Nonetheless, we observe that the anisotropy decay of the carbonyl stretch vibration is quite well described by eq. 9.2, as indicated by the solid lines in figure 9.6, which are the result of a least-squares fit to this equation. For tributyrin, the measured anisotropy initially decays somewhat faster than the Förster formula can capture, most likely due to faster-than-average energy transfer between carbonyl groups located on the same molecule, which does not lead to a full decay of the anisotropy, because the direction of these carbonyl groups is correlated. This is less important for triacetin, as the molecules, and thus the carbonyl groups located on different molecules, are closer together.

From the fit, we obtain Förster radii of 2.6 ± 0.1 Å and 2.5 ± 0.1 Å for triacetin and tributyrin, respectively, independent of the water content. As expected, the Förster radii for triacetin and tributyrin are similar, because the transition dipole moment and spectral width of the carbonyl stretch vibration are similar for these triglycerides (see fig. 9.2). The overall decay of the anisotropy is slower for tributyrin, since the average distance between carbonyl groups is larger for this triglyceride.

9.4 DISCUSSION

We observe that the vibrational relaxation of the carbonyl stretch vibrations of triacetin and tributyrin is very inhomogeneous. The vibrational relaxation can be described well with three spectral components, with associated lifetimes of ∼1.5 ps, ∼7 ps and ∼40 ps. These spectral components probably do not represent specific species of carbonyl vibrations, but rather serve to describe a continuous distribution of vibrational relaxation times across the inhomogeneously broadened carbonyl absorption band. This distribution likely arises from different local conformations of the glycerol backbone and fatty acid chains of the triglyceride. Below the melting point, triglycerides adopt different polycrystalline phases that are thought to persist to some extent in the liquid[22], and that give rise to distinct C=O stretch vibrational frequencies[200,201].

We further observe that adding water to the triglycerides leads to a broadening of the transient C=O vibrational response towards the low-frequency side

and a decrease in vibrational lifetime, due to the response of carbonyl groups that are hydrogen-bonded to water. A similar reduction in vibrational lifetime upon hydrogen-bond formation has been observed for the carbonyl vibrations of methyl and ethyl acetate[202–204], and was explained by the increase in the vibrational density of states (VDOS) as a result of the low-frequency vibrations of the intermolecular hydrogen bond[203]. An alternative explanation is that the lifetime of the carbonyl stretch vibration decreases with decreasing frequency, due to better spectral overlap with a lower-frequency vibrational mode to which the carbonyl stretch vibration relaxes.

We observed that the anisotropy of excited carbonyl stretch vibrations decays via vibrational (Förster) energy transfer between carbonyl stretch vibrations, and that the water content does not influence the anisotropy decay. The insensitivity of the anisotropy decay to the presence of water is likely due to the low water concentration. Since most carbonyl groups are not hydrogen-bonded to a water molecule, the carbonyl groups that are hydrogen-bonded to water are on average located far away from each other, meaning that the anisotropy decay of hydrogen-bonded carbonyl groups is likely dominated by energy transfer to non-hydrogen-bonded carbonyl groups.

9.5 Conclusions

We studied the effect of water on the carbonyl stretch vibration of triacetin and tributyrin, using linear infrared and polarization-resolved femtosecond infrared spectroscopy. We observe that hydrogen-bond formation between a water molecule and the carbonyl group of the triglyceride leads to a frequency downshift of the absorption of the carbonyl stretch vibration from $\sim$1745 cm^{-1} to $\sim$1728 cm^{-1}.

Excitation of the carbonyl stretch vibration induces a transient absorption response that can be described with three spectral components with increasing frequency and associated decay times ranging from 1.3 to 43 picoseconds, reflecting a strongly inhomogeneous vibrational relaxation. This inhomogeneity is present for both the dry triglycerides and the triglycerides with added water. Adding water leads to a broadening of the spectral components and a slight speedup of the vibrational relaxation.

The anisotropy of excited carbonyl stretch vibrations decays via vibrational (Förster) energy transfer between carbonyl stretch vibrations. We find a Förster radius of 2.6 $\pm$ 0.1 Å for triacetin and 2.5 $\pm$ 0.1 Å for tributyrin, independent of the water content.

Bibliography

1. I. Brovchenko and A. Oleinikova. Multiple phases of liquid water. *ChemPhysChem*, 9(18):2660–2675, 2008.

2. M. Chaplin. Water structure and science. www.lsbu.ac.uk/water, june 2016.

3. K. Ichikawa, Y. Kameda, T. Yamaguchi, H. Wakita, and M. Misawa. Neutron-diffraction investigation of the intramolecular structure of a water molecule in the liquid phase at high temperatures. *Mol. Phys.*, 73(1): 79–86, 1991.

4. A. Rastogi, A. K. Ghosh, and S. J. Suresh. Hydrogen bond interactions between water molecules in bulk liquid, near electrode surfaces and around ions. In J. C. M. Piraján, editor, *Thermodynamics - Physical Chemistry of Aqueous Systems*, chapter 13, pages 351–364. InTech, Rijeka, 2011.

5. J. D. Eaves, J. J. Loparo, C. J. Fecko, S. T. Roberts, A. Tokmakoff, and P. L. Geissler. Hydrogen bonds in liquid water are broken only fleetingly. *Proc. Natl. Acad. Sci. U.S.A.*, 102:13019–13022, 2005.

6. C. J. Fecko, J. D. Eaves, J. J. Loparo, A. Tokmakoff, and P. L. Geissler. Ultrafast hydrogen-bond dynamics in the infrared spectroscopy of water. *Science*, 301(5640):1698–1702, 2003.

7. C. J. Fecko, J. J. Loparo, S. T. Roberts, and A. Tokmakoff. Local hydrogen bonding dynamics and collective reorganization in water: Ultrafast infrared spectroscopy of HOD/D_2O. *J. Chem. Phys.*, 122(5):054506, 2005.

8. C. P Lawrence and J. L Skinner. Ultrafast infrared spectroscopy probes hydrogen-bonding dynamics in liquid water. *Chem. Phys. Lett.*, 369(34): 472 – 477, 2003.

9. C. P. Lawrence and J. L. Skinner. Vibrational spectroscopy of HOD in liquid D_2O. III. spectral diffusion, and hydrogen-bonding and rotational dynamics. *J. Chem. Phys.*, 118(1):264–272, 2003.

10. T. Steinel, J. B Asbury, S. A Corcelli, C. P Lawrence, J. L Skinner, and M. D Fayer. Water dynamics: dependence on local structure probed with vibrational echo correlation spectroscopy. *Chem. Phys. Lett.*, 386(46):295 – 300, 2004.

11. H. J. Bakker, Y. L. A. Rezus, and R. L. A. Timmer. Molecular reorientation of liquid water studied with femtosecond midinfrared spectroscopy. *J. Phys. Chem. A*, 112(46):11523–11534, 2008.

12. M. Ji, M. Odelius, and K. J. Gaffney. Large angular jump mechanism observed for hydrogen bond exchange in aqueous perchlorate solution. *Science*, 328(5981):1003–1005, 2010.

13. D. Laage and J. T. Hynes. A molecular jump mechanism of water reorientation. *Science*, 311(5762):832–835, 2006.

14. R. Jimenez, G. R. Fleming, P. V. Kumar, and M. Maroncelli. Femtosecond solvation dynamics of water. *Nature*, 369(6480):471–473, 1994.

15. T. R. Dyke and J. S. Muenter. Electric dipole moments of low J states of H_2O and D_2O. *J. Chem. Phys.*, 59(6):3125–3127, 1973.

16. D. Chandler. Interfaces and the driving force of hydrophobic assembly. *Nature*, 437(7059):640–647, 2005.

17. G. E. Walrafen. Raman spectral studies of HDO in H_2O. *J. Chem. Phys.*, 48(1):244–251, 1968.

18. N. Muller. Is there a region of highly structured water around a nonpolar solute molecule? *J. Solution Chem.*, 17(7):661–672, 1988.

19. B. Bagchi. Water dynamics in the hydration layer around proteins and micelles. *Chem. Rev.*, 105(9):3197–3219, 2005.

20. P. Ball. Water as an active constituent in cell biology. *Chem. Rev.*, 108 (1):74–108, 2008.

21. J. Milhaud. New insights into water-phospholipid model membrane interactions. *Biochim. Biophys. Acta, Biomembranes*, 1663(12):19 – 51, 2004.

22. M. Iwahashi and Y. Kasahara. Dynamic molecular movements and aggregation structures of lipids in a liquid state. *Curr. Opin. Colloid Interface Sci.*, 16(5):359 – 366, 2011.

23. K. A. Dill. Dominant forces in protein folding. *Biochemistry*, 29(31): 7133–7155, 1990.

24. Y. Levy and J. N. Onuchic. Water mediation in protein folding and molecular recognition. *Annu. Rev. Biophys. Biomol. Struc.*, 35:389–415, 2006.

25. G. D. Rose, P. J. Fleming, J. R. Banavar, and A. Maritan. A backbone-based theory of protein folding. *Proc. Natl. Acad. Sci. U.S.A.*, 103(45): 16623–16633, 2006.

26. G. A. Papoian, J. Ulander, M. P. Eastwood, Z. Luthey-Schulten, and P. G. Wolynes. Water in protein structure prediction. *Proc. Natl. Acad. Sci. U.S.A.*, 101(10):3352–3357, 2004.

27. G. Careri, E. Gratton, P.-H. Yang, and J. A. Rupley. Correlation of IR spectroscopic, heat capacity, diamagnetic susceptibility and enzymatic measurements on lysozyme powder. *Nature*, 284(5756):572–573, 1980.

28. R. V. Dunn and R. M. Daniel. The use of gas–phase substrates to study enzyme catalysis at low hydration. *Phil. Trans. R. Soc. B*, 359(1448): 1309–1320, 2004.

29. P. W. Fenimore, H. Frauenfelder, B. H. McMahon, and F. G. Parak. Slaving: Solvent fluctuations dominate protein dynamics and functions. *Proc. Natl. Acad. Sci. U.S.A.*, 99(25):16047–16051, 2002.

30. H. Frauenfelder, G. Chen, J. Berendzen, P. W. Fenimore, H. Jansson, B. H. McMahon, I. R. Stroe, J. Swenson, and R. D. Young. A unified model of protein dynamics. *Proc. Natl. Acad. Sci. U.S.A.*, 106(13):5129–5134, 2009.

31. Y. Qin, L. Wang, and D. Zhong. Dynamics and mechanism of ultrafast water-protein interactions. *Proc. Natl. Acad. Sci. U.S.A.*, 113(30):8424–8429, 2016.

32. F. Autenrieth, E. Tajkhorshid, K. Schulten, and Z. Luthey-Schulten. Role of water in transient cytochrome c2 docking. *J. Phys. Chem. B*, 108(52): 20376–20387, 2004.

33. S. Braun-Sand, M. Strajbl, and A. Warshel. Studies of proton translocations in biological systems: Simulating proton transport in carbonic anhydrase by EVB-based models. *Biophys. J.*, 87(4):2221 – 2239, 2004.

34. B. C. Roberts and R. L. Mancera. Ligand-protein docking with water molecules. *J. Chem. Inf. Model*, 48(2):397–408, 2008.

35. P. H. Yancey, M. E. Clark, S. C. Hand, R. D. Bowlus, and G. N. Somero. Living with water stress: evolution of osmolyte systems. *Science*, 217 (4566):1214–1222, 1982.

36. D. R. Canchi and A. E. García. Cosolvent effects on protein stability. *Annu. Rev. Phys. Chem.*, 64(1):273–293, 2013.

37. S. N. Timasheff. Protein-solvent preferential interactions, protein hydration, and the modulation of biochemical reactions by solvent components. *Proc. Natl. Acad. Sci. U.S.A.*, 99(15):9721–9726, 2002.

38. M. Auton and D. W. Bolen. Predicting the energetics of osmolyte-induced protein folding/unfolding. *Proc. Natl. Acad. Sci. U.S.A.*, 102(42):15065–15068, 2005.

39. L. Hua, R. Zhou, D. Thirumalai, and B. J. Berne. Urea denaturation by stronger dispersion interactions with proteins than water implies a 2-stage unfolding. *Proc. Natl. Acad. Sci. U.S.A.*, 105(44):16928–16933, 2008.

40. D. Tobi, R. Elber, and D. Thirumalai. The dominant interaction between peptide and urea is electrostatic in nature: A molecular dynamics simulation study. *Biopolymers*, 68(3):359–369, 2003.

41. A. Möglich, F. Krieger, and T. Kiefhaber. Molecular basis for the effect of urea and guanidinium chloride on the dynamics of unfolded polypeptide chains. *J. Mol. Biol.*, 345(1):153 – 162, 2005.

42. B. J. Bennion and V. Daggett. The molecular basis for the chemical denaturation of proteins by urea. *Proc. Natl. Acad. Sci. U.S.A.*, 100(9): 5142–5147, 2003.

43. B. J. Bennion and V. Daggett. Counteraction of urea-induced protein denaturation by trimethylamine N-oxide: A chemical chaperone at atomic resolution. *Proc. Natl. Acad. Sci. U.S.A.*, 101(17):6433–6438, 2004.

44. H. S. Frank and F. Franks. Structural approach to the solvent power of water for hydrocarbons; urea as a structure breaker. *J. Chem. Phys.*, 48 (10):4746–4757, 1968.

45. P. K. Verma, H. Lee, J.-Y. Park, J.-H. Lim, M. Maj, J.-H. Choi, K.-W. Kwak, and M. Cho. Modulation of the hydrogen bonding structure of water by renal osmolytes. *J. Phys. Chem. Lett.*, 6(14):2773–2779, 2015.

46. B. Auer, R. Kumar, J. R. Schmidt, and J. L. Skinner. Hydrogen bonding and Raman, IR, and 2D-IR spectroscopy of dilute HOD in liquid D_2O. *Proc. Natl. Acad. Sci. U.S.A.*, 104(36):14215–14220, 2007.

47. B. M. Auer and J. L. Skinner. Water: Hydrogen bonding and vibrational spectroscopy, in the bulk liquid and at the liquid/vapor interface. *Chem. Phys. Lett.*, 470(13):13 – 20, 2009.

48. H. J. Bakker and J. L. Skinner. Vibrational spectroscopy as a probe of structure and dynamics in liquid water. *Chem. Rev.*, 110(3):1498–1517, 2010.

49. J. Tennyson, P. F. Bernath, L. R. Brown, A. Campargue, A. G. Császár, L. Daumont, R. R. Gamache, J. T. Hodges, O. V. Naumenko, O. L. Polyansky, L. S. Rothman, A. Carine Vandaele, N. F. Zobov, A. R. Al Derzi, C. Fábri, A. Z. Fazliev, T. Furtenbacher, I. E. Gordon, L. Lodi, and I. I. Mizus. IUPAC critical evaluation of the rotational-vibrational spectra of water vapor, Part III: Energy levels and transition wavenumbers for $H_2{}^{16}O$. *J. Quant. Spectrosc. Radiat. Transfer*, 117:29 – 58, 2013.

50. R. Laenen, C. Rauscher, and A. Laubereau. Dynamics of local substructures in water observed by ultrafast infrared hole burning. *Phys. Rev. Lett.*, 80:2622–2625, Mar 1998.

51. S. Woutersen and H. J. Bakker. Hydrogen bond in liquid water as a brownian oscillator. *Phys. Rev. Lett.*, 83:2077–2080, Sep 1999.

52. G. Herzberg. *Molecular spectra and molecular structure II: Infrared and Raman spectra of polyatomic molecules.* D. Van Nostrand Company, New York, 1945.

53. E. B. Wilson, J. C. Desius, and P. C. Cross. *Molecular vibrations: the theory of infrared and Raman vibrational spectra.* McGraw-Hill book company Inc., New York, 1955.

54. D. J. Griffiths. *Introduction to quantum mechanics.* Pearson Education International, 1995.

55. P. W. Atkins. *Physical Chemistry, Sixth Edition.* Oxford University Press, 1998.

56. E. R. Lippincott and R. Schroeder. One-dimensional model of the hydrogen bond. *J. Chem. Phys.*, 23(6):1099–1106, 1955.

57. M. Fox. *Quantum Optics: An introduction.* Oxford University Press, 2006.

58. C. P. Lawrence and J. L. Skinner. Vibrational spectroscopy of HOD in liquid D_2O. II. infrared line shapes and vibrational stokes shift. *J. Chem. Phys.*, 117(19):8847–8854, 2002.

59. J. R. Schmidt, S. A. Corcelli, and J. L. Skinner. Pronounced non-condon effects in the ultrafast infrared spectroscopy of water. *J. Chem. Phys.*, 123 (4):044513, 2005.

60. P. Hamm and M. Zanni. *Concepts and Methods of 2D Infrared Spectroscopy.* Cambridge University Press, 2011.

61. S. Mukamel. *Principles of Nonlinear Optical Spectroscopy.* Oxford University Press, New York, 1995. ISBN 0-19-509278-3.

62. V. M. Kenkre, A. Tokmakoff, and M. D. Fayer. Theory of vibrational relaxation of polyatomic molecules in liquids. *J. Chem. Phys.*, 101(12): 10618–10629, 1994.

63. S. T. Roberts, J. J. Loparo, and A. Tokmakoff. Characterization of spectral diffusion from two-dimensional line shapes. *J. Chem. Phys.*, 125(8):084502, 2006.

64. K. Kwac and M. Cho. Two-color pump-probe spectroscopies of two- and three-level systems: 2-dimensional line shapes and solvation dynamics. *J. Phys. Chem. A*, 107(31):5903–5912, 2003.

65. K. Kwak, S. Park, I. J. Finkelstein, and M. D. Fayer. Frequency-frequency correlation functions and apodization in two-dimensional infrared vibrational echo spectroscopy: A new approach. *J. Chem. Phys.*, 127(12): 124503, 2007.

66. T. Förster. Experimentelle und theoretische untersuchung des zwischenmolekularen uberangs von elektronenanregungsenergie. *Z.Naturforschg.*, 4a:321327, 1949.

67. D. Rehm and K. B. Eisenthal. Intermolecular energy transfer studied with picosecond light pulses. *Chem. Phys. Lett.*, 9(5):387 – 389, 1971.

68. B. J. Berne and R. Pecora. *Dynamic Light Scattering*. Dover Publications, Inc., 2000.

69. G. Lipari and A. Szabo. Effect of librational motion on fluorescence depolarization and nuclear magnetic resonance relaxation in macromolecules and membranes. *Biophys. J.*, 30(3):489 – 506, 1980.

70. R. W. Boyd. *Nonlinear Optics*. Elsevier: Academic Press, 2008.

71. R. Bloem, S. Garrett-Roe, H. Strzalka, P. Hamm, and P. Donaldson. Enhancing signal detection and completely eliminating scattering using quasi-phase-cycling in 2D IR experiments. *Opt. Express*, 18(26):27067–27078, Dec 2010.

72. J. Helbing and P. Hamm. Compact implementation of fourier transform two-dimensional IR spectroscopy without phase ambiguity. *J. Opt. Soc. Am. B*, 28(1):171–178, Jan 2011.

73. F. O. Libnau, A. A. Christy, and O. M. Kvalheim. Determination of the equilibrium constant and resolution of the HOD spectrum by alternating least-squares and infrared analysis. *Appl. Spectrosc.*, 49(10):1431–1437, Oct 1995.

74. Y. L. A. Rezus and H. J. Bakker. On the orientational relaxation of HDO in liquid water. *J. Chem. Phys.*, 123(11):114502, 2005.

75. S. Lotze, C. C. M. Groot, C. Vennehaug, and H. J. Bakker. Femtosecond mid-infrared study of the dynamics of water molecules in water-acetone and water-dimethyl sulfoxide mixtures. *J. Phys. Chem. B*, 119(16):5228–5239, 2015.

76. S. T. van der Post and H. J. Bakker. The combined effect of cations and anions on the dynamics of water. *Phys. Chem. Chem. Phys.*, 14:6280–6288, 2012.

77. S. T. van der Post, S. Scheidelaar, and H. J. Bakker. Femtosecond study of the effects of ions on the reorientation dynamics of water. *J. Mol. Liq.*, 176(0):22 – 28, 2012.

78. T. Arakawa and S. N. Timasheff. Stabilization of protein structure by sugars. *Biochemistry*, 21(25):6536–6544, 1982.

79. G. Xie and S. N. Timasheff. The thermodynamic mechanism of protein stabilization by trehalose. *Biophys. Chem.*, 64(13):25 – 43, 1997.

80. D. Corradini, E. G. Strekalova, H. E. Stanley, and Paola Gallo. Microscopic mechanism of protein cryopreservation in an aqueous solution with trehalose. *Sci. Rep.*, 3:1218, 2013.

81. A. Lerbret, F. Affouard, P. Bordat, A. Hédoux, Y. Guinet, and M. Descamps. Slowing down of water dynamics in disaccharide aqueous solutions. *J. Non-Cryst. Solids*, 357(2):695–699, 2011.

82. M. E. Gallina, P. Sassi, M. Paolantoni, A. Morresi, and R. S. Cataliotti. Vibrational analysis of molecular interactions in aqueous glucose solutions. Temperature and concentration effects. *J. Phys. Chem. B*, 110(17):8856–8864, 2006.

83. C. Branca, S. Magazù, G. Maisano, S. M. Bennington, and B. Fåk. Vibrational studies on disaccharide/H_2O systems by inelastic neutron scattering, Raman, and IR spectroscopy. *J. Phys. Chem. B*, 107(6):1444–1451, 2003.

84. J. J. Towey and L. Dougan. Structural examination of the impact of glycerol on water structure. *J. Phys. Chem. B*, 116(5):1633–1641, 2012.

85. P. E. Mason, G. W. Neilson, J. E. Enderby, M.-L. Saboungi, and J. W. Brady. Structure of aqueous glucose solutions as determined by neutron diffraction with isotopic substitution experiments and molecular dynamics calculations. *J. Phys. Chem. B*, 109(27):13104–13111, 2005.

86. S. E. Pagnotta, S. E. McLain, A. K. Soper, F. Bruni, and M. A. Ricci. Water and trehalose: How much do they interact with each other? *J. Phys. Chem. B*, 114(14):4904–4908, 2010.

87. U. Heugen, G. Schwaab, E. Bründermann, M. Heyden, X. Yu, D. M. Leitner, and M. Havenith. Solute-induced retardation of water dynamics probed directly by terahertz spectroscopy. *Proc. Natl. Acad. Sci. U.S.A.*, 103(33):12301–12306, 2006.

88. M. Heyden, E. Bründermann, U. Heugen, G. Niehues, D. M. Leitner, and M. Havenith. Long-range influence of carbohydrates on the solvation dynamics of water - answers from terahertz absorption measurements and molecular modeling simulations. *J. Am. Chem. Soc.*, 130(17):5773–5779, 2008.

89. K. Fuchs and U. Kaatze. Molecular dynamics of carbohydrate aqueous solutions. Dielectric relaxation as a function of glucose and fructose concentration. *J. Phys. Chem. B*, 105(10):2036–2042, 2001.

90. L. R. Winther, J. Qvist, and B. Halle. Hydration and mobility of trehalose in aqueous solution. *J. Phys. Chem. B*, 116(30):9196–9207, 2012.

91. M. Sajadi, F. Berndt, C. Richter, M. Gerecke, R. Mahrwald, and N. P. Ernsting. Observing the hydration layer of trehalose with a linked molecular terahertz probe. *J. Phys. Chem. Lett.*, 5(11):1845–1849, 2014.

92. L. Lupi, L. Comez, M. Paolantoni, S. Perticaroli, P. Sassi, A. Morresi, B. M. Ladanyi, and D. Fioretto. Hydration and aggregation in mono- and disaccharide aqueous solutions by gigahertz-to-terahertz light scattering and molecular dynamics simulations. *J. Phys. Chem. B*, 116(51):14760–14767, 2012.

93. D. Fioretto, L. Comez, M.E. Gallina, A. Morresi, L. Palmieri, M. Paolantoni, P. Sassi, and F. Scarponi. Separate dynamics of solute and solvent in water-glucose solutions by depolarized light scattering. *Chem. Phys. Lett.*, 441(46):232 – 236, 2007.

94. S. L. Lee, P. G. Debenedetti, and J. R. Errington. A computational study of hydration, solution structure, and dynamics in dilute carbohydrate solutions. *J. Chem. Phys.*, 122(20):204511, 2005.

95. A. Magno and P. Gallo. Understanding the mechanisms of bioprotection: A comparative study of aqueous solutions of trehalose and maltose upon supercooling. *J. Phys. Chem. Lett.*, 2(9):977–982, 2011.

96. A. Vila Verde and R. K. Campen. Disaccharide topology induces slowdown in local water dynamics. *J. Phys. Chem. B*, 115(21):7069–7084, 2011.

97. S. T. van der Post. *Love and fear of water : water dynamics around charged and apolar solutes*. PhD thesis, University of Amsterdam, February 7th 2014.

98. A. Lerbret, P. E. Mason, R. M. Venable, A. Cesàro, M. L. Saboungi, R. W. Pastor, and J. W. Brady. Molecular dynamics studies of the conformation of sorbitol. *Carbohyd. Res.*, 344(16):2229 – 2235, 2009.

99. S. T. van der Post, K.-J. Tielrooij, J. Hunger, E. H. G. Backus, and H. J. Bakker. Femtosecond study of the effects of ions and hydrophobes on the dynamics of water. *Farad. Discuss.*, 160:171–189, 2013.

100. J. Hunger, K.-J. Tielrooij, R. Buchner, M. Bonn, and H. J. Bakker. Complex formation in aqueous trimethylamine-N-oxide (TMAO) solutions. *J. Phys. Chem. B*, 116(16):4783–4795, 2012.

101. Y. L. A. Rezus and H. J. Bakker. Observation of immobilized water molecules around hydrophobic groups. *Phys. Rev. Lett.*, 99:148301, Oct 2007.

102. K.-J. Tielrooij, J. Hunger, R. Buchner, M. Bonn, and H. J. Bakker. Influence of concentration and temperature on the dynamics of water in the hydrophobic hydration shell of tetramethylurea. *J. Am. Chem. Soc.*, 132 (44):15671–15678, 2010.

103. S. M. Kelly and N. C. Price. The use of circular dichroism in the investigation of protein structure and function. *Curr. Protein Pept. Sci.*, 1(4): 349–384, 2000.

104. V. P. Denisov and B. Halle. Thermal denaturation of ribonuclease a characterized by water ^{17}O and ^{2}H magnetic relaxation dispersion. *Biochemistry*, 37(26):9595–9604, 1998.

105. V. P. Denisov, B.-H. Jonsson, and B. Halle. Hydration of denatured and molten globule proteins. *Nat. Struct. Mol. Biol.*, 6:253–260, 1999.

106. A. C. Fogarty and D. Laage. Water dynamics in protein hydration shells: The molecular origins of the dynamical perturbation. *J. Phys. Chem. B*, 118(28):7715–7729, 2014.

107. A. Luise, M. Falconi, and A. Desideri. Molecular dynamics simulation of solvated azurin: Correlation between surface solvent accessibility and water residence times. *Proteins: Struct. Funct. Bioinf.*, 39(1):56–67, 2000.

108. V. A. Makarov, B. K. Andrews, P. E. Smith, and B. M. Pettitt. Residence times of water molecules in the hydration sites of myoglobin. *Biophys. J.*, 79(6):2966 – 2974, 2000.

109. F. Sterpone, G. Stirnemann, and D. Laage. Magnitude and molecular origin of water slowdown next to a protein. *J. Am. Chem. Soc.*, 134(9): 4116–4119, 2012.

110. C. Mattea, J. Qvist, and B. Halle. Dynamics at the protein-water interface from ^{17}O spin relaxation in deeply supercooled solutions. *Biophys. J.*, 95 (6):2951 – 2963, 2008.

111. Y.-T. Qiu, W.and Kao, L. Zhang, Y. Yang, L. Wang, W. E. Stites, D. Zhong, and A. H. Zewail. Protein surface hydration mapped by site-specific mutations. *Proc. Natl. Acad. Sci. U.S.A.*, 103(38):13979–13984, 2006.

112. D. Zhong, S. K. Pal, and A. H. Zewail. Biological water: A critique. *Chem. Phys. Lett.*, 503(13):1 – 11, 2011.

113. B. D. Armstrong, J. Choi, C. López, D. A. Wesener, W. Hubbell, S. Cavagnero, and S. Han. Site-specific hydration dynamics in the nonpolar core of a molten globule by dynamic nuclear polarization of water. *J. Am. Chem. Soc.*, 133(15):5987–5995, 2011.

114. N. V. Nucci, M. S. Pometun, and A. J. Wand. Mapping the hydration dynamics of ubiquitin. *J. Am. Chem. Soc.*, 133(32):12326–12329, 2011.

115. K.-J. Tielrooij, C. Petersen, Y. L. A. Rezus, and H. J. Bakker. Reorientation of HDO in liquid H_2O at different temperatures: Comparison of first and second order correlation functions. *Chem. Phys. Lett.*, 471(13):71–74, 2009.

116. C. Petersen, K.-J. Tielrooij, and H. J. Bakker. Strong temperature dependence of water reorientation in hydrophobic hydration shells. *J. Chem. Phys.*, 130(21):214511, 2009.

117. Y. L. A. Rezus and H. J. Bakker. Effect of urea on the structural dynamics of water. *Proc. Natl. Acad. Sci. U.S.A.*, 103(49):18417–18420, 2006.

118. R. Fraczkiewicz and W. Braun. Exact and efficient analytical calculation of the accessible surface areas and their gradients for macromolecules. *J. Comput. Chem.*, 19(3):319–333, 1998.

119. J. Qvist and B. Halle. Thermal signature of hydrophobic hydration dynamics. *J. Am. Chem. Soc.*, 130(31):10345–10353, 2008.

120. Ø. Halskau, R. Perez-Jimenez, B. Ibarra-Molero, J. Underhaug, V. Muñoz, A. Martinez, and J. M. Sanchez-Ruiz. Large-scale modulation of thermodynamic protein folding barriers linked to electrostatics. *Proc. Natl. Acad. Sci. U.S.A.*, 105(25):8625–8630, 2008.

121. A. Hedoux, S. Krenzlin, L. Paccou, Y. Guinet, M.-P. Flament, and J. Siepmann. Influence of urea and guanidine hydrochloride on lysozyme stability and thermal denaturation; a correlation between activity, protein dynamics and conformational changes. *Phys. Chem. Chem. Phys.*, 12:13189–13196, 2010.

122. K. Schlepckow, J. Wirmer, A. Bachmann, T. Kiefhaber, and H. Schwalbe. Conserved folding pathways of α-lactalbumin and lysozyme revealed by kinetic CD, fluorescence, NMR, and interrupted refolding experiments. *J. Mol. Biol.*, 378(3):686 – 698, 2008.

123. S. N. Timasheff and G. Xie. Preferential interactions of urea with lysozyme and their linkage to protein denaturation. *Biophys. Chem.*, 105(23):421–448, 2003.

124. L.-Z. Wu, B.-L. Ma, D.-W. Zou, Z.-X. Tie, J. Wang, and W. Wang. Influence of metal ions on folding pathway and conformational stability of bovine serum albumin. *J. Mol. Struct.*, 877(13):44 – 49, 2008.

125. K. P. Barnes, J. R. Warren, and J. A. Gordon. Effect of urea on the circular dichroism of lysozyme. *J. Biol. Chem.*, 247(6):1708–1712, 1972.

126. S. Emadi and M. Behzadi. A comparative study on the aggregating effects of guanidine thiocyanate, guanidine hydrochloride and urea on lysozyme aggregation. *Biochem. Biophys. Res. Commun.*, 450(4):1339–1344, 2014.

127. T. Kühn and H. Schwalbe. Monitoring the kinetics of ion-dependent protein folding by time-resolved NMR spectroscopy at atomic resolution. *J. Am. Chem. Soc.*, 122(26):6169–6174, 2000.

128. V. N. Uversky and A. L. Fink. The chicken-egg scenario of protein folding revisited. *FEBS Lett.*, 515(13):79 – 83, 2002.

129. J. A. Jones, D. K. Wilkins, L. J. Smith, and C. M. Dobson. Characterisation of protein unfolding by NMR diffusion measurements. *J. Biomol. NMR*, 10(2):199–203, 1997.

130. U. Mahammad Yasin, P. Sashi, and A. K. Bhuyan. Free energy landscape of lysozyme: Multiple near-native conformational states and rollover in the urea dependence of folding energy. *J. Phys. Chem. B*, 118(24):6662–6669, 2014.

131. R. Wijesinha-Bettoni, C. M. Dobson, and C. Redfield. Comparison of the denaturant-induced unfolding of the bovine and human α-lactalbumin molten globules. *J. Mol. Biol.*, 312(1):261 – 273, 2001.

132. S. Yamamoto, S. Fujii, N. Yoshimoto, and P. Akbarzadehlaleh. Effects of protein conformational changes on separation performance in electrostatic interaction chromatography: Unfolded proteins and PEGylated proteins. *J. Biotechnol.*, 132(2):196–201, 2007.

133. K. Kuwajima. The molten globule state of alpha-lactalbumin. *FASEB J.*, 10(1):102–9, 1996.

134. E. W. Chung, E. J. Nettleton, C. J. Morgan, M. Groß, A. Miranker, S. E. Radford, C. M. Dobson, and C. V. Robinson. Hydrogen exchange properties of proteins in native and denatured states monitored by mass spectrometry and NMR. *Protein Sci.*, 6(6):1316–1324, 1997.

135. C. M. Quezada, B. A. Schulman, J. J. Froggatt, C. M. Dobson, and C. Redfield. Local and global cooperativity in the human α-lactalbumin molten globule. *J. Mol. Biol.*, 338(1):149 – 158, 2004.

136. R. Wijesinha-Bettoni, C. M. Dobson, and C. Redfield. Comparison of the structural and dynamical properties of holo and apo bovine α-lactalbumin by NMR spectroscopy. *J. Mol. Biol.*, 307(3):885 – 898, 2001.

137. B. Ibarra-Molero and J. M. Sanchez-Ruiz. Are there equilibrium intermediate states in the urea-induced unfolding of hen egg-white lysozyme? *Biochemistry*, 36(31):9616–9624, 1997.

138. S. E. Radford, C. M. Dobson, and P. A. Evans. The folding of hen lysozyme involves partially structured intermediates and multiple pathways. *Nature*, 358:302–307, 1992.

139. M. Arai and K. Kuwajima. Rapid formation of a molten globule intermediate in refolding of α-lactalbumin. *Fold. Des.*, 1(4):275 – 287, 1996.

140. M. M. G. Krishna, Y. Lin, L. Mayne, and S. W. Englander. Intimate view of a kinetic protein folding intermediate: Residue-resolved structure, interactions, stability, folding and unfolding rates, homogeneity. *J. Mol. Biol.*, 334(3):501 – 513, 2003.

141. P. Liuni, B. Deng, and D. J. Wilson. Comparing equilibrium and kinetic protein unfolding using time-resolved electrospray-coupled ion mobility mass spectrometry. *Analyst*, 140:6973–6979, 2015.

142. T. Mizukami, Y. Abe, and K. Maki. Evidence for a shared mechanism in the formation of urea-induced kinetic and equilibrium intermediates of horse apomyoglobin from ultrarapid mixing experiments. *PLoS One*, 10 (8):1–22, 08 2015.

143. O. B. Ptitsyn. Structures of folding intermediates. *Curr. Opin. Struct. Biol.*, 5(1):74 – 78, 1995.

144. L. Zhu, Y.-X. Fan, S. Perrett, and J.-M. Zhou. Relationship between kinetic and equilibrium folding intermediates of creatine kinase. *Biochem. Biophys. Res. Commun.*, 285(4):857 – 862, 2001.

145. J. A. Raymond and A. L. DeVries. Adsorption inhibition as a mechanism of freezing resistance in polar fishes. *Proc. Natl. Acad. Sci. U.S.A.*, 74(6): 2589–2593, 1977.

146. J. G. Duman. Antifreeze and ice nucleator proteins in terrestrial arthropods. *Annu. Rev. Physiol.*, 63(1):327–357, 2001.

147. R. N. Ben. Antifreeze glycoproteins - preventing the growth of ice. *ChemBioChem*, 2(3):161–166, 2001.

148. R. E. Feeney, T. S. Burcham, and Y. Yeh. Antifreeze glycoproteins from polar fish blood. *Annu. Rev. Biophys. Biophys. Chem.*, 15(1):59–78, 1986.

149. L. L. C. Olijve, K. Meister, A. L. DeVries, J. G. Duman, S. Guo, H. J. Bakker, and I. K. Voets. Blocking rapid ice crystal growth through nonbasal plane adsorption of antifreeze proteins. *Proc. Natl. Acad. Sci. U.S.A.*, 113(14):3740–3745, 2016.

150. C. Budke, A. Dreyer, J. Jaeger, K. Gimpel, T. Berkemeier, A. S. Bonin, L. Nagel, C. Plattner, A. L. DeVries, N. Sewald, and T. Koop. Quantitative efficacy classification of ice recrystallization inhibition agents. *Cryst. Growth Des.*, 14(9):4285–4294, 2014.

151. C. P. Garnham, R. L. Campbell, and P. L. Davies. Anchored clathrate waters bind antifreeze proteins to ice. *Proc. Natl. Acad. Sci. U.S.A.*, 108 (18):7363–7367, 2011.

152. T. Sun, F.-H. Lin, R. L. Campbell, J. S. Allingham, and P. L. Davies. An antifreeze protein folds with an interior network of more than 400 semiclathrate waters. *Science*, 343(6172):795–798, 2014.

153. K. Meister, S. Strazdaite, A. L. DeVries, S. Lotze, L. L. C. Olijve, I. K. Voets, and H. J. Bakker. Observation of ice-like water layers at an aqueous protein surface. *Proc. Natl. Acad. Sci. U.S.A.*, 111(50):17732–17736, 2014.

154. C. Yang and K. A. Sharp. The mechanism of the type III antifreeze protein action: a computational study. *Biophys. Chem.*, 109(1):137 – 148, 2004.

155. D. R. Nutt and J. C. Smith. Dual function of the hydration layer around an antifreeze protein revealed by atomistic molecular dynamics simulations. *J. Am. Chem. Soc.*, 130(39):13066–13073, 2008.

156. N. Smolin and V. Daggett. Formation of ice-like water structure on the surface of an antifreeze protein. *J. Phys. Chem. B*, 112(19):6193–6202, 2008.

157. U. S. Midya and S. Bandyopadhyay. Hydration behavior at the ice-binding surface of the tenebrio molitor antifreeze protein. *J. Phys. Chem. B*, 118 (18):4743–4752, 2014.

158. C. A. Knight, E. Driggers, and A. L. DeVries. Adsorption to ice of fish antifreeze glycopeptides 7 and 8. *Biophys. J.*, 64(1):252 – 259, 1993.

159. S. Ebbinghaus, K. Meister, B. Born, A. L. DeVries, M. Gruebele, and M. Havenith. Antifreeze glycoprotein activity correlates with long-range proteinwater dynamics. *J. Am. Chem. Soc.*, 132(35):12210–12211, 2010.

160. A. N. Krishnamoorthy, C.Holm, and J. Smiatek. Local water dynamics around antifreeze protein residues in the presence of osmolytes: The importance of hydroxyl and disaccharide groups. *J. Phys. Chem. B*, 118(40): 11613–11621, 2014.

161. J. A. Ahlgren and A. L. DeVries. Comparison of antifreeze glycopeptides from several antarctic fishes. *Polar Biol.*, 3(2):93–97, 1984.

162. C. C. M. Groot and H. J. Bakker. Proteins take up water before unfolding. *J. Phys. Chem. Lett.*, 7(10):1800–1804, 2016.

163. A. L. DeVries. Glycoproteins as biological antifreeze agents in antarctic fishes. *Science*, 172(3988):1152–1155, 1971.

164. A. I. Ahmed, Y. Yeh, Y. Y. Osuga, and R. E. Feeney. Antifreeze glycoproteins from antarctic fish. inactivation by borate. *J. Biol. Chem.*, 251 (10):3033–3036, 1976.

165. C. C. M. Groot, K. Meister, A. L. DeVries, and H. J. Bakker. Dynamics of the hydration water of antifreeze glycoproteins. *J. Phys. Chem. Lett.*, 7:4836–4840, 2016.

166. A. L. DeVries. The role of antifreeze glycopeptides and peptides in the freezing avoidance of antarctic fishes. *Comp. Biochem. Physiol. B - Comp. Biochem.*, 90(3):611 – 621, 1988.

167. T. S. Burcham, M. J. Knauf, D. T. Osuga, R. E. Feeney, and Y. Yeh. Antifreeze glycoproteins: Influence of polymer length and ice crystal habit on activity. *Biopolymers*, 23(7):1379–1395, 1984.

168. K. Meister, S. Ebbinghaus, Y. Xu, J. G. Duman, A. DeVries, M. Gruebele, D. M. Leitner, and M. Havenith. Long-range protein-water dynamics in hyperactive insect antifreeze proteins. *Proc. Natl. Acad. Sci. U.S.A.*, 110 (5):1617–1622, 2013.

169. A. N. Lane, L. M. Hays, N. Tsvetkova, R. E. Feeney, L. M. Crowe, and J. H. Crowe. Comparison of the solution conformation and dynamics of antifreeze glycoproteins from antarctic fish. *Biophys. J.*, 78(6):3195 – 3207, 2000.

170. N. M. Tsvetkova, B. L. Phillips, V. V. Krishnan, R. E. Feeney, W. H. Fink, J. H. Crowe, S. H. Risbud, F. Tablin, and Y. Yeh. Dynamics of antifreeze glycoproteins in the presence of ice. *Biophys. J.*, 82(1):464 – 473, 2002.

171. C. A. Knight, J. Hallett, and A. L. DeVries. Solute effects on ice recrystallization: An assessment technique. *Cryobiology*, 25(1):55 – 60, 1988.

172. C. A. Knight, D. Wen, and R. A. Laursen. Nonequilibrium antifreeze peptides and the recrystallization of ice. *Cryobiology*, 32(1):23 – 34, 1995.

173. C. Mattos and A. C. Clark. Minimizing frustration by folding in an aqueous environment. *Arch. Biochem. Biophys.*, 469(1):118 – 131, 2008.

174. B. Halle. Protein hydration dynamics in solution: a critical survey. *Philos. T. Roy. Soc. B*, 359(1448):1207–1224, 2004.

175. J. D. Watson and F. H. C. Crick. Molecular structure of nucleic acids: A structure for deoxyribose nucleic acid. *Nature*, 171:737–738, 1953.

176. Ł. Szyc, M. Yang, E.T.J. Nibbering, and T. Elsaesser. Ultrafast vibrational dynamics and local interactions of hydrated DNA. *Angew. Chem. Int. Ed.*, 49(21):3598–3610, 2010.

177. V. V. Volkov, D. J. Palmer, and R. Righini. Distinct water species confined at the interface of a phospholipid membrane. *Phys. Rev. Lett.*, 99:078302, 2007.

178. K. Larsson. On the structure of the liquid state of triglycerides. *J. Am. Oil Chem. Soc.*, 69(8):835–836, 1992.

179. D. J. Cebula, D. J. McClements, M. J. W. Povey, and P. R. Smith. Neutron diffraction studies of liquid and crystalline trilaurin. *J. Am. Oil Chem. Soc.*, 69(2):130–136, 1992.

180. R. W. Corkery, D. Rousseau, P. Smith, D. A. Pink, and C. B. Hanna. A case for discotic liquid crystals in molten triglycerides. *Langmuir*, 23(13): 7241–7246, 2007.

181. H. Kawachi, R. Tanaka, M. Hirano, K. Igarashi, and H. Ooshima. Crystallization of β-sitosterol using a water-immiscible solvent hexane. *J. Chem. Eng. Jpn.*, 39(8):869–875, 2006.

182. L. I. Christiansen, J. T. Rantanen, A. K. von Bonsdorff, M. A. Karjalainen, and J. K. Yliruusi. A novel method of producing a microcrystalline β-sitosterol suspension in oil. *Eur. J. Pharm. Sci.*, 15(3):261 – 269, 2002.

183. R. den Adel, P. C. M. Heussen, and A. Bot. Effect of water on self-assembled tubules in β-sitosterol + γ-oryzanol-based organogels. *JPCS*, 247(1):012025, 2010.

184. W. Ostwald. *Lehrbuch der Allgemeinen Chemie, vol. 2, part 1.* W. Engelmann, Leipzig, 1896.

185. J. Kurashige, K. Takaoka, M. Takasago, Y. Taru, and K. Kobayashi. State of dissolved water in triglycerides as determined by fourier transform infrared and near infrared spectroscopy. *J. Jpn. Oil Chem. Soc.*, 40(7): 549–553, 1991.

186. S. A. Moreira, J. Sarraguça, D. F. Saraiva, R. Carvalho, and J. A. Lopes. Optimization of NIR spectroscopy based PLSR models for critical properties of vegetable oils used in biodiesel production. *Fuel*, 150:697 – 704, 2015.

187. M. R. Monteiro, A. R. P. Ambrozin, L. M. Lião, and A. G. Ferreira. Critical review on analytical methods for biodiesel characterization. *Talanta*, 77 (2):593 – 605, 2008.

188. J. J. Gilijamse, A. J. Lock, and H. J. Bakker. Dynamics of confined water molecules. *Proc. Natl. Acad. Sci. U.S.A.*, 102(9):3202–3207, 2005.

189. A. Wulf and R. Ludwig. Structure and dynamics of water confined in dimethyl sulfoxide. *ChemPhysChem*, 7(1):266–272, 2006.

190. R. Lemus. Vibrational excitations in H_2O in the framework of a local model. *J. Mol. Spectrosc.*, 225(1):73 – 92, 2004.

191. S. Park, D. E. Moilanen, and M. D. Fayer. Water dynamics - the effects of ions and nanoconfinement. *J. Phys. Chem. B*, 112(17):5279–5290, 2008.

192. D. Cringus, S. Yeremenko, M. S. Pshenichnikov, and D. A. Wiersma. Hydrogen bonding and vibrational energy relaxation in water-acetonitrile mixtures. *J. Phys. Chem. B*, 108(29):10376–10387, 2004.

193. D. B. Wong, K. P. Sokolowsky, M. I. El-Barghouthi, E. E. Fenn, C. H. Giammanco, A. L. Stopturlaugson, and M. D. Fayer. Water dynamics in water/DMSO binary mixtures. *J. Phys. Chem. B*, 116(18):5479–5490, 2012.

194. E. E. Fenn, D. E. Moilanen, N. E. Levinger, and M. D. Fayer. Water dynamics and interactions in waterpolyether binary mixtures. *J. Am. Chem. Soc.*, 131(15):5530–5539, 2009.

195. T. Q. Luong, P. K. Verma, R. K. Mitra, and M. Havenith. Onset of hydrogen bonded collective network of water in 1,4-dioxane. *J. Phys. Chem. A*, 115(50):14462–14469, 2011.

196. O. Selig, R. Siffels, and Y. L. A. Rezus. Ultrasensitive ultrafast vibrational spectroscopy employing the near field of gold nanoantennas. *Phys. Rev. Lett.*, 114:233004, Jun 2015.

197. M. Candelaresi, M. Pagliai, M. Lima, and R. Righini. Chemical equilibrium probed by two-dimensional IR spectroscopy: Hydrogen bond dynamics of methyl acetate in water. *J. Phys. Chem. A*, 113(46):12783–12790, 2009.

198. I. M. Pazos, A. Ghosh, M. J. Tucker, and F. Gai. Ester carbonyl vibration as a sensitive probe of protein local electric field. *Angew. Chem. Int. Ed.*, 53(24):6080–6084, 2014.

199. S. E. Braslavsky, E. Fron, H. B. Rodriguez, E. S. Roman, G. D. Scholes, G. Schweitzer, B. Valeur, and J. Wirz. Pitfalls and limitations in the practical use of Förster's theory of resonance energy transfer. *Photochem. Photobiol. Sci.*, 7:1444–1448, 2008.

200. S. Bresson, M. El Marssi, and B. Khelifa. Raman spectroscopy investigation of various saturated monoacid triglycerides. *Chem. Phys. Lipids*, 134 (2):119 – 129, 2005.

201. S. Bresson, M. El Marssi, and B. Khelifa. Conformational influences of the polymorphic forms on the CO and C-H stretching modes of five saturated monoacid triglycerides studied by Raman spectroscopy at various temperatures. *Vib. Spectrosc.*, 40(2):263 – 269, 2006.

202. L. Chuntonov, I. M. Pazos, J. Ma, and F. Gai. Kinetics of exchange between zero-, one-, and two-hydrogen-bonded states of methyl and ethyl acetate in methanol. *The Journal of Physical Chemistry B*, 119(12):4512–4520, 2015.

203. M. Banno, K. Ohta, and K. Tominaga. Ultrafast vibrational dynamics and solvation complexes of methyl acetate in methanol studied by subpicosecond infrared spectroscopy. *J. Raman Spectrosc.*, 39(11):1531–1537, 2008.

204. S. M. Kashid, G. Y. Jin, S. Bagchi, and Y. S. Kim. Cosolvent effects on solutesolvent hydrogen-bond dynamics: Ultrafast 2D IR investigations. *J. Phys. Chem. B*, 119(49):15334–15343, 2015.

Appendix: The value of science

Science: The intellectual and practical activity encompassing the systematic study of the structure and behaviour of the physical and natural world through observation and experiment.

the Oxford dictionary

Science, simply put, is the systematic study of the natural world. The foremost task of a scientist is therefore to study, i.e., to acquire knowledge towards a more comprehensive understanding of the natural world. Around the world, people devote a lot of time and resources to scientific projects, building giant observatories, installing particle accelerators, gathering large groups of study participants and even sending experiments to space. What drives this quest for knowledge? For many scientists, it is a sense of fascination: understanding the complexity of nature, be it in the physical or social domain, is the primary goal. It is the yearning to know more, and the satisfaction that comes with solving the next puzzle.

At the same time, the generation of knowledge often has consequences. New insights and technologies can impact society in many ways[1,2]. The way most people live nowadays is heavily influenced by discoveries in the past. Consider for example the discovery of electricity by Michael Faraday in 1820, now essential to any modern household, and the realization of Louis Pasteur in the 1860's that many diseases are caused by microorganisms, which saved millions of lives ever since. Less benign examples also exist: the invention of the atomic bomb for instance provided the world with such an effective weapon that it changed the entire political landscape. Even though only few discoveries have such far-reaching implications, it makes clear that scientific findings can have a great impact on society.

With this in mind, perhaps, the term "valorization" has entered the scientific world. That is, the creation of value from knowledge, by transferring this knowledge into products, services or processes. The term was first coined by public policy makers wishing to see return on their investments: in return for funding, scientists across all disciplines are expected to contribute to societal benefits[3]. Scientific advance does indeed hold promise to provide solutions to societal problems. We can for example foresee answers towards more efficient and cheaper clean energy sources, more sustainable food production and better treatment of diseases. On a global scale, the major societal objectives have been formulated in the UN Millenium Development Goals, and science and technology are expected to be crucial factors in reaching these goals[1,4]. On a national level, scientific knowledge has been shown to stimulate the economy, thereby

enhancing the standard of living. The economist Robert Solow (winner of the Nobel prize in 1987) and later colleagues identified technological progress as the main factor of economic growth[5,6]. It is hard to estimate how much science, as a driver of technological progress, contributes to growth, but economists estimate a substantial 20%-60% return on investments in science[7,8].

In my eyes, the fact that scientific insights can be used to improve people's lives makes science very valuable. The term valorization emphasizes this fact, and encourages scientists to think about the consequences and possible applications of their results.

At the same time, in attempts to stimulate valorization, scientists are increasingly evaluated on societal relevance[9–11]. This creates some complications. Firstly, the very nature of science, as the study of the unknown, prevents a reliable prediction of the long-term societal impact of a study, especially in the case of basic research. A famous example is the experiments by Heinrich Hertz on radio waves. These experiments are at the base of many of the modern communication technologies, but Hertz himself remarked[12]: "It's of no use whatsoever[...] this is just an experiment that proves Maestro Maxwell was right - we just have these mysterious electromagnetic waves that we cannot see with the naked eye. But they are there." As a result of this unpredictability, scientists conducting basic research have a harder time convincing funding boards about the merits of their research, and budget is moving from basic science to applied science, and from creative ideas to short-term low-risk projects.[a] The question is whether this approach will in the end lead to the most benefit for society. Applied research may have the most impact on the short term, but radically new approaches to societal problems will likely not emerge.

A second complication is how to evaluate societal impact. What is beneficial for the local economy, such as partnerships with private organizations and the creation of patents, is not necessarily beneficial for the larger society, or even for science itself. From an economic viewpoint, for instance, it is best to develop medicines targeted to the demands of the rich, which does not help the societal aim of eradicating diseases that primarily affect the poor[1]. From the same viewpoint it is vital to protect generated knowledge with patents, such that a competitive position on the market can be maintained. Patents and other intellectual property (IP) rights, however, can also hinder innovation, as patents might be too expensive for new players to use the knowledge. It can furthermore clash with the openness and knowledge transfer that is so crucial for scientific advancement[1,13]. In recent years, absurd situations occurred where scientists working together with private organizations are expected to investigate materials or devices without knowing what they are made of, in light of IP rights. This likely does not help science nor the private organizations involved. Too much focus on economic indicators of valorization might thus lead to the opposite of the desired effect.

So we find that stimulating and evaluating valorization is not so simple.

[a] This trend is also driven by the fact that discoveries in basic science usually don't directly benefit the investor, who takes the financial risk, but benefit all, as findings travel with internet-speed across the world[7].

Currently, valorization mechanisms are to let scientists write about the future use of their future knowledge, and to list performance indicators like the amount of collaborations inside and outside academia, public lectures, outreach activities, patents, and received prizes. It remains to be seen whether the scientists that are most excellent on paper are actually the ones that turn out to find the answers that contribute most to society. We must especially be careful not to focus too much on the particular performance indicator of high-impact papers. In the current scientific climate of extreme competition, a high-impact paper can make or break a scientist's career. To publish in a high-impact journal, an exciting and novel discovery is needed, while attempts to thoroughly reproduce studies often end up in less highly regarded journals. The number of irreproducable studies is consequently alarmingly high[14]. It would be tragic if the way we try to stimulate science and its societal impact led to the loss of science itself, as in the systematic study of the natural world, and the search for the truth, or as close to it as we can get[13]. Without proper science, we cannot expect benefits for society at all.

History has shown us enough examples of scientific discoveries with great impact and many benefits for society. Let us therefore reward rigorous science, look critically beyond the numbers at real quality and societal impact, and continue to reap the benefits.

References

1. B. De Jonge and N. Louwaars. Valorizing science: whose values? *EMBO Press*, 10(6):535-539, 2009.
2. R. E. McGinn. *Science, technology, and society.* Prentice Hall, 1991.
3. S. de Jong. *Engaging Scientists: Organising Valorisation in the Netherlands.* PhD thesis, Leiden University, September 10$^{\text{th}}$ 2015.
4. C. Juma, Y.-C. Lee, UN Millenium project task force on science, innovation and technology. *Innovation: Applying knowledge in development.* Eartscan, 2005.
5. R. M. Solow. Technical change and the aggregate production function. *Rev. Econ. Stat.*, 39(3):312-320, 1957.
6. K. Arrow. Economic welfare and the allocation of resources for invention. In R. Nelson (ed.) *The rate and direction of inventive activity: economic and social factors.* Princeton Univ. Press, 1962.
7. W. H. Press. What's so special about science (and how much should we spend on it?) *Science*, 342(6160):817-822, 2013.
8. A. J. Salter and B. R. Martin. The economic benefits of publicly funded basic research: a critical review. *Res. Policy*, 30(3):509-532, 2001.
9. Standard Evaluation Protocol 2015-2021: Protocol for research assessments in the Netherlands. VSNU, KNAW and NWO, 2014.
10. Dutch Top Sector policy. www.topsectoren.nl, November 2016.

11. 2025 - Vision for science choices for the future. Dutch Ministry of Education, Culture and Science, 2014.

12. A. Z. Capri. *Quips, quotes, and quanta: an anecdotal history of physics.* World Scientific, 2007.

13. K. R. Popper. *Conjectures and Refutations: The Growth of Scientific Knowledge.* Routledge, 1963.

14. M. Baker. 1,500 scientists lift the lid on reproducibility. *Nature*, 533(7604):452-454, 2016.

Summary

Life as we know it takes place in liquid water. This water is not merely a passive solvent, but plays an active role in many biological processes. Understanding the subtle interplay between water and biomolecules is therefore crucial for understanding the mechanics and chemistry of life. In this thesis, we present a series of spectroscopic experiments that elucidate the hydrogen-bond structure and dynamics of water molecules in solutions of different biologically relevant molecules. As a tool, we use vibrational pump-probe spectroscopy. This technique uses a short, intense infrared pump pulse to excite molecular vibrations that we can follow over time by monitoring the infrared absorption of a second, weaker probe pulse. The main vibrational mode of water, the OH stretch vibration, is very sensitive to the hydrogen-bond strength of water and can therefore supply information on water structure: the OH stretch vibrational frequency can indicate whether water molecules are hydrogen-bonded to other water molecules, to other hydrophilic molecules, or not hydrogen-bonded at all. After excitation by the pump pulse, the water OH stretch vibrations decay back to the ground state on a picosecond (10^{-12}s) timescale. The timescale of vibrational relaxation can provide structural information as well. Furthermore, by exciting at different frequencies we can probe the typical timescale of structural fluctuations of the dynamical water hydrogen-bond network and explore the coupling between different vibrations. Finally, by exploiting the polarization-dependence of the pump-probe signal, we can measure the rate of water reorientation.

Water dynamics in sugar solutions In a first series of experiments, we investigated the water reorientation dynamics in aqueous sugar solutions. Sugars are an important class of biomolecules, serving for example as energy source, signalling group, or stabilizing osmolyte of proteins under environmental stress conditions. This latter property is still not fully understood, though it has been hypothesized that sugars stabilize proteins indirectly, via the water solvent. We find that the water reorientation dynamics in a sugar solution of a particular concentration can be described by a single reorientation time constant. With increasing sugar concentration, the water reorientation time constant increases from 2.5 picoseconds to a value of about 15 picoseconds. Compared to other small solutes, the influence of sugars on the dynamics of water is relatively long-ranged, and involves collective structural effects. These results are in line with an indirect protein stabilization mechanism of sugars via the water solvent.

Water dynamics at a protein surface Secondly, we focused on the water reorientation dynamics in solutions of globular proteins at different degrees of

unfolding. Proteins perform specific biological functions that strongly depend on their three-dimensional folded structure that in turn is influenced by the interaction between the protein and the water solvent. We find that a fraction of the water molecules is strongly slowed down by their interaction with the protein surface. The slow water fraction is a measure of the amount of water-exposed surface. In the process of urea-induced protein unfolding, we observe that the water-exposed surface increases by almost 50%, before the protein secondary structure is affected. This indicates that protein unfolding starts with the protein structure becoming less tight, thereby allowing water to enter.

HYDRATION OF ANTIFREEZE GLYCOPROTEINS A special class of proteins are the antifreeze glycoproteins (AFGPs) that enable the survival of arctic fish by inhibiting the growth of ice crystals. The molecular mechanism of antifreeze protection is still unclear. We measured the water reorientation dynamics in solutions of AFGPs, and find that a fraction of the water molecules is strongly slowed down. The fraction of slow water molecules scales with the size and concentration of AFGP, and is comparable to the fraction of slow water observed for non-antifreeze proteins, both at room temperature and close to biologically working temperatures. We find that inhibiting AFGP antifreeze activity using borate buffer induces no changes in the dynamics of water hydrating the AFGP. At the same time, borate induces gel formation by forming cross-links between the AFGP sugar groups. Our findings support a local mechanism in which the sugar unit of AFGP forms the active ice-binding site.

WATER MOLECULES IN TRIGLYCERIDE OILS The last series of experiments described in this thesis focuses on the hydrogen-bond structure and dynamics of water in triglyceride oils. Triglycerides are crucial for metabolic functions and are used in daily life as foods, pharmaceuticals, cosmetics and raw material for biodiesel. Even though triglycerides are considerably hydrophobic, small amounts of water can accumulate in the oil. We find that these water molecules form several stable species that do not interconvert on the 20 picosecond timescale of the experiment: waters with a single strong hydrogen bond to the triglyceride, waters with two weaker hydrogen bonds to the triglycerides, and water clusters. The water molecules with two weaker hydrogen bonds to the triglyceride correspond to a single, specific hydrogen-bond configuration; these molecules likely bridge the carbonyl groups of adjacent triglyceride molecules, which can have a large influence on the properties of triglyceride oils.

WATER MOLECULES IN TRIGLYCERIDE OILS - PROBING THE CARBONYL STRETCH VIBRATION We further investigated the interaction between water and triglyceride oil by studying the transient response of the carbonyl stretch vibration of the triglycerides. We find that the hydrogen-bond formation between a water molecule and the carbonyl group of the triglyceride leads to a frequency downshift of the absorption of the carbonyl stretch vibration. This hydrogen-bond formation affects the transient response of the carbonyl stretch vibration, and slightly speeds up the vibrational relaxation. We also observe that the relaxation rate strongly varies with frequency, and that the C=O

vibrations rapidly exchange vibrational energy as a result of Förster energy transfer.

Samenvatting

Leven speelt zich af in vloeibaar water. Het menselijk lichaam bestaat bijvoorbeeld voor gemiddeld 65% uit water, en de meeste levende wezens kunnen niet zonder. Water lijkt zelfs zo essentieel voor leven dat astrofysici enthousiast worden wanneer er ergens vloeibaar water wordt gevonden in het universum, want waar water is, kan ook leven zijn... Zeker is dat water niet een passief oplosmiddel is, maar een actieve rol speelt in veel biologische processen. Gedetailleerde kennis van de subtiele wisselwerking tussen water en biomoleculen is dus cruciaal om we de mechanica en scheikunde van levende wezens te kunnen begrijpen. In dit proefschrift presenteren we een serie spectroscopische experimenten die de structuur en dynamica ontrafelen van water moleculen in oplossingen van verschillende biologisch relevante moleculen. Ons experimenteel gereedschap is vibrationele pomp-probe spectroscopie. In deze vorm van spectroscopie, exciteert een korte, intense infrarode lichtpuls (de pomp) moleculaire vibraties, die we vervolgens kunnen bekijken door de infrarood absorptie van een tweede, zwakkere lichtpuls (de probe) te meten. De voornaamste vibratie van water, de water zuurstof-waterstof (OH) strek vibratie, is erg gevoelig voor de waterstofbrugsterkte van water en kan als zodanig informatie verschaffen over de structuur van water: de frequentie van de OH strek vibratie kan bijvoorbeeld aangeven of water moleculen waterstofbruggen vormen met andere water moleculen, met andere hydrofiele moleculen, of dat ze ongebrugd zijn. Na excitatie door de pomp puls vervallen de water OH strek vibraties terug naar de grondtoestand binnen enkele picoseconden (10^{-12}s). Deze vibratierelaxatietijd kan ook structurele informatie verschaffen. Bovendien is het mogelijk om de typische tijdschaal van structurele fluctuaties te meten en de koppeling tussen moleculen te bekijken door te exciteren bij verschillende pompfrequenties. Tenslotte kunnen we de water oriëntatiesnelheid bepalen door gebruik te maken van de polarisatieafhankelijkheid van het pomp-probe signaal.

Waterdynamica in suikeroplossingen De eerste experimenten beschreven in dit proefschrift richten zich op de oriëntatiesnelheid van watermoleculen in suikeroplossingen. Suikers zijn een belangrijke groep biomoleculen die dienst doen als energiebron, signaalgroep of stabiliserende factor voor de structuur van eiwitten. Deze laatste eigenschap is nog steeds niet volledig begrepen, maar vermoedt wordt dat suikers de structuur van eiwitten indirect stabiliseren door de eigenschappen van het omringende water te veranderen. We vinden dat de water oriëntatiesnelheid in een suikeroplossing van een bepaalde concentratie te beschrijven is met een enkele tijdsconstante. Deze tijdsconstante neemt toe met toenemende suikerconcentratie, van 2.5 picoseconden tot een waarde van 15 picoseconden. In vergelijking met andere kleine moleculen beïnvloeden suikers

de dynamica van water over een relatief lange afstand, en spelen collectieve structurele effecten een rol. Deze resultaten zijn consistent met een indirect stabilisatie-effect van suikers op eiwitten via het omringende water.

WATERDYNAMICA AAN HET OPPERVLAK VAN EIWITTEN Ten tweede richten we ons op de waterdynamica in oplossingen van globulaire eiwitten, waarbij de eiwitten in verschillende mate ontvouwen zijn. Eiwitten verrichten specifieke biologische taken die sterk afhangen van de driedimensionale gevouwen eiwitstructuur, die op zijn beurt weer afhangt van de interactie tussen het eiwit en het omringende water. We observeren dat een fractie van de water moleculen in eiwitoplossingen sterk wordt vertraagd door hun interactie met het eiwitoppervlak. De fractie langzame watermoleculen is een maat voor de hoeveelheid eiwitoppervlak dat aan water wordt blootgesteld. Wanneer het eiwit wordt ontvouwen met behulp van ureum, observeren we een toename van het blootgestelde oppervlak van bijna 50%, terwijl de secondaire eiwitstructuur intact blijft. Hieruit volgt dat het ontvouwen van eiwitten begint met het losser worden van de eiwitstructuur en het binnendringen van water.

HYDRATIE VAN ANTIVRIESGLYCOPROTEÏNEN Een speciale klasse van eiwitten zijn de antivriesglycoproteïnen (AVGPs). Deze eiwitten verhinderen dat ijskristallen kunnen groeien, waardoor ze ervoor zorgen dat vissen in de poolcirkel kunnen overleven. Het moleculaire mechanisme van deze antivriesbescherming is niet bekend. We meten de waterdynamica in oplossingen van AVGPs, en constateren dat een fractie van de watermoleculen sterk is vertraagd. De fractie langzame watermoleculen schaalt met de concentratie en grootte van de AVGPs en is vergelijkbaar met de fractie langzame watermoleculen voor eiwitten zonder antivrieswerking, zowel bij kamertemperatuur als bij biologisch relevante temperaturen vlak bij het vriespunt. We observeren dat het toevoegen van boraat, dat de antivriesactiviteit remt, geen effect heeft op de waterdynamica rondom AVGPs. Boraat zorgt er wel voor dat de oplossing een gel vormt, doordat boraat moleculen bruggen vormen tussen de suikergroepen van de AVGPs. Onze bevindingen wijzen op een antivriesmechanisme waarbij het vooral de suikergroepen van AVGPs zijn die zich binden aan het ijs.

WATERMOLECULEN IN TRIGLYCERIDE OLIËN De laatste serie experimenten beschreven in dit proefschrift richten zich op de waterstofbrugstructuur en dynamica van water in triglyceride oliën. Triglyceriden zijn cruciaal voor metabolisme en worden in het dagelijks leven gebruikt in voedsel, medicijnen, cosmetica en als grondstof voor biobrandstof. Hoewel triglyceriden sterk hydrofoob zijn, kunnen zich toch kleine hoeveelheden water in de olie ophopen. We observeren dat deze watermoleculen verschillende stabiele structuren vormen: we identificeren watermoleculen met een enkele sterke waterstofbrug naar de triglyceride, watermoleculen met twee zwakkere waterstofbruggen naar de triglyceriden en water clusters. De watermoleculen met twee zwakkere waterstofbruggen naar de triglyceriden vormen een enkele, specifieke waterstofbrugconfiguratie: deze moleculen overbruggen waarschijnlijk de carbonylgroepen van aangrenzende triglyceridemoleculen en zouden zo een groot effect kunnen

hebben op de eigenschappen van triglyceride oliën.

WATERMOLECULEN IN TRIGLYCERIDE OLIËN - OBSERVATIE VIA DE CARBONYL STREK VIBRATIE We hebben de interactie tussen water en triglyceride oliën in meer detail onderzocht door de transiente respons van de C=O strek vibratie van de triglyceriden te bestuderen. We nemen waar dat de waterstofbrugformatie tussen een watermolecuul en een triglyceride C=O groep leidt tot een verschuiving van de absorptie van de C=O strek vibratie naar lagere frequenties. Deze waterstofbrugformatie leidt tot een kleine versnelling van de vibratierelaxatie. We vinden dat de vibratierelaxatie sterk afhankelijk is van de frequentie van de C=O vibratie, en dat de C=O vibraties energie uitwisselen als gevolg van hun dipool-dipool (Förster) interacties.

Acknowledgements

With the completion of this thesis a 4.5-year period of conducting research at AMOLF comes to an end. It was an interesting time: moving to Amsterdam, meeting new people, learning a lot about science, about the interactions between water and biomolecules, and about other things. The completion of this thesis was made possible by the help and support of many people, whom I would like to thank here.

Allereerst wil ik graag mijn promotor Huib Bakker bedanken, voor de kans om aan een interessant onderwerp te werken en voor de fijne samenwerking. Ik heb grote bewondering voor hoezeer dingen kunnen verbeteren - een artikel, een fysische verklaring van meetdata, de opbouw van een presentatie, of het nemen van een beslissing - na een kort advies van Huib.

My direct colleagues contributed a lot to the good atmosphere I experienced at AMOLF. In the beginning, Sietse and Marcin got me started with spectroscopy, and Sietse explained all the details of data analysis. For any question regarding theory, I could always count on Yves, and in case of an experimental problem, Jan was there to ensure that the laser and setup were running smoothly. I'd further like to thank Niklas for the interesting conversations, Konrad for the strategic view and help by thinking along, Simona for the friendliness, Wilbert for the enthusiasm, Oleg for always being willing to help, Eliane for enhancing the office gezelligheid, and all the older and newer members of our department: Artem, Stephan, Liyuan, Christina, Stefanie, Lianne, Jiri, Roel, Giulia, Bart, Roberto, Biplap, Johannes, Andrea, Aleksandr, Harmen, and Cateryn.

Als er iets gefixt moest worden, waren er ook veel mensen waar ik op kon rekenen. Hinco, Niels en Dion wil ik bedanken voor de technische ondersteuning en de enthusiaste houding van "dat gaan we regelen". Idsart, Duncan, Sjoerd, Ivo, Mark, Wiebe en Rutger bedank ik voor hulp met elektronica, software, scheikunde en computerproblemen.

In addition I had the privilege to collaborate with people outside the Molecular Biophysics department at AMOLF. I'd like to thank Krassimir Velikov for the fruitful collaboration and the helpful result-oriented questions, Faidon and Peter Bolhuis for contributing to the theoretical understanding of water and proteins, Leonardo Cornacchia for the project on milk proteins and Stijn, Nicholas, Bart and Gijsje for involving me in the interesting project looking into fibrinogen.

Als ik denk aan mijn promotietijd in Amsterdam, dan denk ik ook aan het Studentenkoor Amsterdam: altijd garant voor gezelligheid op woensdagavond en mooie concerten. Hetzelfde geld voor Boeuf Majeur, daarom aan alle

medezangers: bedankt.

Gezelligheid en afleiding van werk was er ook bij de "burgerchicks", toevallig weer verenigd in Amsterdam, en met alle andere vrienden die ik heb leren kennen in Enschede, of eerder nog in Amersfoort. Team awesome did its name justice and contributed to many good times as well. I want to thank you all for your friendship and for keeping in touch.

Voor vriendschap en ondersteuning wil ik ook mijn familie bedanken, de Grootjes, de Klavers, de Mensinks, bij wie ik me thuis voel en altijd terecht kan. And finally, Jacob: you contributed to this thesis by thoroughly checking it for grammar mistakes, but more so by being there. Us meeting again was the best thing that happened during my PhD, and I'll be forever grateful for that.